# Self-interacting neutrinos, the Hubble parameter tension, and the cosmic microwave background

Thejs Brinckmann<sup>®</sup>, <sup>1,\*</sup> Jae Hyeok Chang<sup>®</sup>, <sup>2,3</sup> and Marilena LoVerde<sup>®</sup> <sup>1</sup>C. N. Yang Institute for Theoretical Physics and Department of Physics & Astronomy, Stony Brook University, Stony Brook, New York 11794, USA <sup>2</sup>Maryland Center for Fundamental Physics, University of Maryland, College Park, Maryland 20742, USA <sup>3</sup>Department of Physics and Astronomy, Johns Hopkins University, Baltimore, Maryland 21218, USA

(Received 18 February 2021; accepted 1 July 2021; published 13 September 2021)

We perform a comprehensive study of cosmological constraints on nonstandard neutrino self-interactions using cosmic microwave background and baryon acoustic oscillation data. We consider different scenarios for neutrino self-interactions distinguished by the fraction of neutrino states allowed to participate in self-interactions and how the relativistic energy density,  $N_{\rm eff}$ , is allowed to vary. Specifically, we study cases in which all neutrino states self-interact and  $N_{\rm eff}$  varies; two species free-stream, which we show alleviates tension with laboratory constraints, while the energy in the additional interacting states varies; and a variable fraction of neutrinos self-interact with either the total  $N_{\rm eff}$  fixed to the Standard Model value or allowed to vary. In no case do we find compelling evidence for new neutrino interactions or nonstandard values of  $N_{\rm eff}$ . In several cases, we find additional modes with neutrino decoupling occurring at lower redshifts  $z_{\rm dec} \sim 10^{3-4}$ . We do a careful analysis to examine whether new neutrino self-interactions solve or alleviate the so-called  $H_0$  tension and find that, when all Planck 2018 CMB temperature and polarization data are included, none of these examples eases the tension more than allowing a variable  $N_{\rm eff}$  comprised of free-streaming particles. Although we focus on neutrino interactions, these constraints are applicable to any light relic particle.

#### DOI: 10.1103/PhysRevD.104.063523

#### I. INTRODUCTION

Neutrinos are among the least understood particles in the Standard Model. The origin of neutrino mass is unknown, as is their Dirac or Majorana nature. Moreover, a range of anomalies persists in laboratory neutrino experiments (for a review, see, e.g., Refs. [1,2]). Cosmological datasets, which are sensitive to the gravitational effects of neutrinos throughout cosmic history, offer complementary information about neutrinos and may therefore shed light on these neutrino puzzles. In this paper, we will generalize the phenomenological description of neutrinos as pertains to cosmological datasets to determine constraints on a variety of nonstandard neutrino scenarios.

In the standard cosmology, neutrinos were in thermal equilibrium with the rest of the Standard Model particles at temperatures much greater than 2 MeV. As the Universe expanded and cooled, neutrinos ceased to scatter frequently, a process referred to as *neutrino decoupling*. Neutrinos contribute a substantial fraction to the energy budget of the early Universe, comprising roughly 40% of the radiation density at epochs probed by the cosmic microwave background (CMB). CMB anisotropies are

sensitive to both the total energy in neutrinos, through their contribution to the energy density and therefore the expansion rate, as well as inhomogeneities in the neutrino energy density (for a review, see, e.g., Ref. [3]).

The cosmological epochs probed by the CMB anisotropies are well after neutrino decoupling. That is, from the perspective of CMB data, standard neutrinos are freestreaming particles. While the total energy in neutrinos is unaffected by the decoupling transition, the behavior of neutrino perturbations changes qualitatively. If neutrinos scatter frequently, neutrino perturbations behave as a relativistic fluid and will participate in acoustic oscillations along with photons and baryons. After neutrino decoupling, neutrinos free-stream to cosmological distances, sourcing large anisotropic stress, which in turn modifies the behavior of the photon-baryon fluid [4]. For standard neutrinos, neutrinos are free-streaming for the entire epoch probed by the CMB, and the decoupling transition leaves no impact. On the other hand, if neutrinos have additional self-interactions, neutrino-neutrino scattering can persist until late enough times to have an observable impact on CMB data. In this paper, we will study CMB constraints on the decoupling of neutrino self-interactions. From now on, we refer to neutrino decoupling from the photon bath as standard neutrino

<sup>\*</sup>thejs.brinckmann@gmail.com

decoupling to distinguish from the decoupling of neutrino self-interactions.

Before proceeding, let us review related literature. The assumption of free-streaming neutrinos at CMB times has been relaxed to study a variety of specific nonstandard neutrino scenarios (see, e.g., Refs. [5–24]). Other works have modified the behavior of neutrino perturbations by introducing a viscosity parameter to quantify the anisotropic stress and put constraints on that parameter with CMB data (e.g., Refs. [25–30]). A general framework for studying the impact of neutrino self-interactions and their decoupling on CMB data, along with constraints, was presented in Ref. [31] and the subsequent work [32]. Recently, neutrino self-interactions have been proposed as a solution to the Hubble tension [33], which has since been studied by Refs. [34–40]. Related work studies selfinteracting dark radiation, which will have similar consequences on CMB observables (e.g., Refs. [41-45]).

In this paper, we go beyond the previous works in several ways. First, we use the latest Planck 2018 data for our constraints. Second, we consider several different implementations of new neutrino interactions. In addition to studying interactions among all species of neutrinos, with a free total number of neutrino states, as in Refs. [31–33] (our case 1), we consider a scenario with two free-streaming neutrinos states and free number of self-interacting neutrino states (case 2), which we will see alleviates some of the tension with current experimental constraints on new neutrino interactions [46,47]. For *case 3*, we fix the early Universe energy density of neutrinos to the Standard Model value ( $N_{\rm eff} = 3.046$ ) and produce constraints on the fraction of those neutrinos that can have self-interactions. Finally, for case 4, we allow both the total energy in relativistic neutrinos to vary and the self-interacting fraction. We remind the reader that while we use the term "neutrino" to describe the particles we are constraining, the physical effects of these particles on CMB and baryon acousting oscillation (BAO) data are purely gravitational, and therefore the constraints on the energy density (parametrized by  $N_{\rm eff}$ ) and decoupling epoch described in this paper apply to any light relic particle (for a review see, e.g., Ref. [48]).

A second motivation for our work is the existence of tensions between different cosmological datasets. In recent years, increasingly precise measurements of the Hubble parameter have led to a statistically significant tension between direct measurements of the Hubble expansion rate using supernovae calibrated with the distance ladder (e.g., Refs. [49–51]), which find a high value of the Hubble parameter, and a host of alternative methods that do not make use of the distance ladder (see, e.g., Ref. [52] for a review). These include supernovae (i.e., the Pantheon [53] or Dark Energy Survey (DES) samples [54]) calibrated by alternative means, e.g., using the BAO scale (e.g., measured by DES [54]); the so-called inverse distance ladder approach, as well as inferences of the Hubble parameter

using early-time probes, such as the CMB (e.g., from Planck [30,55] or Atacama Cosmology Telescope (ACT) [56]); or, independently from the CMB, from the BAO scale in combination with measurements of the abundance of primordial elements from big bang nucleosynthesis (BBN), either the two alone (see, e.g., Refs. [57–59]) or with galaxy clustering and weak lensing measurements (e.g., including DES [60]).

Similarly, recent measurements of the amplitude of matter fluctuations (quantified in this case by  $\sigma_8$ , the root mean square amplitude of fluctuations within 8 Mpc spheres, or by  $S_8 = \sigma_8(\Omega_m/0.3)^{0.5}$ , a parameter that folds in the matter density in the Universe,  $\Omega_m$ ) in the late Universe have seen a notable discrepancy between earlyand late-time measurements. Specifically, a discrepancy exists between values inferred from Planck CMB data and late-time cosmic shear measurements from, e.g., KiDS + VIKING-450 alone [61] and with DES [62,63], as well as the new cosmic shear and galaxy clustering results from KIDS-1000 [64,65], although note some analyses find a larger value for  $S_8$  that is closer to Planck, e.g., KiDS-450 +GAMA [66], HSC SSP [67], and DES-Y3 [68]. This tension is not as severe as that of the Hubble tension, but it behooves us to keep it in mind when searching for solutions to the latter, as many natural solutions to the Hubble tension (e.g., simply increasing the amount of free-streaming relativistic species in the early Universe) will worsen the aforementioned tension, thereby making those models not viable candidates for alleviating the Hubble tension.

These tensions between cosmological datasets have led to a number of models being proposed to resolve or alleviate one or both of them. Examples of these include the introduction of extra dark radiation coupled to dark matter [69–74], which has the potential to alleviate both tensions, a phase of so-called early dark energy [75], which can largely solve the Hubble tension (but may worsen the discrepancy related to the amplitude of matter fluctuations [76–78], although attempts are being made to develop similar models that avoid this problem; see, e.g., Refs. [79–81]), and sterile neutrino secret interactions [17,82–84]. Notably, the introduction of self-interactions between active neutrinos and extra relativistic species has been posited as a way to alleviate both tensions [33], which is a topic we attempt to address in this work.

Finally, before proceeding, we will mention two closely related papers that were recently posted. Reference [39] uses CMB, BAO, and  $f\sigma_8$  data to constrain self-interacting neutrinos, primarily in cases where a fixed number of neutrino states self-interact (one, two, or three neutrino states) for a fixed  $N_{\rm eff}=3.046$  and assuming massless neutrinos. The analysis in Ref. [40] considers all species of neutrinos to be self-interacting and varying both  $N_{\rm eff}$  and  $\sum m$ , matching our case 1. The particular dataset combinations in Ref. [40] differ somewhat from our choices

(for instance, we always include CMB lensing in our analyses). Despite this, our results for case 1 are in qualitative agreement.

This paper is organized as follows. In Sec. II, we review self-interacting neutrinos using the example of an interaction mediated by a Majoron and present relationships between the Majoran-neutrino coupling, effective neutrino self-interaction parameters, and the associated redshift at which neutrino self-interactions will decouple. We also review experimental constrains on neutrino interactions. In Sec. III, we describe our phenomenological parametrization of self-interacting neutrinos, which builds on Ref. [43] and how this is implemented in the CLASS code [85] and illustrate the changes to CMB temperature, polarization, and lensing power spectra induced by a self-interacting neutrino component. In Sec. IV, we present our analysis method and choice of datasets. The results of our analyses are presented in Sec. V. Conclusions are presented in Sec. VI. Details of the computation of neutrino opacity functions discussed in Sec. II are given in Appendix A. A study of the sensitivity of our analyses to the assumed duration of neutrino decoupling is in Appendix B. Complete parameter constraints plots for all scenarios are given in Appendix C.

#### II. SELF-INTERACTING NEUTRINOS

In this section, we review self-interacting neutrinos using the example of an interaction mediated via a massive scalar  $\phi$ , called the Majoron, the Goldstone boson associated with spontaneous breaking of neutrino flavor symmetry [86,87]. Our goal here is to connect the neutrino interaction parameters with the redshift and duration of neutrino decoupling, which impact the CMB power spectra. The Lagrangian for the Majoron reads

$$\mathcal{L} = \frac{1}{2} \partial_{\mu} \phi \partial^{\mu} \phi - \frac{1}{2} m_{\phi}^2 \phi^2 + \frac{1}{2} g_{ij} \bar{\nu}_i \nu_j \phi, \tag{1}$$

where  $m_{\phi}$  is the Majoron mass,  $\nu_i$  is a mass eigenstate of neutrinos, and  $g_{ij}$  are the coupling constants between neutrinos and the Majoron. We assume interactions among mass eigenstates so that when we study interactions among only a fraction of the mass eigenstates the number of interacting neutrinos is not changed by neutrino oscillations. We assume neutrinos are Majorana fermions because the Dirac neutrino case is widely constrained from  $\Delta N_{\rm eff}$  during BBN [47]. For simplicity, we choose a diagonal and universal coupling,  $g_{ij} \equiv g_{\phi} \delta_{ij}$ . Neutrinos can interact with each other by exchanging the Majoron, and the effective Lagrangian for neutrino self-interaction with a heavy enough  $\phi$  can be written as [88]

$$\mathcal{L} = \frac{1}{8} G_{\nu} \bar{\nu}_i \nu_i \bar{\nu}_j \nu_j, \tag{2}$$

where  $G_{\nu} \equiv g_{\phi}^2/m_{\phi}^2$ . If  $G_{\nu} \gg G_F$ , neutrinos continue to interact with each other even after they decouple from the Standard Model thermal bath at  $T \sim 2$  MeV.

#### A. Decoupling of neutrino self-interactions

The neutrino self-interaction rate drops as the Universe expands and the number density of neutrino decreases, eventually ceasing entirely. We define the decoupling redshift  $z_{\rm dec}$ , as the redshift when neutrinos decouple from self-interactions (more concretely, when the neutrino opacity drops to 1/2). The decoupling occurs roughly at  $\Gamma_{\nu} \sim H$ , where the  $\Gamma_{\nu}$  is the neutrino self-interaction rate and H is the Hubble parameter. From dimensional analysis, one finds  $\Gamma_{\nu} \sim G_{\nu}^2 T^5$  and  $H \sim T^2/m_{pl}$ , which gives  $z_{\rm dec} \sim (G_{\nu}^2 T_0^3 m_{pl})^{-1/3}$ , where  $T_0$  is the CMB temperature today and  $m_{pl}$  is the Planck mass. As we shall see, this estimate gives a correct  $z_{\rm dec}$  up to an  $\mathcal{O}(1)$  factor.

We will now study  $z_{\rm dec}$  in more detail. The exact form of  $\Gamma_{\nu}$  for a neutrino  $\nu_i$  with energy  $E_1$  for the process  $\nu_i(p_1) + \nu_i(p_2) \rightarrow \nu_k(p_3) + \nu_l(p_4)$  is

$$\Gamma_{\nu}(E_{1}) = \frac{1}{2E_{1}} \int d\Pi_{2} d\Pi_{3} d\Pi_{4} f_{\nu}(E_{2})$$

$$\times (1 - f_{\nu}(E_{3}))(1 - f_{\nu}(E_{4})) |\mathcal{M}|^{2} (2\pi)^{4} \delta^{(4)}$$

$$\times (p_{1} + p_{2} - p_{3} - p_{4}), \tag{3}$$

where  $d\Pi_i = \frac{g_\nu d^3 p_i}{(2\pi)^3 2E_i}$  with the spin degeneracy  $g_\nu = 2$ ,  $f_\nu(E) = \frac{1}{\exp(E/T_\nu)+1}$  is the Fermi-Dirac distribution, and  $|\mathcal{M}|^2$  is the spin-averaged matrix element of the process, which is

$$|\mathcal{M}_{\nu\nu\to\nu\nu}|^2 = \frac{1}{2} |\mathcal{M}_{\nu_i\nu_i\to\nu_i\nu_i}|^2 + \frac{1}{2} \times 2|\mathcal{M}_{\nu_i\nu_i\to\nu_j\nu_j}|^2 + 2|\mathcal{M}_{\nu_i\nu_i\to\nu_i\nu_j}|^2, \tag{4}$$

where

$$|\mathcal{M}_{\nu_i \nu_i \to \nu_i \nu_i}|^2 = G_{\nu}^2 (s^2 + st + t^2),$$
 (5)

$$|\mathcal{M}_{\nu_i \nu_i \to \nu_j \nu_j}|^2 = G_{\nu}^2 s^2 \quad (i \neq j), \tag{6}$$

$$|\mathcal{M}_{\nu_i \nu_i \to \nu_i \nu_i}|^2 = G_{\nu}^2 t^2 \quad (i \neq j). \tag{7}$$

Here,  $s=(p_1+p_2)^2$  and  $t=(p_3-p_1)^2$  are Mandelstam variables, and the factor of  $\frac{1}{2}$  in the first and the second terms in Eq. (4) accounts for the symmetric factor for identical outgoing particles. Note that, since we are discussing neutrino scattering at  $T\gg m_{\nu}$ , we ignore neutrino masses throughout this section. If we ignore the Pauli-blocking factors  $(1-f_{\nu})$ ,  $\Gamma_{\nu}$  reduces to

$$\Gamma_{\nu}(E_1) = \int \frac{d^3 p_2}{(2\pi)^3} g_{\nu} f_{\nu}(E_2) \frac{s}{2E_1 E_2} \sigma_{\nu\nu \to \nu\nu}$$
 (8)

$$=\frac{35\pi}{1728}G_{\nu}^{2}E_{1}T_{\nu}^{4},\tag{9}$$

where  $\sigma_{\nu\nu\to\nu\nu}=\int d\cos\theta_{\rm CM}\,\frac{|\mathcal{M}_{\nu\to\nu\nu}|^2}{32\pi s}$  is the neutrino self-interaction cross section and  $\theta_{\rm CM}$  is the angle between incoming and outgoing particles in the center-of-momentum frame. Neglecting the Pauli blocking factors gives  $\mathcal{O}(10\%)$  errors on the rate, but we have checked this does not change the results of our computations of  $z_{\rm dec}$  significantly. This is discussed further in Appendix A.

Now, we define the neutrino opacity function for scattering rate  $\Gamma_{\nu}(E_1)$  as

$$O(T, E_1) = 1 - \exp\left[-\int_{t(T)}^{t_0} \Gamma_{\nu} dt\right],$$
 (10)

$$= 1 - \exp\left[-\int_{T_0}^T \frac{\Gamma_{\nu}}{H(T')T'} dT'\right]. \tag{11}$$

In this expression, T is the temperature of the photon bath, and H(T) is the Hubble parameter at temperature T. We take the neutrino temperature to be  $T_{\nu} = (\frac{4}{11})^{1/3}T$ . The opacity function averaged over neutrino energies is

$$\langle O(T) \rangle = \frac{1}{n_{\nu}} \int \frac{d^3 p_1}{(2\pi)^3} g_{\nu} f_{\nu}(E_1) O(T, E_1),$$
 (12)

where  $n_{\nu}=\frac{3\zeta(3)}{2\pi^2}T_{\nu}^3$  is the number density of each neutrino species.

To find the decoupling redshift  $z_{\rm dec}$ , we fit the opacity function in terms of the redshift  $O_z(z) = \langle O((1+z)T_0) \rangle$  to the transition function from [43],

$$\mathcal{T}(z) = \frac{1}{2} \left( \tanh \left( \frac{z - z_{\text{dec}}}{\Delta z_{\text{dec}}} \right) + 1 \right). \tag{13}$$

We show the decoupling redshifts in terms of  $G_{\nu}$  in Fig. 1. In Fig. 1, we also show the results for the case of partially interacting neutrinos as uniform couplings for neutrino self-interactions are widely constrained by terrestrial experiments, yet these constraints can be weakened by assuming only certain species of neutrinos are self-interacting [47] (see Sec. II B for more detail). The amplitudes for one and two interacting neutrino species are

$$|\mathcal{M}_{\nu\nu\to\nu\nu}^{1-\text{int}}|^2 = \frac{1}{2} |\mathcal{M}_{\nu_i\nu_i\to\nu_i\nu_i}|^2, \tag{14}$$

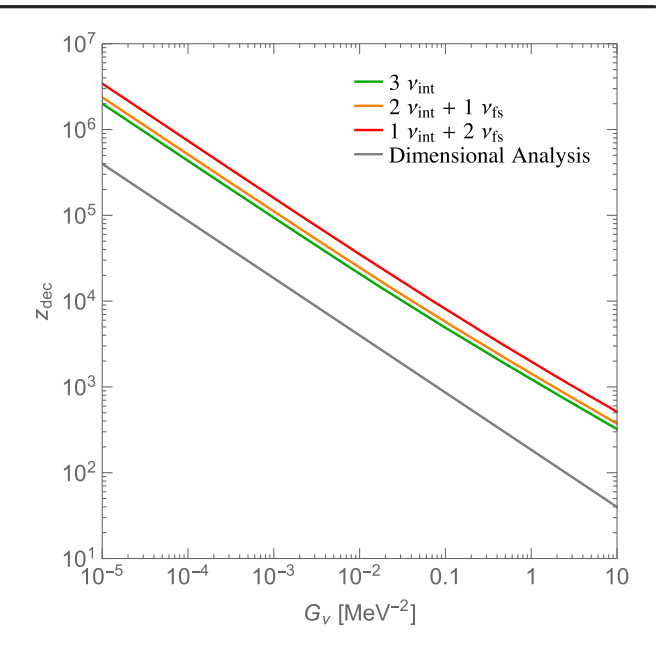


FIG. 1. The relationship between the redshift of neutrino decoupling,  $z_{\rm dec}$ , and the effective neutrino self-interaction strength  $G_{\nu}$ . Plotted is the relationship for different numbers of interacting neutrino species. The red, orange, and green lines correspond to one, two, and three self-interacting neutrino species, respectively. The gray line is result from dimensional analysis,  $z_{\rm dec} \sim (G_{\nu}^2 T_0^3 m_{pl})^{-1/3}$ .

$$|\mathcal{M}_{\nu\nu\to\nu\nu}^{2-\text{int}}|^2 = \frac{1}{2} |\mathcal{M}_{\nu_i\nu_i\to\nu_i\nu_i}|^2 + \frac{1}{2} |\mathcal{M}_{\nu_i\nu_i\to\nu_j\nu_j}|^2 + |\mathcal{M}_{\nu_i\nu_j\to\nu_i\nu_j}|^2.$$
(15)

And the scattering rates are

$$\Gamma_{\nu}^{1-\text{int}}(E_1) = \frac{7\pi}{1728} G_{\nu}^2 E_1 T_{\nu}^4, \tag{16}$$

$$\Gamma_{\nu}^{2-\text{int}}(E_1) = \frac{7\pi}{576} G_{\nu}^2 E_1 T_{\nu}^4. \tag{17}$$

Note that neutrino oscillation does not change the number of interacting neutrino species since we assume diagonal couplings in the mass eigenstates.

We find  $\Delta z_{\rm dec} \sim 0.4 z_{\rm dec}$  is a good description of the Majoron case. See Appendix A for comparison with the actual opacity function. This is a generic feature of decoupling from a dimension-6 operator with the number density of particles changing only from the expansion. Precise values for  $\Delta z_{\rm dec}$  vary with  $z_{\rm dec}$ , but we have checked that this approximation is enough for the purpose of the work. A study of the (in)sensitivity of our results to the assumed decoupling width is presented in Appendix B.

<sup>&</sup>lt;sup>1</sup>We assume the scale factor is inversely proportional to the temperature to get Eq. (11) from Eq. (10), so Eq. (11) is only exact for temperatures after electron-positron annihilations.

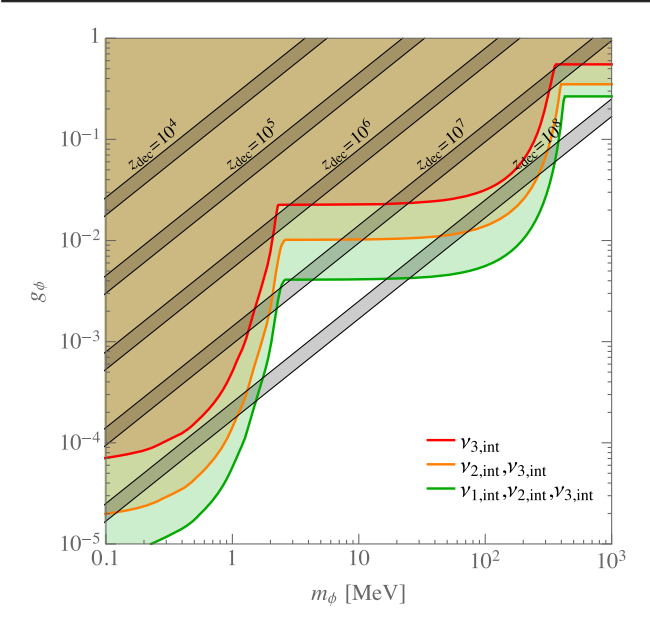


FIG. 2. Experimental constraints for the Majoron coupled to neutrino mass eigenstates in the  $g_{\phi}-m_{\phi}$  plane translated from the constraints on the coupling to neutrino flavor eigenstates in Ref. [47]. We show these constraints translated under different assumptions about the number of interacting neutrinos. The gray bands show different values of  $z_{\rm dec}$  in this parameter space with the upper lines of the bands corresponding to the one-interacting-neutrino case and the lower lines corresponding to the three-interacting-neutrinos case.

### B. Experimental constraints on neutrino self-interactions

Experimental constraints on neutrino self-interactions have been studied in previous works [47,88-92], and we review most relevant constraints on the model with the Majoron, mostly following Ref. [47].<sup>2</sup> Reference [47] discusses the experimental constraints on the coupling between the Majoron and the neutrino flavor eigenstates. The strongest constraints on the coupling to  $\nu_e$  come from kaon decay ( $K \rightarrow e\nu\phi$ ) and neutrinoless double-beta decay, while the coupling to  $\nu_{\mu}$  is constrained from kaon decay to muon  $(K \to \mu\nu\phi)$  and coupling to  $\nu_{\tau}$  from  $\tau$  decay  $(\tau \to \ell \nu \nu \phi)$ . In this work, we consider the Majoron coupling to be diagonal to the neutrino mass eigenstates instead of neutrino flavor eigenstates as in Ref. [47], and we translate the constraints with the Pontecorvo-Maki-Nakagawa-Sakata (PMNS) matrix, where we take the values in the PMNS matrix from Ref. [93].

The Majoron couplings to mass eigenstates can be converted to couplings to flavor eigenstates with the PMNS matrix U by

$$g_{\alpha\beta} = U_{\alpha i} g_{ij} (U^{\dagger})_{i\beta}. \tag{18}$$

For the all-interacting-neutrinos case (our case 1) where the Majoron couplings to neutrino mass eigenstates are diagonal and universal,  $g_{ij} = g_{\phi} \delta_{ij}$ , we have  $g_{ij} = g_{\alpha\beta}$ ; hence, the constraints on  $g_{\phi}$  are the same as the universal case in Ref. [47]. For partially interacting cases (our cases 2–4), we calculate  $g_{\alpha\beta}$  in terms of  $g_{\phi}$  and demand that each component obeys the constraints in  $g_{\alpha\beta}$ . We show the results in Fig. 2. For partially interacting neutrinos, we choose the cases that are minimally constrained. Since  $\nu_{\tau}$ is the least-constrained flavor eigenstate, choosing the mass eigenstates that contain more  $\nu_{\tau}$  gives the desired combination. As a result, we consider  $\nu_3$  for one interacting neutrino and  $\nu_2$  and  $\nu_3$  for two interacting neutrinos. As we shall see, current CMB data are only able to probe neutrino decoupling that occurs at redshifts below  $z_{\rm dec} \lesssim 10^6$ , so Fig. 2 demonstrates that laboratory constraints on new neutrino interactions are stronger than CMB constraints, with the possible exception of interactions mediated exclusively through  $\nu_3$ .

### III. PARAMETRIZATION, IMPLEMENTATION, AND EFFECT ON CMB POWER SPECTRA

To model the impact of self-interacting neutrinos on CMB observables, we extend the decoupling redshift approach of Ref. [43]. Neutrino self-interactions have the effect of suppressing higher moments of the Boltzmann hierarchy (i.e., moments of the perturbation to the neutrino distribution function,  $F_{\nu,\ell}$ , are suppressed for  $\ell > 2$ ), causing neutrino perturbations to evolve as a relativistic fluid. After decoupling, neutrinos free-stream, allowing the higher moments of the Boltzmann hierarchy to take nonzero values. The transition between these two epochs is imposed manually with the transition function in Eq. (13). In this paper, we extend the implementation in Ref. [43] to allow for massive self-interacting species in combination with ordinary, massive, free-streaming neutrinos. Where Ref. [43] considers a near-instantaneous decoupling width  $\Delta z_{\rm dec} = 0.01 z_{\rm dec}$ , we approximately match the opacity function for the case of neutrino decoupling with the Majoron as stated in Sec. II, which is closer to  $\Delta z_{\rm dec} = 0.4 z_{\rm dec}$ . This approach also gives CMB power spectra that are in excellent agreement with those in Refs. [31–33,94], and, as shown in Appendix B, our final results are relatively insensitive to the precise value of  $\Delta z_{\rm dec}$  for  $\Delta z_{\rm dec}/z_{\rm dec}$  in the range [0.1, 0.8].

#### A. Parametrization

As usual, the radiation density in the early Universe is parametrized by

$$\rho_{\rm rad}(T \lesssim 1 \text{ MeV}) = \rho_{\gamma} \left[ 1 + \frac{7}{8} \left( \frac{4}{11} \right)^{4/3} N_{\rm eff} \right], (19)$$

<sup>&</sup>lt;sup>2</sup>Note that we ignore terms from the UV completion considered in Ref. [88]. As pointed out in Ref. [47], UV completion of self-interacting neutrinos cannot be a minimal seesaw mechanism but needs separate seesaw mechanisms for the neutrino masses and the Majoron coupling.

where  $\rho_{\gamma}=(\pi^2/15)T_{\gamma}^4$  is the energy density in CMB photons and  $T_{\gamma}=2.725K$  today (see, e.g., Ref. [30]). With this definition,  $N_{\rm eff}=3$  corresponds to the radiation energy density expected from three Standard Model neutrinos that decouple instantaneously. In the standard cosmology,  $N_{\rm eff}\approx 3.046$ , due to residual heating of neutrinos from electron-positron annihilation [95–107].

We further split the  $N_{\rm eff}$  parameter into two components:  $N_{\rm eff,fs}$ , the effective number of free-streaming relativistic species, and  $N_{\rm eff,int}$ , the effective number of interacting relativistic species. The total energy in relativistic species is then given by

$$N_{\rm eff} = N_{\rm eff,fs} + N_{\rm eff,int} \tag{20}$$

the interacting species  $N_{\rm eff,int}$  is assumed to decouple at a redshift  $z_{\rm dec}$  with a duration  $\Delta z_{\rm dec}$  that is fixed to  $\Delta z_{\rm dec} = 0.4 z_{\rm dec}$  (see Sec. II and Appendix B). The effective mass of all species is given by  $\sum m = \sum_i N_{{\rm eff},i} \times m_i$ . We will always use the degenerate neutrino mass approximation where all interacting or free-streaming species are presumed to have the same mass.<sup>3</sup>

In this paper, we will consider four cases of parameter choices, designed to mimic different scenarios for interacting neutrinos:

- (i) Case 1: All species interacting.—In this example, all neutrino species are presumed to participate in the new self-interactions, which decouple at  $z_{\rm dec}$ , a free parameter. The total energy in self-interacting neutrinos,  $N_{\rm eff,int}$ , and the masses of self-interacting neutrinos are both allowed to vary. This is implemented by allowing variable  $N_{\rm eff,int}$ ,  $z_{\rm dec}$ , and  $\sum m$  with  $N_{\rm eff,fs} = 0$ .
- (ii) Case 2: Two free-streaming species plus interacting species.—In this example, we force two neutrino states to be free-streaming, as a way to account for laboratory constraints on new neutrino self-interactions (see Sec. II B). This is implemented by fixing  $N_{\rm eff,fs} = 2$  and allowing the additional interacting relativistic degrees of freedom, characterized by  $N_{\rm eff,int}$  to vary. We assume  $N_{\rm eff,fs}$  degrees of freedom are massless and the masses of  $N_{\rm eff,int}$  are  $\sum m/N_{\rm eff,int}$ .
- (iii) Case 3: Fixed number of relativistic species and varying fraction of interacting species.—In this example, we fix the number of relativistic species to  $N_{\rm eff} = 3.046$ , but vary the fraction that is self-interacting. The mass sum of all relativistic species is

<sup>3</sup>This has been shown to be sufficiently accurate for all current and most future cosmological analyses, see e.g., [108–111].

- also allowed to vary. This is implemented by allowing variable  $N_{\rm eff,int}$ ,  $z_{\rm dec}$ , and  $\sum m$  while fixing  $N_{\rm eff} = N_{\rm eff,fs} + N_{\rm eff,int} = 3.046$ .
- (iv) Case 4: Varying fraction of interacting species.— Finally, we consider an example where both the free-streaming and self-interacting degrees of freedom are allowed to vary. This is implemented by allowing variable  $N_{\rm eff,int}$ ,  $N_{\rm eff,fs}$ , and  $z_{\rm dec}$ . This is equivalent to treating the total relativistic degrees of freedom  $(N_{\rm eff}=N_{\rm eff,int}+N_{\rm eff,fs})$  as a free parameter, as well as the interacting fraction. For simplicity, in this case, we fixed to  $\sum m=0.11$  eV, by setting the individual mass of the interacting and the free-streaming species to  $\sum m/N_{\rm eff}$ .
- (v) Reference cosmologies.—We have one reference cosmology per case, which uses a standard implementation of variable  $N_{\rm eff}$ , where all degrees of freedom contributing to  $N_{\rm eff}$  are free-streaming. Masses are arranged as in cases 1–4 (i.e., for case 4 all relativistic species are massless, for cases 1 and 3, all species are massive; and for case 2, only species in excess of  $N_{\rm eff}=2.0328$  are massive). In either cases with a massive relativistic species, the mass is characterized by  $\sum m$ . Specifically, we allow variable  $N_{\rm eff,fs}$  (except reference case 3) and  $\sum m$  (except reference case 4) and fix  $N_{\rm eff,int}=0$ .

For cases 2, 3, and 4, we also study the pure fluidlike limit, equivalent to setting  $z_{\rm dec}$  to a value in the future so that  $N_{\rm eff,int}$  remains interacting through today. Case 1 is analogous to that considered in Ref. [33], with the exception that we treat the neutrinos as having degenerate masses, rather than putting all the mass associated with  $\sum m_{\nu}$  into a single mass state.

#### **B.** Implementation in class

We generalize the implementation of a decoupling non-cold-dark-matter species from Ref. [43] by modifying CLASS2.7 to add a new species DDEC, which is similar to the existing NCDM species. This separation allows us to control all aspects of the DDEC species, while maintaining the current implementation of the NCDM species, and allows for flexible computation options with both active (or sterile) neutrinos and/or a new class of self-interacting species, each with their own precision parameters and settings. We verified that the implementation is still valid when considering massive species and a wider decoupling width, tuning the precision parameters where needed. The neutrino self-interaction is added as a function modifying the

<sup>&</sup>lt;sup>4</sup>Technically, because of the way CLASS computes  $N_{\rm eff}$  we set the number of extra free-streaming species to  $N_{\rm eff,fs}=2.0328$  so that we get  $N_{\rm eff}=3.046$  if we add exactly one massive extra relativistic species.

<sup>&</sup>lt;sup>5</sup>Since Ref. [43] only considered massless species and instantaneous decoupling.

<sup>&</sup>lt;sup>6</sup>This primarily involves turning off the fluid approximation and increasing the precision requirements for the other DDEC precision parameters (which match the NCDM ones); see Appendix D for details.

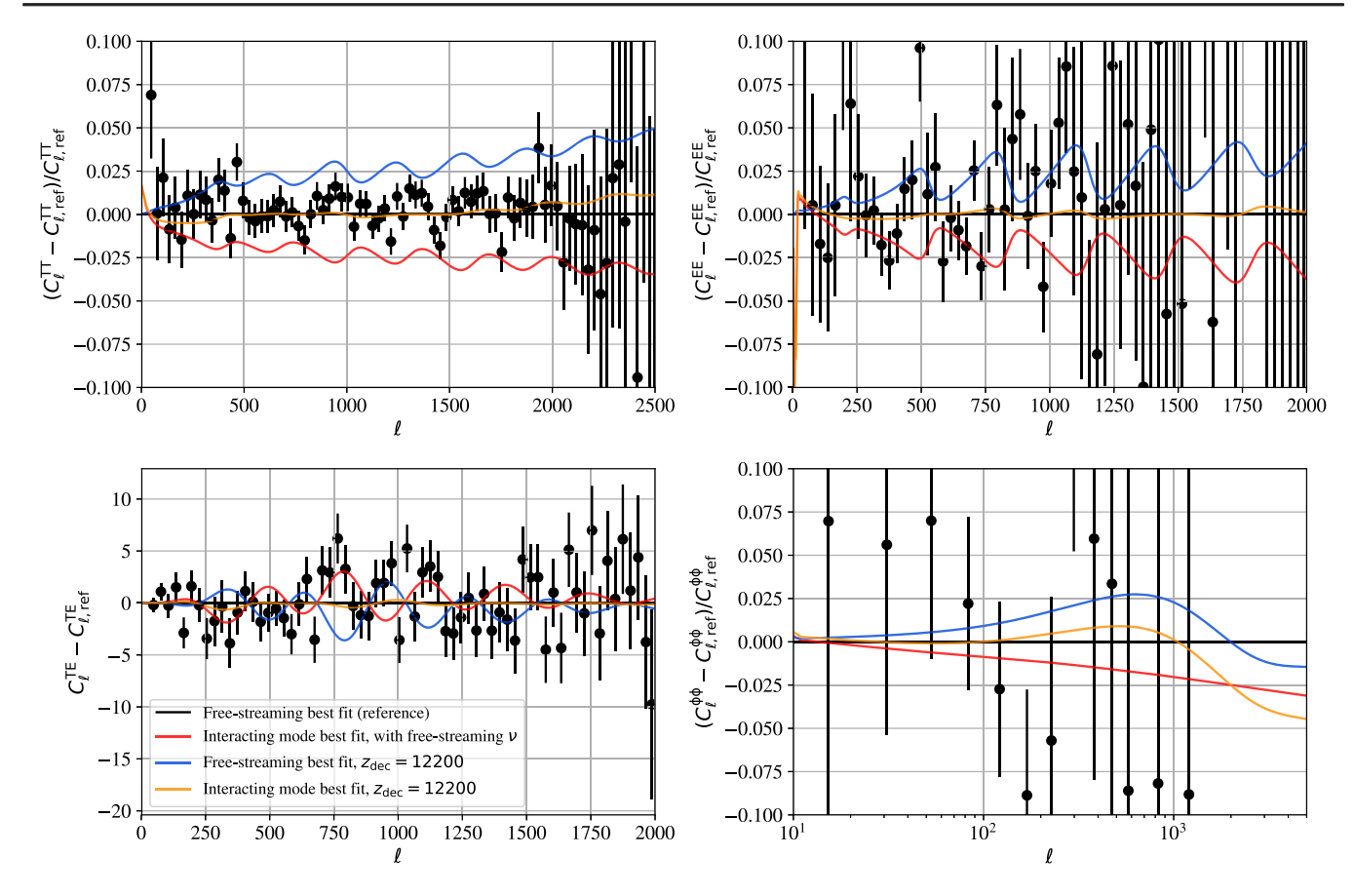


FIG. 3. Fractional differences between CMB temperature (top left) and polarization (top right) autocorrelation and cross-correlation (bottom left, showing difference rather than fractional difference) angular power spectra and the CMB lensing power spectrum (bottom right). In all panels, the Planck 2018 binned data [113,114] are shown in black, for comparison. Fractional differences are computed with respect to a best-fit free-streaming neutrinos comparison case. The orange curves show power spectra in a model with both free-streaming and self-interacting neutrinos (case 2), computed at the best-fit cosmological parameters for that model with a decoupling redshift of  $z_{\rm dec} = 12,200$ . In red, the same cosmological parameters are assumed as for the orange curve, but the power spectra are computed assuming only free-streaming neutrinos. In blue, the power spectra are computed in a cosmology with interacting neutrinos assuming  $z_{\rm dec} = 12,200$  using the best-fit cosmological parameters for the free-streaming reference case. See Sec. III A for a description of the reference and interacting neutrino models and Table IV (P18 + lens + BAO) for the precise parameter choices.

Boltzmann hierarchy, so the species behaves as a perfect fluid prior to decoupling and is free-streaming after decoupling, with some intermediate region defined by the decoupling width. For this work, we define the decoupling width as 40% of the decoupling redshift,  $\Delta z_{\rm dec} = 0.4 z_{\rm dec}$ , since we find this to be a good approximation for an effective self-interaction (see Sec. II). In Appendix B, we discuss how this choice affects bounds on the time of decoupling.

#### C. Effects on CMB power spectra

Let us now review the effects of neutrino self-interactions on CMB power spectra. Neutrino self-interactions qualitatively change the evolution of neutrino perturbations. Perturbations in free-streaming neutrinos propagate at the speed of light c, while perturbations in a relativistic fluid of self-interacting neutrinos propagate at smaller speed

 $c_s \approx c/\sqrt{3}$ . This difference leads to changes in the phase and amplitude of acoustic oscillations in the photon-baryon fluid in the early Universe (see, e.g., Refs. [4,42,43,112]). In what follows, we illustrate the changes to the CMB power spectra caused by neutrino self-interactions that decouple at different epochs, using example parameter choices from our results in Sec. V, paying particular attention to how these changes can be mimicked by changing other cosmological parameters.

In Fig. 3, we show the effect of neutrino self-interactions on the CMB temperature and polarization autocorrelation  $(C_\ell^{TT}, C_\ell^{EE})$  and cross-correlation  $(C_\ell^{TE})$  angular power spectra and the CMB lensing power spectrum  $(C_\ell^{\phi\phi})$ . We compare power spectra computed assuming different cosmologies with either free-streaming or a combination of free-streaming and self-interacting neutrinos (e.g., case 2 from Sec. III A). The reference ("ref") cosmology is the

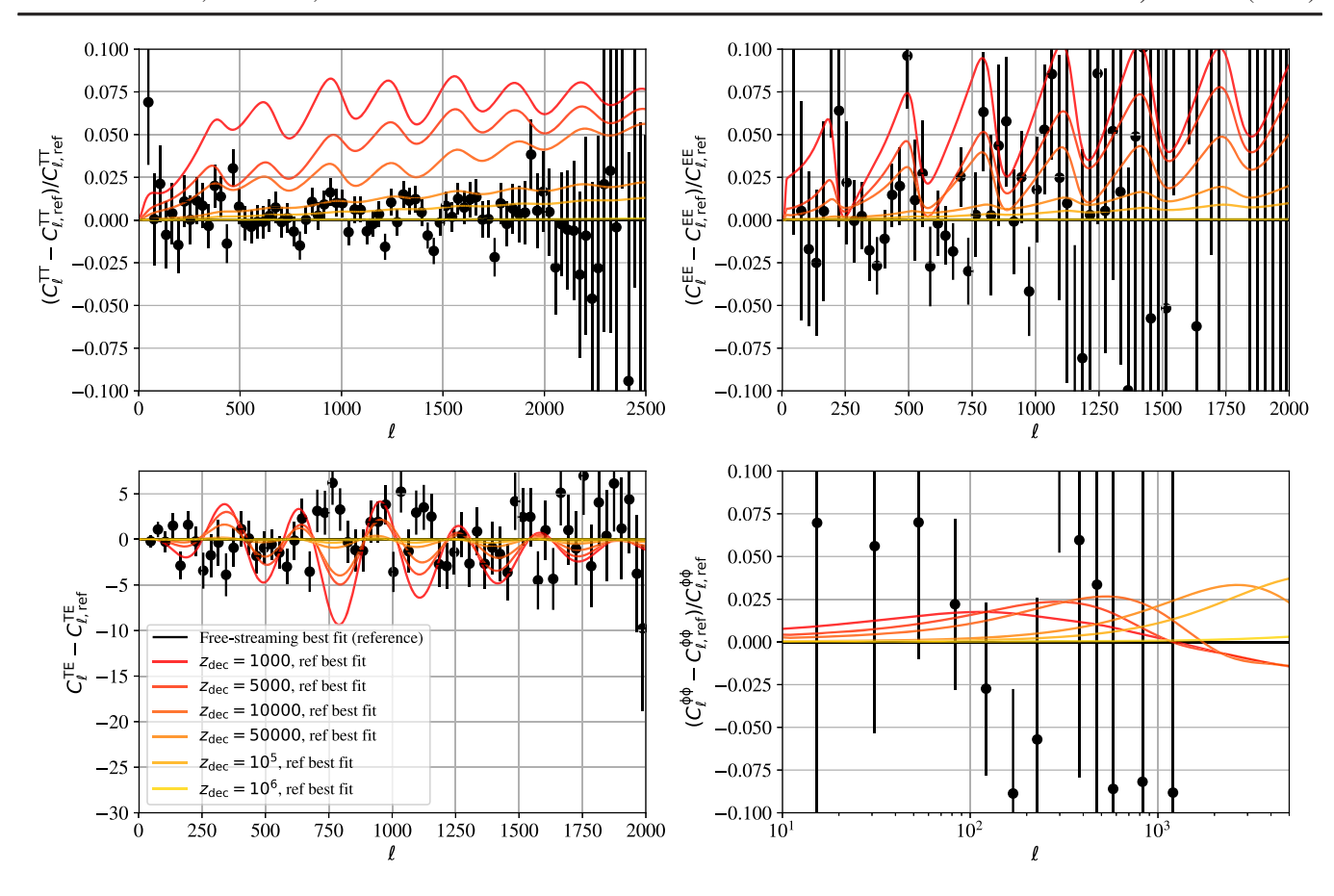


FIG. 4. Fractional differences between the CMB power spectra computed in a model with self-interacting and free-streaming neutrinos (case 2; see Sec. III A), as compared to a model with only free-streaming neutrinos. Each curve shows a different assumed value of  $z_{\rm dec}$ , with all other parameters held fixed. Shown are CMB temperature (top left) and polarization (top right) autocorrelation and cross-correlation (bottom left, showing difference rather than fractional difference) angular power spectra and the CMB lensing power spectrum (bottom right). In all panels, the Planck 2018 binned data [113,114] are shown in black, for comparison.

best-fit parameters assuming a free  $N_{\rm eff}$ , all free-streaming  $(\Lambda CDM + \nu_{fs}; \text{ see } P18 + \text{lens} + BAO \text{ on Table IV for}$ the precise parameter values). In orange, we show the best fit of a  $\Lambda$ CDM +  $\nu_{fs}$  +  $\nu_{int}$  case (case 2 in Sec. III A above) for  $z_{\text{dec}} = 12,200$  (the low-z decoupling mode discussed later in Sec. VB). In red, we show the power spectra for a free-streaming cosmology but computed using the best-fit cosmological parameters for the interacting scenario (including the total  $N_{\rm eff}$  value). In blue, we show the converse: the power spectra for an interacting neutrino cosmology with  $z_{dec} = 12,200$  but computed using the best-fit parameters from the free-streaming comparison case. In all panels, the Planck 2018 binned data [113,114] are shown in black, for comparison. As was noted in Refs. [32,33], a significant change in cosmological parameters is nearly offset by changing the decoupling redshift (or equivalently, neutrino interaction strength),  $z_{dec}$ . This is illustrated by the orange curve, which is also approximately the sum of the blue and red curves, where for most scales the difference compared to the free-streaming comparison case is subpercent, with percent-level differences at very small scales (high multipole,  $\ell$ ).

In Fig. 4, we isolate the effect of varying the decoupling redshift  $z_{\rm dec}$ , holding all other parameters fixed to the best-fit free-streaming ( $\Lambda {\rm CDM} + \nu_{\rm fs}$ ) comparison case (ref). We can see that varying  $z_{\rm dec}$  does not just shift the phase and overall amplitude of the acoustic peaks but introduces more subtle changes, depending on the value of  $z_{\rm dec}$ :

- (i) The amplitude always increases across all scales with lower  $z_{\rm dec}$ , but not in a scale-independent way (this is easier to see in the  $C_\ell^{TT}$  plot, but the effect persists in the  $C_\ell^{EE}$  plot).
- (ii) Going from later decoupling redshifts to earlier, between  $z_{\rm dec} = 10{,}000$  and  $z_{\rm dec} = 1000$ , we see that at higher values the spectra experience a fairly regular scale-dependent amplitude shift roughly corresponding to a larger effect with smaller  $z_{\rm dec}$ , but at low  $z_{\rm dec}$  values, it is not this simple.
- (iii) At  $\ell > 800$ , the amplitude increases across all scales in roughly the same way as between  $z_{\rm dec} = 1000$  and  $z_{\rm dec} = 10,000$ , except for a small change of the damping tail, where the amplitude increases more slowly with lower  $z_{\rm dec}$  and goes from increasing with

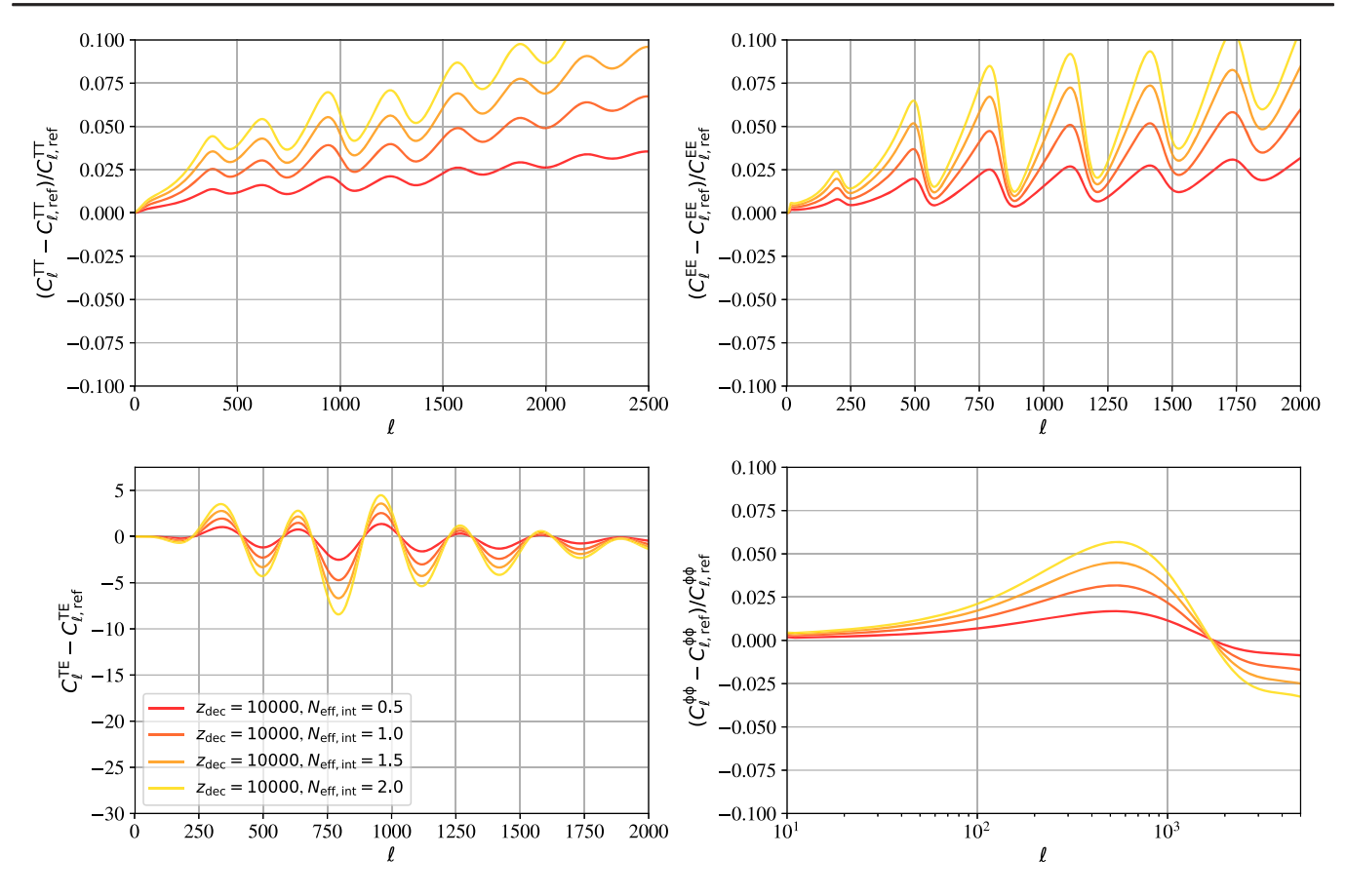


FIG. 5. The fractional differences between CMB power spectra computed in a scenario with a varying fraction of interacting neutrinos that decouple from self-interactions at  $z_{\rm dec}=10{,}000$ , as compared to those computed in a cosmology with the same total  $N_{\rm eff}$  comprised of all free-streaming neutrinos (all other parameters are also held fixed). Shown are the CMB temperature (top left) and polarization (top right) autocorrelation and cross-correlation (bottom left, showing difference rather than fractional difference) angular power spectra and the CMB lensing power spectrum (bottom right).

 $\ell$  in a scale-dependent way for  $z_{\text{dec}} = 10,000$  to a roughly flat amplitude increase at  $z_{\text{dec}} = 1000$ .

(iv) At  $\ell$  < 800, the amplitude increases steadily up until around  $z_{\rm dec} = 10{,}000$  and then barely changes through  $z_{\rm dec} = 5000$  before going back to changing in a regular way at  $z_{\rm dec} = 1000$ . This change coincides with the transition from radiation to matter domination.

Finally, in Fig. 5, we isolate the effect of varying the total  $N_{\rm eff,int}$  with fixed  $z_{\rm dec}=10{,}000$ , in comparison to a predictions for power spectra with the same total  $N_{\rm eff}$ . Precisely, we consider power spectra computed in a cosmology with two free-streaming massless neutrinos and variable amount of  $N_{\rm eff,int}$  ranging from  $N_{\rm eff,int}=0.5$  to  $N_{\rm eff,int}=2$ . We compare those power spectra to ones computed a cosmology with only free-streaming neutrinos with the same abundances set by  $N_{\rm eff,fs}=2+N_{\rm eff,int}$ , where  $N_{\rm eff,int}$  takes the same values ranging from 0.5 to 2. In this case, the binned Planck data are omitted. Since we do not use a universal reference case (with  $N_{\rm eff,fs}$  varying), the Planck residuals would get shifted for each

curve. From Fig. 5, we see that the overall shape for  $C_\ell^{TT}$  and  $C_\ell^{EE}$  is changed by increasing the self-interacting fraction. The fractional difference between the  $C_\ell^{TE}$  are very similar to that shown in the varying  $z_{\rm dec}$  plot. The changes to  $C_\ell^{\phi\phi}$  with varying interacting fraction are instead purely an amplitude shift with the same peak value and zero crossing point irrespective of  $N_{\rm eff,int}$ .

#### IV. METHOD AND DATASETS

For our analyses, we use the cosmological sampling package MontePython3.2<sup>7</sup> [115,116], interfaced with a modified version of the Boltzmann Solver CLASS2.7<sup>8</sup> [85,117,118] and with the MultiNest sampler [119–121] via the PyMultiNest wrapper [122] (see Appendix D for the MultiNest sampling settings used for the runs in this paper).

<sup>&</sup>lt;sup>7</sup>Get the new MontePython3.4 at https://github.com/brinckmann/montepython\_public.

<sup>&</sup>lt;sup>8</sup>Get the current CLASS2.9 at https://github.com/lesgourg/class\_public.

In the following, we use shorthand notation to refer to the following datasets:

- (i) P18: Planck 2018 CMB temperature and polarization auto- and cross-correlation, both high  $\ell$  and low  $\ell$  [113].
- (ii) TT: Planck 2018 CMB temperature autocorrelation, both high  $\ell$  and low  $\ell$  [113].
- (iii) lowEE: Planck 2018 CMB polarization autocorrelation, low  $\ell$  [113].
- (iv) lens: Planck 2018 CMB lensing [114].
- (v) BAO: Six-degree Field Galaxy Survey (6dFGS, z = 0.106) [123], Sloan Digital Sky Survey Data Release 7 Main Galaxy Sample (SDSS DR7 MGS, z = 0.15) [124], and Baryon Oscillation Spectroscopic Survey (BOSS DR12, z = 0.38, 0.51, 0.61) three redshift bin sample [125] (formerly the CMASS and LOWZ galaxy samples [126]).
- (vi) R19: Prior on the Hubble parameter today,  $H_0$ , from Riess *et al.* [51].

Note that we make use of the "lite" version of the Planck likelihoods in order to speed up the rate of convergence, as the full set of nuisance parameters is expected to have only a small effect on cosmological constraints for most models. Although not an ideal choice, the use of MultiNest requires we restrict the total number of parameters to make the analysis feasible, and we checked that the resulting bias is less than about  $0.2\sigma$  shifts in all parameters (with  $N_{\rm eff}$  biased toward lower values). We consider P18 + lens and P18 + lens + BAO as our baseline configurations (we always include lensing) but sometimes add R19 to explore whether the model in question helps alleviate the Hubble tension. We also consider the case without high- $\ell$ polarization with and without the R19 prior for the model with all neutrinos self-interacting, in order to compare to previous work.

# A. Discussion of tensions and analysis choices

Cosmology has seen a number of tensions between datasets grow in recent years, most notably the  $H_0$  and  $S_8$  tensions. Aside from the possibility of unresolved systematics, these tensions could arise from the assumption

of an incorrect model, as (nearly) all cosmological analyses assume a model to conduct the analysis. As a result, many works have striven to address this tension by changing assumptions within the cosmological model, e.g., on the nature of dark matter or dark energy. Before proceeding, we discuss our philosophy on exercising great caution when combining discrepant datasets when performing parameter inference analyses.

When combining two discrepant datasets, we will generally expect to find a result between the two measurements, e.g., between Planck CMB extrapolations of the  $H_0$  value and late-time cepheid calibrated supernovae measurements of the same. Note that this does not mean a model alleviates the tension, as it is merely a consequence of the statistical analysis. In cases where a model does not resolve (or at least significantly alleviate) the tension in question, a combination of discrepant datasets is not consistent, and these dataset combinations should be avoided (e.g., Refs. [128,129]).

In the following, we will test our models by combining datasets that are discrepant within ACDM, specifically by including a prior on the Hubble parameter from Riess et al. [51]. We evaluate whether the addition of an  $H_0$  prior appears to be reasonable, by comparing to a control case (a free-streaming only model) that does not help resolve the  $H_0$  tension (see, e.g., Ref. [133]) and for which, therefore, the combination of datasets is not consistent. In many cases, the analysis will show that our model does not help alleviate the  $H_0$  tension beyond what we find for the free-streaming control case. As such, the combination of discrepant datasets is suspect. We include these null results in order to further the discussion of which types of models work to resolve the tensions but also what does *not* work to resolve the  $H_0$ tension. In all cases, the validity of this combination for a particular model will always be discussed in the text.

#### V. RESULTS

In this section, we present the results of our analyses. As introduced in Sec. III A, we consider four scenarios for interacting neutrinos and a corresponding reference example with free-streaming neutrinos.

<sup>&</sup>lt;sup>9</sup>Note that, since neutrino self-interactions introduce a phase shift in the acoustic peaks, it is possible constraints using the standard BAO approach are biased. However, Ref. [127] studied the reliability of this approach when confronted with some beyond ACDM cosmologies, including a model with interactions between dark matter and neutrinos, which exhibit a similar phase shift. As such, for current data, the self-interacting neutrino model is unlikely to result in large biases from the BAO analysis, especially when BAO data are combined with other datasets, such as CMB data. However, for future data, it would be prudent to ideally analyze the BAO data consistently or at least to redo the analysis of Ref. [127] for the self-interacting neutrino case in question in order to ensure that any possible bias is sufficiently small.

 $<sup>^{10}</sup>$ Note that it was recently pointed out that, rather than including a prior on  $H_0$ , from, e.g., the SH0ES Collaboration [51], it is more appropriate to include the Pantheon supernovae sample [53] along with a prior on the absolute peak magnitude  $M_B$  from SH0ES [130–132] (see those works for details). While the authors would encourage doing so in the future irrespective of the cosmological model being studied (or indeed to not include a prior from a discrepant dataset at all, as discussed in this section), we stress that for a change to early-time cosmology, such as the self-interacting neutrinos studied in this work, the inferred value for  $H_0$  by SH0ES would be expected to correct (with all the usual caveats), and the use of a prior on  $H_0$  should not differ significantly from a prior on  $M_B$ . However, for models that change the late-time evolution of the Universe, correct use of the  $M_B$  prior is crucial.

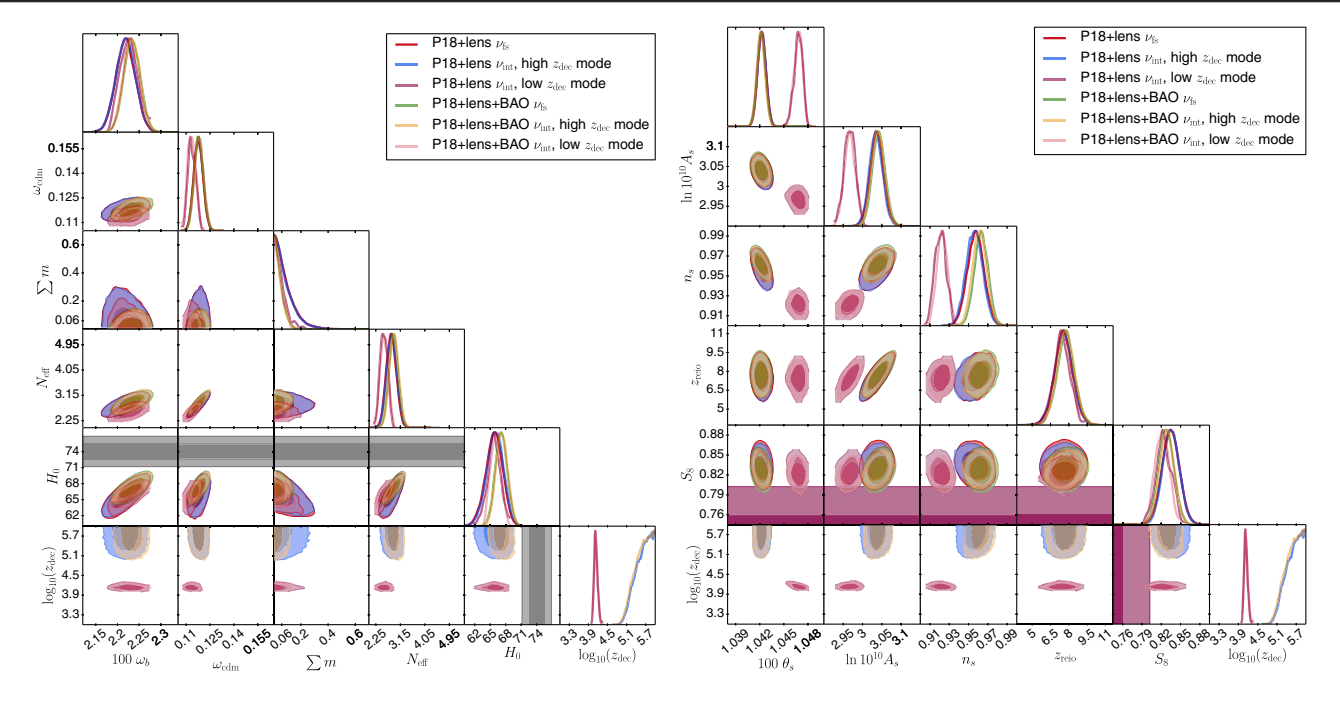


FIG. 6. Case 1: all species interacting. Plotted are parameter constraints from models with all free-streaming neutrinos (red and green) vs all species interacting separated into high- $z_{\rm dec}$  (blue and yellow) and low- $z_{\rm dec}$  modes (purple and pink) for Planck only (red, blue, and purple) and Planck + BAO (green, yellow, and pink). The gray bands correspond to the  $H_0$  measurement from Riess et~al.~[51], while the purple band is the  $S_8$  measurement from KiDS + VIKING-450 [134]. See Appendix C, Fig. 18 for the full parameter space plot. Left and right panels: both show the same cases, but different cosmological parameters. Left panel: energy density parameters. Right panel: power spectrum shape and amplitude parameters. Note that beyond  $z_{\rm dec} > 10^6$  the one-dimensional posterior flattens out and is very slowly increasing until a peak near standard neutrino decoupling. In several cases, it can be hard to see some contours as they are neatly overlapping, e.g., red and blue as well as green and yellow, which in these cases signify minimal difference between the free-streaming comparison case and the high- $z_{\rm dec}$  mode. The same is also true to a lesser degree for the two strongly interacting modes in purple and pink. This figure shows that enabling self-interactions for all neutrinos is not a solution to the Hubble tension when including all Planck primary anisotropies and lensing. This can be seen from the self-interacting cases closely overlapping with the free-streaming cases for  $H_0$  (left panel); i.e., there is no improvement over free-streaming neutrinos.

#### A. Case 1: All species interacting

#### 1. Baseline data configurations

To compare to Ref. [33], we include a case with all neutrinos interacting. Note that in our case the mass is distributed across all of the neutrino mass states in a degenerate mass hierarchy instead of one massive and the rest massless like in Ref. [33]. In this section, we present our baseline data configurations for case 1 (all species interacting), consisting of Planck primary anisotropies plus lensing, alone and with BAO data (see Fig. 6). Additionally, we add a prior corresponding to the Hubble constant measurement from Riess *et al.* [51], in order to see if this decoupling model alleviates the Hubble tension and whether this data combination is reasonable for this decoupling model (see Fig. 7).

In this section, we refer to these figures, datasets, and configurations:

(i) Figure 6. P18 + lens Red (all free-streaming), blue (all interacting, high- $z_{\rm dec}$  mode), and purple (all interacting, low  $z_{\rm dec}$  mode).

- (ii) Figure 6. P18 + lens + BAO. Green (all free-streaming), yellow (all interacting, high- $z_{\rm dec}$  mode), and pink (all interacting, low  $z_{\rm dec}$  mode).
- (iii) Figure 7. P18 + lens + BAO + R19. Light green (all free-streaming) and cyan (all interacting).
- (iv) Figure 8. TT + lowEE + lens + BAO (no high- $\ell$  polarization). Red (all free-streaming) and blue (all interacting).
- (v) Figure 8. TT + lowEE + lens + BAO + R19 (no high- $\ell$  polarization). Green (all free-streaming), yellow (all interacting, high- $z_{\rm dec}$  mode), and pink (all interacting, low  $z_{\rm dec}$  mode).

When considering the full set of Planck primary anisotropies and lensing (see Fig. 6, purple and pink), referred to here as P18 + lens, we find the data allow for a low  $z_{\rm dec}$  mode with  $\log_{10}(z_{\rm dec}) = 4.14 \pm 0.58$  ( $\log_{10}(z_{\rm dec}) = 4.14 \pm 0.56$  when including BAO). Note, however, that this mode is disfavored by the data. In itself, the low- $z_{\rm dec}$  mode is a slightly worse fit to the data compared to the free-streaming and high- $z_{\rm dec}$  cases (see Table I), which is unfortunate considering that we have added a free

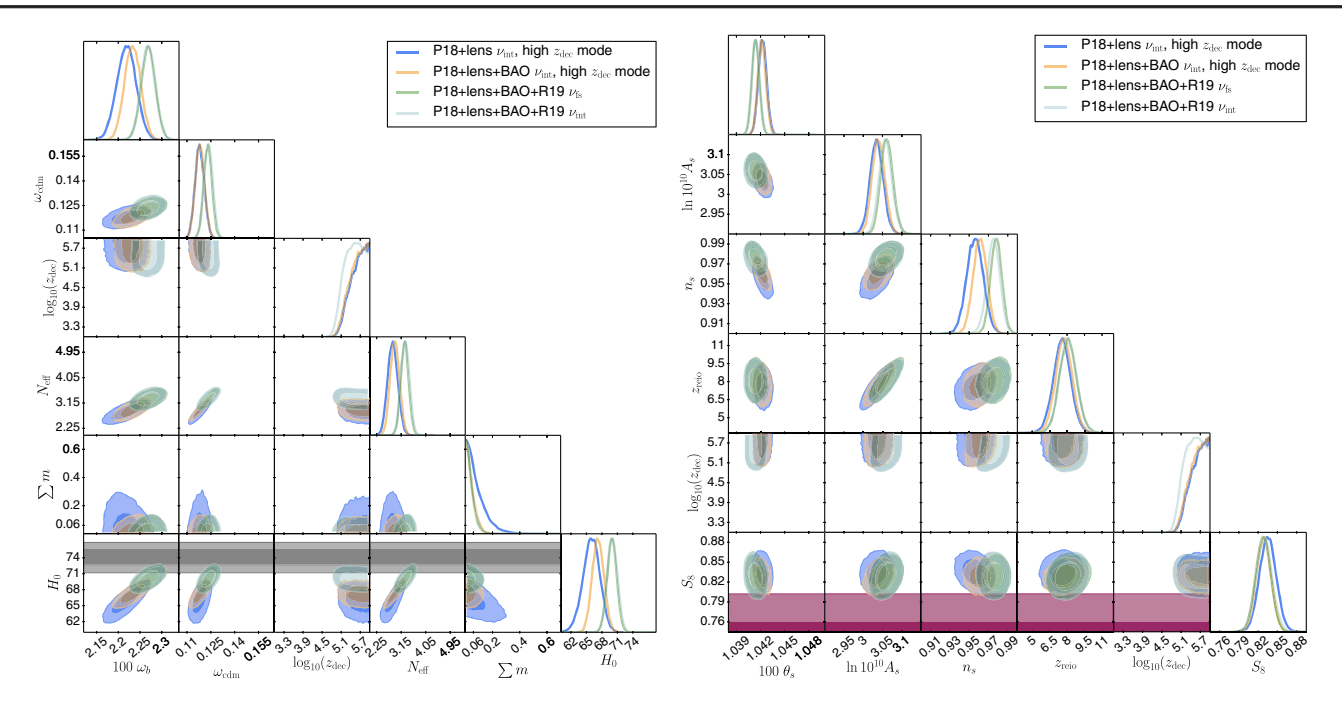


FIG. 7. Case 1: all species interacting, including  $H_0$  prior. Parameter constraints comparing models with all free-streaming neutrinos (light green) vs all species interacting separated (cyan) for Planck + BAO + R19. For comparison, we also show the high- $z_{\rm dec}$  modes from Fig. 6 for Planck-only (blue) and Planck + BAO (yellow). The gray bands correspond to the  $H_0$  measurement from Riess et al. [51], while the purple band is the  $S_8$  measurement from KiDS + VIKING-450 [134]. See Appendix C, Fig. 19 for the full parameter space plot. Left and right panels: both show the same cases, but different cosmological parameters. Left panel: energy density parameters. Right panel: power spectrum shape and amplitude parameters. Note that beyond  $z_{\rm dec} > 10^6$  the one-dimensional posterior is approximately flat up to standard neutrino decoupling. This figure shows that enabling self-interactions for all neutrinos is not a solution to the Hubble tension when including all Planck primary anisotropies and lensing, as well as a prior on  $H_0$ . This can be seen from the self-interacting case (cyan) neatly overlapping with the free-streaming case (green) for  $H_0$  (left panel); i.e., there is no improvement over free-streaming neutrinos. Note that this makes the inclusion of the  $H_0$  prior suspect and those results should be regarded with caution.

parameter. Additionally, once we consider the parameter volume effects using Bayesian evidences, this mode is further disfavored; we have a large allowed parameter space for  $z_{\text{dec}}$ , where the posterior for the high- $z_{\text{dec}}$  mode (Fig. 6, blue and yellow) flattens out above  $z_{\rm dec} \sim 10^6$  and is very slowly increasing all the way to standard neutrino decoupling  $(z \sim 10^9)$ . This is because variations in  $z_{\text{dec}}$  values above  $z_{\rm dec} \gtrsim 10^6$  do not have distinguishable effects on observables so that values of  $z_{\rm dec} \sim 10^6$  produce power spectra that closely resemble those for free-streaming neutrinos. As such, the high-z<sub>dec</sub> mode gives us a bound of  $\log_{10}(z_{\text{dec}}) > 5.2$  for P18 + lens and  $\log_{10}(z_{\text{dec}}) > 5.1$ for P18 + lens + BAO (both 68% C.L.; note that these bounds depend weakly on the prior range as pointed out in the Table I caption) and has a cosmology fairly similar to a free-streaming one, and the data show no preference for it over a free-streaming case.

The low- $z_{\rm dec}$  mode has a significantly different cosmology, as reported by, e.g., Ref. [33], with wildly different  $\theta_s$ ,  $A_s$  and  $n_s$  values compared to the free-streaming neutrino comparison case (Fig. 6, red and green) and the high- $z_{\rm dec}$  mode (Fig. 6, blue and yellow). There is, however, virtually no change in  $H_0 = 65.7 \pm 1.3 \, ({\rm km/s})/{\rm Mpc}$ 

for P18 + lens ( $H_0=66.1\pm1.0~({\rm km/s})/{\rm Mpc}$  for P18 + lens + BAO), compared to  $H_0=65.8\pm1.6~({\rm km/s})/{\rm Mpc}$  for P18 + lens ( $H_0=67.2\pm1.1~({\rm km/s})/{\rm Mpc}$  for P18 + lens + BAO) for the free-streaming case, as any increase of  $H_0$  allowed by the self-interactions is neatly of-set by a lower value for  $N_{\rm eff}=2.55\pm0.14$  for P18 + lens ( $N_{\rm eff}=2.57\pm0.14$  for P18 + lens + BAO) compared to the free-streaming value of  $N_{\rm eff}=2.82\pm0.18$  for P18 + lens ( $N_{\rm eff}=2.90\pm0.17$  for P18 + lens + BAO). On its own, with the baseline data configurations, all neutrinos self-interacting does not help alleviate the  $H_0$  tension.

Since this model has been proposed as a solution to the Hubble tension [33], let us examine if that picture changes if we include a prior on the Hubble parameter from Riess *et al.* [51] (R19) of  $H_0 = 74.04 \pm 1.42 \text{ (km/s)/Mpc}$  (see Fig. 7), and if such a combination is consistent in the first place.

Perhaps surprisingly, once we include the  $H_0$  prior, the low- $z_{\rm dec}$  mode is ruled out by the data (Fig. 7, cyan). We already saw a hint this might happen from Fig. 6. To accommodate a larger  $H_0$  value, we need to increase the effective number of relativistic species  $N_{\rm eff}$ . However, because the effect on observables when all species are

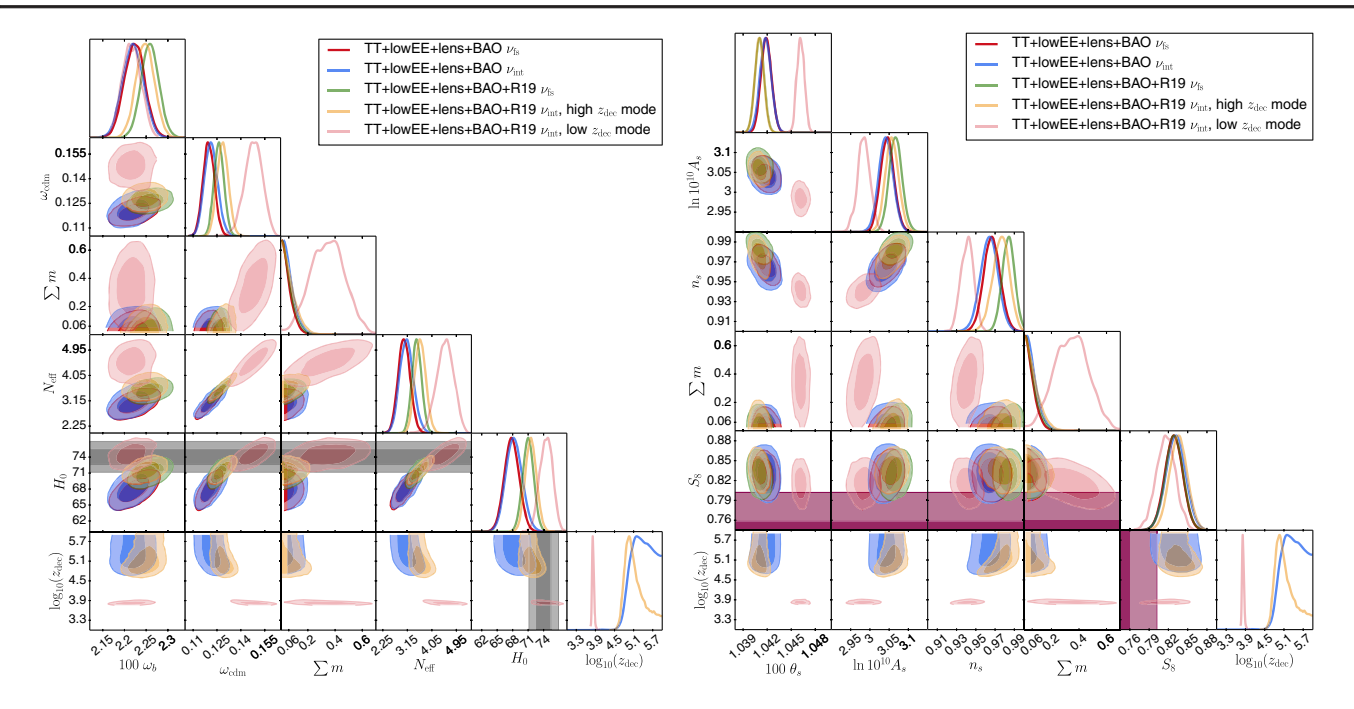


FIG. 8. Case 1: all species interacting, no high- $\ell$  polarization. All free-streaming (red and green) vs all species interacting separated into high- $z_{\rm dec}$  (blue and yellow) and low- $z_{\rm dec}$  modes (pink) for Planck-only with no high- $\ell$  polarization (red and blue) and the same plus BAO (green, yellow, and pink). The gray bands correspond to the  $H_0$  measurement from Riess et al. [51], while the purple band is the  $S_8$  measurement from KiDS + VIKING-450 [134]. See Appendix C, Fig. 20 for the full parameter space plot. Left and right panels: both show the same cases, but different cosmological parameters. Left panel: energy density parameters. Right panel: power spectrum shape and amplitude parameters. Note that beyond  $z_{\rm dec} > 10^6$  the one-dimensional posterior is approximately flat up to standard neutrino decoupling. It can be hard to see some contours, e.g., red and blue, as they are nearly overlapping as there is only a small difference between the free-streaming comparison case and the high- $z_{\rm dec}$  mode. In agreement with Ref. [33], once we exclude high- $\ell$  polarization and include a prior on  $H_0$ , we get a dramatically different cosmology for the low-log<sub>10</sub>( $z_{\rm dec}$ ) = 3.83 ± 0.03 mode (pink), including a very large neutrino mass sum  $\sum m = 0.35 \pm 0.13$  (68% C.L.), a very large number of extra relativistic species  $N_{\rm eff} = 4.53 \pm 0.32$  (68% C.L.), a low- $S_8 = 0.816 \pm 0.015$  value closer to those of late-time weak lensing surveys such as KiDS and DES, and a very high  $H_0 = 74.5 \pm 1.2$  (km/s)/Mpc in perfect agreement with Riess et al. [51] (in fact, the value of  $H_0$  we find is larger and in even better agreement with Riess et al. than the one reported in Ref. [33]).

interacting is so strong, the data do not allow for a large amount of it, and instead the mode is ruled out and we are left with a bound  $\log_{10}(z_{\rm dec}) > 5.3$  (68% C.L.). For the remaining high- $z_{\rm dec}$  mode (for which the posterior is approximately flat from the edge of the plotted parameter space to standard neutrino decoupling), we find  $N_{\rm eff} = 3.30 \pm 0.15$ , which is comparable to the free-streaming value of  $N_{\rm eff} = 3.28 \pm 0.14$  and is much larger than the low- $z_{\rm dec}$  value without R19 from before of  $N_{\rm eff} = 2.55 \pm 0.14$  for P18 + lens ( $N_{\rm eff} = 2.57 \pm 0.14$  for P18 + lens + BAO).

Finally, comparing the self-interacting case (cyan) and free-streaming comparison case (light green) from Fig. 7, it is clear that neutrino self-interactions are not a solution to the Hubble parameter tension. The  $H_0=70.05\pm0.94~({\rm km/s})/{\rm Mpc}$  value inferred in the self-interacting case is almost identical to that for the free-streaming case  $H_0=69.93\pm0.92~({\rm km/s})/{\rm Mpc}$  (the curves are neatly on top of one another, making it hard to tell them apart). The higher value compared to the cases without R19 is simply due to combining discrepant datasets, where the value for

 $H_0$  is increased at the expense of worsening the fit to the CMB data (see Table II, where the best-fit chi square contribution from Planck is 1011.4 for the free-streaming case without R19, compared to 1016.0 and 1016.7 when including R19 for the free-streaming and interacting cases, respectively). Moreover, neutrino self-interactions do not help improve the consistency with the Riess *et al.*  $H_0$  value compared to simply adding free-streaming neutrinos. For any case where this is true, we recommend viewing any such combination of discrepant datasets with caution.

#### 2. Removing high-\( \epsilon \) polarization

To fully compare to Ref. [33], we also produce parameter constraints removing high- $\ell$  polarization data. This is the choice of datasets that produced the most convincing argument for neutrino self-interactions as a solution to the Hubble tension [33]. Note that, although there have been questions about Planck high- $\ell$  polarization in the past [135], we do not have a convincing argument for excluding high- $\ell$  polarization from the analysis at present and leave

TABLE I. Case 1: statistical information for our baseline configurations.  $\chi^2_{\rm eff} = -2 \ln \mathcal{L}$  is the minimum effective chi square,  $\Delta \chi^2_{\rm eff}$  is with regard to the corresponding free-streaming case,  $\ln(E)$  is the Bayesian evidence, and  $E_{\rm int}/E_{\rm fs}$  is the Bayesian evidence ratio with regard to the corresponding free-streaming case. All credibility intervals are 68% C.L. centered around the mean unless otherwise noted. Note that because the 1-d marginalized posterior distribution above  $z_{\rm dec} > 10^6$  is not quite flat the bound on  $z_{\rm dec}$  for mode 1 (high- $z_{\rm dec}$  mode) is somewhat prior dependent. The results listed in the table were derived with a prior bound of  $10^2 < z_{\rm dec} < 10^6$  as the posterior distribution is close to flat beyond this range, this was done in order to speed up sampling while properly resolving the low- $z_{\rm dec}$  mode. If we allow sampling up to around standard neutrino decoupling ( $z_{\rm dec} < 10^9$ ) the bound for P18 + lens and P18 + lens + BAO are both  $\log_{10}(z_{\rm dec}) > 5.5$  (95% C.L.), so slightly larger than the values listed in the table. The other bounds are largely unaffected by this prior choice and the shape of the posterior for  $z_{\rm dec}$  shown in Fig. 6 is also insensitive to the allowed range of  $z_{\rm dec}$ .

	Free-str	reaming	Self-interacting (case 1)				
	P18 + lens +BAO		P18 -	⊢ lens	+BAO		
_			Mode 1	Mode 2	Mode 1	Mode 2	
$\omega_b$	$0.02219 \pm 0.00022$	$0.02234 \pm 0.00019$	$0.02219 \pm 0.00022$	$0.02226 \pm 0.00020$	$0.02233 \pm 0.018$	$0.02230 \pm 0.0017$	
$\omega_{cdm}$	$0.1177 \pm 0.0029$	$0.1179 \pm 0.0028$	$0.1180 \pm 0.0029$	$0.1136 \pm 0.0024$	$0.1182 \pm 0.0029$	$0.1135 \pm 0.0025$	
$100 \times \theta_s$	$1.04226 \pm 0.00051$	$1.04217 \pm 0.00050$	$1.04225 \pm 0.00051$	$1.04679 \pm 0.00055$	$1.04217 \pm 0.00049$	$1.04678 \pm 0.00055$	
$\ln(10^{10}A_s)$	$3.037 \pm 0.017$	$3.042 \pm 0.017$	$3.035 \pm 0.017$	$2.967 \pm 0.014$	$3.040 \pm 0.016$	$2.967 \pm 0.014$	
$n_s$	$0.9573 \pm 0.0085$	$0.9631 \pm 0.0071$	$0.9560 \pm 0.0085$	$0.9209 \pm 0.0061$	$0.9613 \pm 0.0071$	$0.9226 \pm 0.0055$	
$Z_{reio}$	$7.57 \pm 0.76$	$7.75 \pm 0.73$	$7.56 \pm 0.76$	$7.56 \pm 0.76$ $7.45 \pm 0.67$		$7.48 \pm 0.65$	
$\log_{10}(z_{\rm dec})$			>5.2 (95% C.L.)	$4.14\pm0.058$	>5.1 (95% C.L.)	$4.14\pm0.056$	
$N_{ m eff}$	$2.82 \pm 0.18$	$2.90 \pm 0.17$	$2.84 \pm 0.18$	$2.55 \pm 0.14$	$2.92 \pm 0.17$	$2.57 \pm 0.14$	
$\sum m$	<0.227 (95% C.L.)	<0.108 (95% C.L.)	<0.225 (95% C.L.)	<0.160 (95% C.L.)	<0.107 (95% C.L.)	<0.108 (95% C.L.)	
$H_0 \left[ \frac{(\text{km/s})}{\text{Mpc}} \right]$	$65.8 \pm 1.6$	$67.2 \pm 1.1$	$65.9 \pm 1.7$	$65.7 \pm 1.3$	$67.3 \pm 1.1$	$66.1 \pm 1.0$	
$S_8$	$0.835 \pm 0.013$	$0.828 \pm 0.012$	$0.835 \pm 0.013$	$0.825 \pm 0.013$	$0.829 \pm 0.011$	$0.821 \pm 0.011$	
ln(E)	$-0.5282 \times 10^3$	$-0.5320 \times 10^3$	$-0.5333 \times 10^3$	$-0.5388 \times 10^3$	$-0.5370 \times 10^3$	$-0.5418 \times 10^3$	
$E_{ m int}/E_{ m fs}$			$6.1 \times 10^{-3}$ $2.5 \times 10^{-5}$		$6.7 \times 10^{-3}$	$5.5 \times 10^{-5}$	
	Best fit						
$N_{ m eff}$	2.846	2.922	2.859	2.572	2.819	2.519	
$\log_{10}(z_{\rm dec})$	• • •	• • •	5.953	4.119	5.997	4.126	
$\chi^2_{ m eff}$	1011.08	1016.72	1011.67	1018.35	1016.94	1023.39	
$\Delta \chi^2_{\rm eff}$			+0.59	+7.27	+0.22	+6.67	

the interpretation of that choice and these results up to the reader. In this subsection, we refer to these figures, datasets, and configurations:

- (i) Figure 8. TT + lowEE + lens + BAO (no high- $\ell$  polarization). Red (all free-streaming) and blue (all interacting).
- (ii) Figure 8. TT + lowEE + lens + BAO + R19 (no high- $\ell$  polarization). Green (all free-streaming), yellow (all interacting, high- $z_{\rm dec}$  mode), and pink (all interacting, low- $z_{\rm dec}$  mode).

High- $\ell$  polarization strongly constrains the number of relativistic degrees of freedom,  $N_{\rm eff}$ , and the neutrino mass sum,  $\sum m$ . Additionally, neutrino self-interactions leave a clear signature on the polarization power spectrum. Therefore, when removing high- $\ell$  polarization, the picture changes dramatically (see Fig. 8), as reported by Ref. [33]. In this section, we update their results for Planck 2018.

When all relativistic species are self-interacting and the prior on the Hubble parameter,  $H_0$ , from Riess *et al.* [51] is included (Fig. 8, yellow and pink contours), the data allow for a very high value of  $N_{\rm eff}=4.53\pm0.32$  for the low- $z_{\rm dec}$  mode (Fig. 8, pink contours), which in turn leads to a high

value for  $H_0 = 74.5 \pm 1.2 \text{ (km/s)/Mpc}$ , which is larger and in even better agreement with Riess *et al.* than the one reported in Ref. [33] and is even slightly larger than the Riess *et al.* [51] measurement of  $H_0 = 74.04 \pm 1.42 \text{ (km/s)/Mpc}$  and completely eliminates the Hubble parameter tension, and indicating the combination of datasets is valid (with the strong assumption that there is a problem with the Planck high- $\ell$  polarization).

These remarkably high values for  $N_{\rm eff}$  and  $H_0$  are only allowed because of the strong neutrino self-interactions of the low- $z_{\rm dec}$  mode and are a consequence of the  $H_0$  prior. In comparison, still with the  $H_0$  prior included, the high- $z_{\rm dec}$  mode (Fig. 8, yellow contours) has much lower values of  $N_{\rm eff}=3.63\pm0.20$  and  $H_0=71.5\pm1.1~({\rm km/s})/{\rm Mpc}$ . Similarly, when all species are free-streaming, we find  $N_{\rm eff}=3.50\pm0.18$  and  $H_0=71.0\pm1.1~({\rm km/s})/{\rm Mpc}$  (Fig. 8, green contours). In both of these examples, the  $H_0$  constraint is simply the result of combining two discrepant datasets making the combination suspect, as we are degrading the fit to the CMB data in order to accommodate a larger  $H_0$  value. The degradation to the fit to CMB data can be seen from the individual  $\chi^2_{\rm eff}$ 

TABLE II. Case 1: statistical information including a prior on  $H_0$  from Riess *et al.* [51].  $\chi^2_{\rm eff} = -2 \ln \mathcal{L}$  is the minimum effective chi square,  $\Delta \chi^2_{\rm eff}$  is with regard to the corresponding free-streaming case,  $\ln(E)$  is the Bayesian evidence, and  $E_{\rm int}/E_{\rm fs}$  is the Bayesian evidence ratio with regard to the corresponding free-streaming case. All credibility intervals are 68% C.L. centered around the mean unless otherwise noted. The baseline case without R19 is included for comparison, to show how adding R19 degrades the fit to the CMB.

	Free	Self-interacting (case 1)			
	$\overline{P18 + lens + BAO}$	P18 + lens + BAO + R19	9 $P18 + lens + BAO + R19$		
$\overline{\omega_b}$	$0.02234 \pm 0.00019$	$0.02270 \pm 0.00016$	$0.2268 \pm 0.0016$		
$\omega_{cdm}$	$0.1179 \pm 0.0028$	$0.1231 \pm 0.0026$	$0.1235 \pm 0.0027$		
$100 \times \theta_s$	$1.04217 \pm 0.00050$	$1.04139 \pm 0.00043$	$1.04139 \pm 0.00045$		
$ln(10^{10}A_s)$	$3.042 \pm 0.017$	$3.062 \pm 0.016$	$3.058 \pm 0.016$		
$n_s$	$0.9631 \pm 0.0071$	$0.9780 \pm 0.0058$	$0.9751 \pm 0.0066$		
$z_{\rm reio}$	$7.75 \pm 0.73$	$8.10 \pm 0.74$	$8.07 \pm 0.74$		
$\log_{10}(z_{\rm dec})$		• • •	>5.3 (68% C.L.)		
$N_{ m eff}$	$2.90 \pm 0.17$	$3.28 \pm 0.14$	$3.30 \pm 0.15$		
$\sum m$	<0.108 (95% C.L.)	<0.0965 (95% C.L.)	<0.102 (95% C.L.)		
$\overline{H}_0 \left[ \frac{(\text{km/s})}{\text{Mpc}} \right]$	$67.2 \pm 1.1$	$69.93 \pm 0.92$	$70.05 \pm 0.94$		
$S_8$	$0.828 \pm 0.012$	$0.828 \pm 0.012$	$0.829 \pm 0.012$		
ln(E)	$-0.5320 \times 10^3$	$-0.5393 \times 10^3$	$-0.5439 \times 10^3$		
$E_{ m int}/E_{ m fs}$	• • •	• • •	$1.0 \times 10^{-2}$		
		Best fit			
$N_{ m eff}$	2.922	3.209	3.254		
$\log_{10}(z_{\rm dec})$		• • •	5.571		
P18 highTTTEEE	583.23	588.54	589.17		
P18 lowTT	23.45	21.95	22.17		
P18 lowEE	396.01	396.43	396.26		
P18 lensing	8.73	9.08	9.08		
P18 total	1011.4	1016.0	1016.7		
BAO	5.30	5.69	5.78		
R19	• • •	9.14	8.17		
$\chi^2_{ m eff}$	1016.72	1030.83	1030.64		
$\Delta \chi^2_{ m eff}$		•••	-0.19		

contributions from the different datasets shown in Table III, where the fit to the CMB data worsens when R19 is added, in particular Planck high- $\ell$  temperature autocorrelation (P18 highTT) and Planck lensing, with a fairly large chi square contribution increase from all the Planck likelihoods for the best-fit cosmology from 633.5 without R19 to 638.5 with R19 for the free-streaming case and to 636.4 with R19 for the high- $z_{\rm dec}$  mode. So, even though the  $H_0$  tension is alleviated, it comes at the expense of a worse fit to the CMB data.

For the high- $z_{\rm dec}$  mode, we do find a better fit overall for the best-fit cosmology, with a  $\Delta\chi^2_{\rm eff}=-2.98$  compared to the free-streaming case including R19, but this is offset by the increased complexity of the model as seen from the Bayesian evidence ratio  $E_{\rm int}/E_{\rm fs}=2.7\times10^{-2}$ , where a value less than 1 means the free-streaming comparison model is favored. However, for the low- $z_{\rm dec}$  mode, it looks even worse. The  $H_0$  tension is completely eliminated, but the fit to the CMB data is severely degraded with a chi square contribution from the Planck likelihoods of 647.5,

resulting in an overall best fit  $\Delta\chi^2_{\rm eff}=+3.98$  compared to the free-streaming comparison case (with R19), resulting in a lower Bayesian evidence ratio of  $E_{\rm int}/E_{\rm fs}=2.7\times 10^{-4}$ . So, although this model is technically allowed by the data, it is disfavored compared to a free-streaming scenario. If we disregard the  $H_0$  prior, we instead find a bound on  $\log_{10}(z_{\rm dec})>4.9$  (95% C.L.) (Fig. 8, blue contours) and lower values of  $N_{\rm eff}=3.13\pm0.25$  and  $H_0=68.3\pm1.5$  (km/s)/Mpc for all extra relativistic species self-interacting and  $N_{\rm eff}=3.04\pm0.22$  and  $H_0=67.8\pm1.4$  (km/s)/Mpc for all extra relativistic species free-streaming.

### B. Case 2: Two free-streaming species plus interacting species

Considering the bounds on electron and muon self-interactions pointed out by Ref. [47], we want to consider a case of two free-streaming neutrinos plus one interacting neutrino, while simultaneously allowing for additional

TABLE III. Case 1: statistical information when excluding high- $\ell$  polarization.  $\chi^2_{\rm eff} = -2 \ln \mathcal{L}$  is the minimum effective chi square,  $\Delta \chi^2_{\rm eff}$  is with regard to the corresponding free-streaming case,  $\ln(E)$  is the Bayesian evidence, and  $E_{\rm int}/E_{\rm fs}$  is the Bayesian evidence ratio with regard to the corresponding free-streaming case. All credibility intervals are 68% C.L. centered around the mean unless otherwise noted.

	Free-stream	ing	Self-interacting (case 1)			
	$\overline{\text{TT} + \text{lowEE} + \text{lens} + \text{BAO}}$	+R19	$\overline{\text{TT} + \text{lowEE} + \text{lens} + \text{BAO}}$	+R	R19	
·	-		_	Mode 1	Mode 2	
$\omega_b$	$0.02223 \pm 0.00023$	$0.02259 \pm 0.00020$	$0.02219 \pm 0.00024$	$0.02248 \pm 0.021$	$0.02216 \pm 0.0021$	
$\omega_{cdm}$	$0.1199 \pm 0.0036$	$0.1263 \pm 0.0031$	$0.1213 \pm 0.0041$	$0.1286 \pm 0.0036$	$0.1478 \pm 0.0057$	
$100 \times \theta_s$	$1.04189 \pm 0.00063$	$1.04204 \pm 0.00054$	$1.04103 \pm 0.00056$	$1.04217 \pm 0.00049$	$1.04617 \pm 0.00046$	
$ln(10^{10}A_s)$	$3.045 \pm 0.018$	$3.067 \pm 0.017$	$3.041 \pm 0.018$	$3.057 \pm 0.018$	$2.984 \pm 0.016$	
$n_s$	$0.9668 \pm 0.0085$	$0.9839 \pm 0.0065$	$0.9639 \pm 0.0092$	$0.9760 \pm 0.0087$	$0.9411 \pm 0.0067$	
$z_{\rm reio}$	$7.74 \pm 0.76$	$8.10 \pm 0.78$	$7.69 \pm 0.77$	$7.95 \pm 0.78$	$7.63 \pm 0.87$	
$\log_{10}(z_{\rm dec})$	• • •		>4.9 (95% C.L.)	$5.15^{+0.40}_{-0.16}$	$3.83 \pm 0.03$	
$N_{ m eff}$	$3.04 \pm 0.22$	$3.50 \pm 0.18$	$3.13 \pm 0.25$	$3.63 \pm 0.20$	$4.53 \pm 0.32$	
$\sum_{i=1}^{n} m_i$	<0.130 (95% C.L.)	<0.144 (95% C.L.)	<0.151 (95% C.L.)	<0.173 (95% C.L.)	$0.35 \pm 0.13$	
$H_0 \left[ \frac{(\text{km/s})}{\text{Mpc}} \right]$	$67.8 \pm 1.4$	$71.0 \pm 1.0$	$68.3 \pm 1.5$	$71.5 \pm 1.1$	$74.5\pm1.2$	
$S_8$	$0.828 \pm 0.014$	$0.829 \pm 0.014$	$0.832 \pm 0.015$	$0.836 \pm 0.014$	$0.816 \pm 0.015$	
ln(E)	$-0.3419 \times 10^3$	$-0.3468 \times 10^3$	$-0.3462 \times 10^3$	$-0.3504 \times 10^3$	$-0.3550 \times 10^3$	
$E_{\rm int}/E_{\rm fs}$	• • •	• • •	$1.4 \times 10^{-2}$	$2.7 \times 10^{-2}$	$2.7 \times 10^{-4}$	
			Best fit			
$N_{ m eff}$	2.971	3.494	3.123	3.591	4.653	
$\log_{10}(z_{\rm dec})$	• • •	• • •	5.224	4.970	3.8208	
P18 highTT	205.34	211.24	204.95	208.11	216.01	
P18 lowTT	23.58	21.56	23.95	22.74	24.44	
P18 highEE	• • •	• • •	• • •		• • •	
P18 lowEE	395.77	396.28	395.75	396.15	395.87	
P18 lensing	8.81	9.46	8.88	9.36	11.20	
P18 total	633.5	638.5	633.5	636.4	647.5	
BAO	5.40	6.54	5.25	6.53	4.96	
R19	• • •	3.75	• • •	2.97	0.33	
$\chi^2_{ m eff}$	638.89	648.83	638.79	645.85	652.81	
$\Delta \chi^2_{\rm eff}$	•••	•••	-0.10	-2.98	+3.98	

interacting species. We use the normal hierarchy approximation for the neutrino masses, <sup>11</sup> treating the two lighter mass states as massless. This should allow us to approximately equate a flavor state with a mass state, a translation that might otherwise be nontrivial. The extra relativistic species share the mass of the massive standard neutrino.

In this section, we refer to these figures, datasets, and configurations:

- (i) Figure 9. P18 + lens. Red (all free-streaming) and blue (partially interacting).
- (ii) Figure 9. P18 + lens + BAO. Green (all free-streaming) and yellow (partially interacting).
- (iii) Figure 9. P18 + lens + BAO + R19. Light green (all free-streaming) and cyan (partially interacting).

- (iv) Figure 10. P18 + lens + BAO. Red (all free-streaming), blue (partially interacting), and purple (partially fluidlike).
- (v) Figure 10. P18 + lens + BAO + R19. Green (all free-streaming), yellow (partially interacting), and pink (partially fluidlike).

We find the strongly interacting mode at  $\log_{10}(z_{\rm dec}) \approx 4.09$  from the previous Sec. VA, although with less significance than shown there (MultiNest does not consider it a separate mode as the intermediate  $z_{\rm dec}$  values are not ruled out). Note that beyond  $\log_{10}(z_{\rm dec}) \gtrsim 5.5$  the posterior continues to be approximately flat all the way to standard neutrino decoupling, as the data prefer free-streaming neutrinos and cannot distinguish between free-streaming and slightly interacting species with such an early decoupling time. Given the shape of the posterior (see Fig. 9), highly non-Gaussian with two modes not clearly separated in parameter space, any attempt to derive bounds on  $z_{\rm dec}$  will naturally be prior dependent, so we instead refer the

<sup>&</sup>lt;sup>11</sup>Known to not be reliable enough for precise neutrino mass sum estimates (see, e.g., Refs. [108–110]), but nevertheless good enough for our purposes as the mass constraint is not the focus of our study.

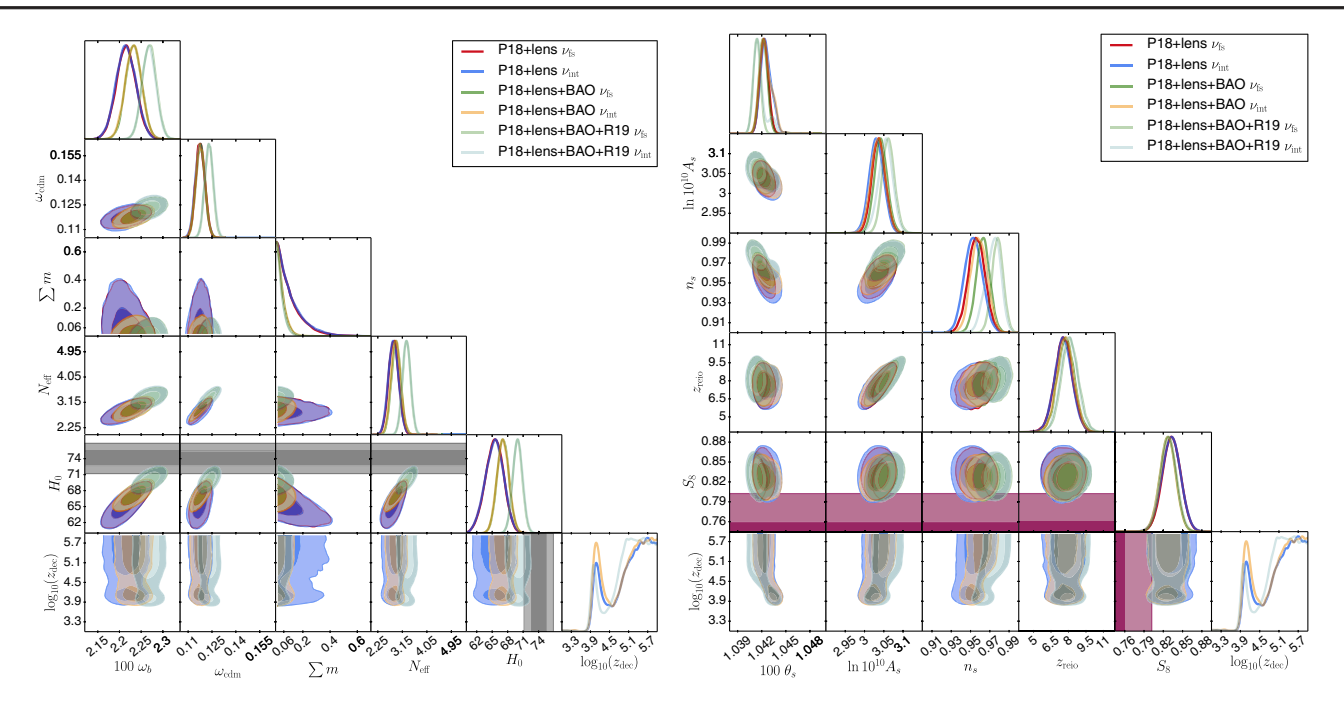


FIG. 9. Case 2: two free-streaming neutrinos plus self-interacting relativistic species. All free-streaming (red, green, and light green) vs self-interacting species (blue, yellow, and cyan) for Planck-only (red and blue), Planck + BAO (green and yellow), and Planck + BAO +  $H_0$  prior (light green and cyan). The gray bands correspond to the  $H_0$  measurement from Riess *et al.* [51], while the purple band is the  $S_8$  measurement from KiDS + VIKING-450 [134]. See Appendix C, Fig. 21 for the full parameter space plot. Left and right panels: both show the same cases, but different cosmological parameters. Left panel: energy density parameters. Right panel: power spectrum shape and amplitude parameters. Note that beyond  $z_{dec} > 10^6$  the one-dimensional posterior is approximately flat up to standard neutrino decoupling. Several of the contours are hard to see as the self-interacting cases are nearly on top of the free-streaming ones, i.e., red and blue, green, and yellow, as well as light green and cyan, indicating that this case is not a solution to the Hubble tension. Even though we find a low- $z_{dec}$  mode, it shows no improvement compared to the free-streaming comparison case, even when including the  $H_0$  prior (on the left panel, the cyan contour is directly on top of the light green one). Indeed, this is further confirmed when considering the low- $z_{dec}$  part of parameter space (bottom row), where we see the low- $z_{dec}$  mode separated at greater than  $1\sigma$  from the high- $z_{dec}$  mode, but still showing a low value for  $H_0$  in line with the free-streaming case (note that this makes the inclusion of the  $H_0$  prior suspect and those results should be regarded with caution). Similarly to case 1 (Sec. VA), the low- $z_{dec}$  mode has a significantly different cosmology than the free-streaming comparison case, including a much larger  $\theta_s$ , related to the scale of the first peak, and lower values for the primordial power spectrum tilt,  $n_s$ , and amplitude,  $A_s$ .

reader to the  $z_{\text{dec}}$  posterior on Fig. 9 and the discussion in the caption of Table IV.

Although the low- $z_{dec}$  mode does have a significantly different cosmology (most notably with larger  $\theta_s$  and lower  $A_s$  and  $n_s$  values), this case does not help with the current cosmological tension related to  $H_0$ . For all combinations of datasets, the free-streaming and interacting lines are neatly on top of each other in the one-dimensional plot for  $H_0$  (left panel of Fig. 9), i.e., red and blue lines for Planck-only (P18 + lens), green and yellow for P18 + lens + BAO, and cyan and light green for P18 + lens + BAO + R19. This is further confirmed when considering the two-dimensional plot for  $H_0 - z_{dec}$  and comparing the high- and low- $z_{dec}$ parts of parameter space, where  $H_0$  for the low- $z_{dec}$  part of parameter space is actually very slightly lower. This can be understood by the self-interactions being slightly disfavored by the data and therefore allowing for a lower value of  $N_{\rm eff}$  (which reduces the effect of the interactions as illustrated by Fig. 5), which in turn leads to a smaller value for  $H_0$ . The fluidlike case (i.e., setting decoupling to today) similarly does not help with the  $H_0$  tension (see Fig. 10, left panel). Note that Ref. [44] also considered fluidlike radiation but did not consider the same cases we do here. The  $S_8$  tension, on the other hand, although it is not improved at all for the marginalized one-dimensional posterior distribution for the self-interacting case, it is very slightly improved for the low- $z_{\rm dec}$  mode (Fig. 9, right panel) and significantly improved for the fluidlike case (Fig. 10, right panel, purple, and pink contours). Note, however, that a self-interaction this strong would appear to be strongly ruled out for the most massive standard neutrino mass state, unless we can construct a scenario where, e.g., these early Universe cosmological neutrinos are not exactly the same ones we measure on Earth today.

However, we do not consider late-time large-scale structure data in the analysis, so it is hard to say if this shift in  $S_8$  helps the model compared to free-streaming neutrinos and extra relativistic species. But when considering only

TABLE IV. Case 2: statistical information for our baseline configurations and the one including a prior on  $H_0$ .  $\chi^2_{\rm eff} = -2\ln\mathcal{L}$  is the effective chi square,  $\Delta\chi^2_{\rm eff}$  is with regard to the corresponding free-streaming case,  $\ln(E)$  is the Bayesian evidence, and  $E_{\rm int}/E_{\rm fs}$  is the Bayesian evidence ratio with regard to the corresponding free-streaming case.  $\chi^2_{\rm eff}$  is presented for the best-fit cosmology (giving the minimum effective chi square) and for the best-fit cosmology of the second mode (note that the best-fit cosmology does not always correspond to the same  $z_{\rm dec}$  mode). All credibility intervals are 68% C.L. centered around the mean unless otherwise noted. Note that the best fit  $N_{\rm eff} = 2.0328 + N_{\rm eff,int}$  is distinct from the mean value of  $N_{\rm eff}$  in line 7. For the  $z_{\rm dec}$  parameter, we refer the reader to Fig. 9, as the posterior distribution for  $z_{\rm dec}$  is multimodal and highly non-Gaussian, which means attempts to derive bounds on  $z_{\rm dec}$  naturally end up being prior dependent with  $\log_{10}(z_{\rm dec}) > 4.9$  at 68% C.L.  $(\log_{10}(z_{\rm dec}) > 3.9$  at 95% C.L.) when the sampling range is  $10^2 < z_{\rm dec} < 10^6$ , compared to  $\log_{10}(z_{\rm dec}) > 6.1$  at 68% C.L.  $(\log_{10}(z_{\rm dec}) > 4.5$  at 95% C.L.) when allowing  $z_{\rm dec}$  to vary freely up to around standard neutrino decoupling  $z_{\rm dec} < 10^9$ . As the posterior distribution is nearly flat beyond the range  $10^2 < z_{\rm dec} < 10^6$ , we chose this prior range in order to accurately resolve the low- $z_{\rm dec}$  mode. The other bounds are largely unaffected by this prior choice.

	Free-streaming			Self-interacting (case 2)			Self-interacting (fluidlike)	
	P18+lens	+BAO	+R19	P18+lens	+BAO	+R19	P18+lens+BAO	+R19
$\overline{\omega_b}$	$0.02216 \pm 0.00023$	$0.02233 \pm 0.00019$	$0.02269 \pm 0.00016$	$0.02215 \pm 0.00023$	$0.02232 \pm 0.00019$	$0.02268 \pm 0.00016$	$0.02235 \pm 0.00021$	$0.02281 \pm 0.00018$
$\omega_{cdm}$	$0.1177 \pm 0.0029$	$0.1178 \pm 0.0029$	$0.1231 \pm 0.0026$	$0.1175^{+0.0029}_{-0.0031}$	$0.1177 \pm 0.0029$	$0.1232^{+0.0028}_{-0.0027}$	$0.1162 \pm 0.0030$	$0.1224^{+0.0025}_{-0.0029}$
$100 \times \theta_s$	$1.04229 \pm 0.00051$	$1.04219 \pm 0.00050$	$1.04140 \pm 0.00044$	$1.04257^{+0.00056}_{-0.00082}$	$1.04254^{+0.00056}_{-0.00093}$	$1.04173^{+0.00032}_{-0.00088}$	$1.04510 \pm 0.00032$	$1.04537 \pm 0.00030$
$\ln(10^{10}A_s)$	$3.036 \pm 0.017$	$3.042 \pm 0.017$	$3.062 \pm 0.016$	$3.031^{+0.019}_{-0.018}$	$3.035 \pm 0.018$	$3.054^{+0.020}_{-0.018}$	$2.992 \pm 0.015$	$2.994 \pm 0.030$
$n_s$	$0.9563 \pm 0.0087$	$0.9629 \pm 0.0071$	$0.9781 \pm 0.0059$	$0.9530^{+0.0092}_{-0.0095}$	$0.9588^{+0.0084}_{-0.0085}$	$0.9735^{+0.0091}_{-0.0067}$	$0.9389 \pm 0.0044$	$0.9465 \pm 0.0040$
$z_{\rm reio}$	$7.58 \pm 0.77$	$7.78 \pm 0.74$	$8.12 \pm 0.74$	$7.56 \pm 0.75$	$7.73 \pm 0.72$	$8.06^{+0.72}_{-0.74}$	$7.81 \pm 0.73$	$8.24 \pm 0.75$
$N_{ m eff}$	$2.83 \pm 0.18$	$2.92 \pm 0.17$	$3.30 \pm 0.15$	$2.83_{-0.19}^{+0.18}$	$2.91^{+0.18}_{-0.17}$	$3.30^{+0.15}_{-0.16}$	$2.76 \pm 0.17$	$3.16 \pm 0.14$
$\sum m$	<0.301 (95% C.L.)	<0.108 (95% C.L.)	<0.095 (95% C.L.)	<0.312 (95% C.L.)			<0.122 (95% C.L.)	<0.110 (95% C.L.)
$H_0 \left[ \frac{(\text{km/s})}{\text{Mpc}} \right]$	$65.4 \pm 1.7$	$67.1 \pm 1.1$	$69.9 \pm 0.9$	$65.4^{+1.9}_{-1.7}$	$67.1 \pm 1.2$	$70.0\pm1.0$	$66.7 \pm 1.2$	$69.9 \pm 1.0$
$S_8$	$0.833 \pm 0.014$	$0.827 \pm 0.012$	$0.828 \pm 0.012$	$0.832^{+0.015}_{-0.014}$	$0.827 \pm 0.012$	$0.828 \pm 0.012$	$0.804 \pm 0.012$	$0.796 \pm 0.011$
ln(E)	$-0.5280 \times 10^3$	$-0.5322 \times 10^3$	$-0.5394 \times 10^3$	$-0.5324 \times 10^3$	$-0.5323 \times 10^3$	$-0.5436 \times 10^3$	$-0.5365 \times 10^3$	$-0.5444 \times 10^3$
$E_{ m int}/E_{ m fs}$	•••	•••	•••	$1.3 \times 10^{-2}$	0.86	$1.6 \times 10^{-2}$	$1.4 \times 10^{-2}$	$6.8 \times 10^{-3}$
				Best fit				
$N_{ m eff,int}$	•••	•••	•••	0.834	0.787	1.239	0.646	1.153
$\log_{10} z_{\mathrm{dec}}$	•••	•••	•••	5.442	4.085	5.163	•••	•••
$\chi^2_{ m eff}$	1011.10	1016.79	1030.98	1011.24	1016.62	1030.85	1025.76	1041.15
$\Delta\chi^2_{ m eff}$	•••	•••	•••	+0.14	-0.16	-0.12	+8.97	+10.17
				Second mode be	est fit			
$N_{ m eff,int}$	•••	•••	•••	0.687	0.822	1.127	•••	•••
$\log_{10} z_{\rm dec}$	•••	•••	•••	4.118	5.456	4.002	•••	•••
$\chi^2_{ m eff}$	•••	•••		1011.43	1016.71	1031.39	•••	
$\Delta \chi^2_{ m eff}$	•••	•••	•••	+0.33	-0.08	+0.41	•••	•••

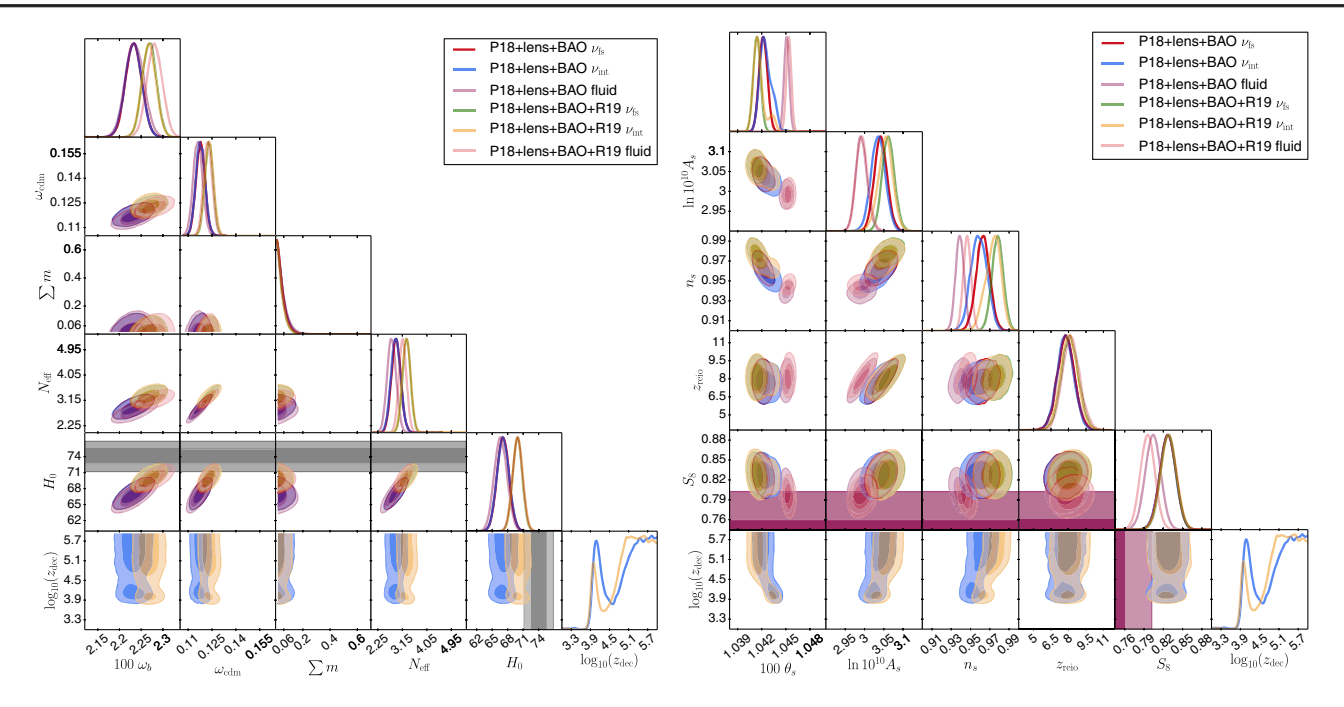


FIG. 10. Case 2: two free-streaming neutrinos plus self-interacting relativistic species, including fluidlike. All free-streaming (red and green) vs self-interacting species (blue and yellow) and fluidlike (purple and pink) for Planck + BAO (red, blue, and purple) and Planck + BAO +  $H_0$  prior (green, yellow, and pink). The gray bands correspond to the  $H_0$  measurement from Riess et al. [51], while the purple band is the  $S_8$  measurement from KiDS + VIKING-450 [134]. See Appendix C, Fig. 22 for the full parameter space plot. Left and right panels: both show the same cases, but different cosmological parameters. Left panel: energy density parameters. Right panel: power spectrum shape and amplitude parameters. Note that beyond  $z_{\rm dec} > 10^6$  the one-dimensional posterior is approximately flat up to standard neutrino decoupling. Some contours are hard to see as they are neatly on top of each other, i.e., red and blue as well as green and yellow. In this figure, we include a fluidlike case, corresponding to a species decoupling after recombination up until today, in the future, or never. The fluidlike cases reduce the  $S_8$  tension to about  $2\sigma$  for the case without the  $H_0$  prior (note that, although the largest improvement is for the case with the  $H_0$  prior, this combination of datasets is suspect as this case does not alleviate the  $H_0$  tension) and displays a different cosmology similar to the low- $z_{\rm dec}$  mode, but with parameter values for  $\theta_s$ ,  $n_s$ , and  $A_s$  even further away from the free-streaming case.

Planck, with or without BAO, we find all of these cases are disfavored compared to free-streaming species (see Table IV). The best-fit cosmologies of the self-interacting modes have slightly better  $\chi^2_{\rm eff}$  values than the free-streaming comparison cases, but this is outweighed by the added complexity of the model resulting in a Bayesian evidence ratio of less than 1.

# C. Case 3: Fixed number of relativistic species and varying fraction of interacting species

Simplifying to only including standard model neutrinos, we want to see whether having one or more species that are self-interacting is allowed by current cosmological data. This case includes free-streaming massive neutrinos plus massive interacting species. The total effective number of

relativistic species is fixed to that expected from the Standard Model,  $N_{\rm eff}=3.046$ , so this case amounts to varying the fraction that is self-interacting, while also varying the total mass sum  $\sum m$ .

In this section, we refer to the following figure, dataset, and configurations:

(i) Figure 11. P18 + lens + BAO. Red (all free-streaming), blue (partially interacting), and purple (partially fluidlike).

We see a small local maximum at around  $z_{\rm dec} \sim 10,000$  (Fig. 11, left panel), roughly at the  $z_{\rm dec}$  of the strongly interacting mode of the other cases, that allows for about  $N_{\rm eff,int} \lesssim 1$  at around  $2\sigma$ . However, it is clearly disfavored compared to higher values of  $z_{\rm dec}$  that are approximately free-streaming (again, the one-dimensional

posterior remains flat from  $z_{\rm dec}=10^6$  to around standard neutrino decoupling), as  $z_{\rm dec}\gtrsim 10^5$  is preferred by the data (with  $N_{\rm eff,int}\lesssim 1$ , at about  $1\sigma$ ). This picture does not change significantly depending on whether BAO data are included or when considering fluidlike vs strongly interacting, although the bounds on allowed  $N_{\rm eff,int}$  values tighten slightly for the fluidlike case. Insofar that bounds were possible to derive, they are summarized in Table V.

#### D. Case 4: Varying fraction of interacting species

We want to open up parameter space and allow for a freely varying number of free-streaming effective degrees of freedom, while still varying the fraction that is interacting. To keep the total number of varying parameters fixed, we fix the effective mass to roughly the current  $2\sigma$  upper bound on the neutrino mass sum [55]. This case has free-streaming massless neutrinos with varying  $N_{\rm eff,fs}$ , plus massive interacting species with a fixed mass sum  $\sum m = 0.11$  eV and varying  $N_{\rm eff,int}$  and  $z_{\rm dec}$ .

In this section, we refer to these figures, datasets, and configurations:

- (i) Figure 12. P18 + lens. Red (all free-streaming) and blue (partially interacting).
- (ii) Figure 12. P18 + lens + BAO. Green (all free-streaming) and yellow (partially interacting).
- (iii) Figure 12. P18 + lens + BAO + R19. Light green (all free-streaming) and cyan (partially interacting).

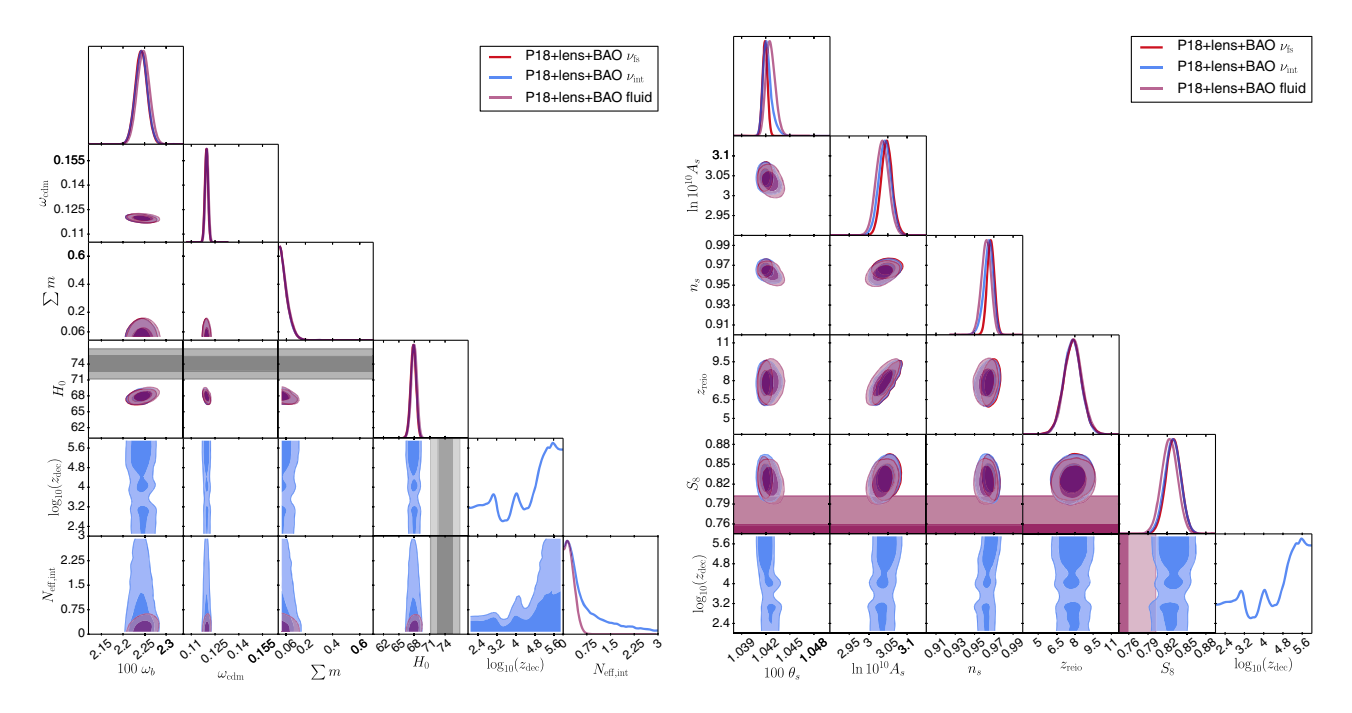


FIG. 11. Case 3: varying fraction of self-interacting relativistic species, including fluid, with fixed  $N_{\rm eff} = 3.046$ . All free-streaming (red) vs fraction of self-interacting (blue) and fraction of fluidlike (purple) for Planck + BAO. The gray bands correspond to the  $H_0$  measurement from Riess et al. [51], while the purple band is the  $S_8$  measurement from KiDS + VIKING-450 [134]. See Appendix C, Fig. 23 for the full parameter space plot. Left and right panels: both show the same cases, but different cosmological parameters. Left panel: energy density parameters. Right panel: power spectrum shape and amplitude parameters. Note that beyond  $z_{\rm dec} > 10^6$  up to standard neutrino decoupling and below  $z_{\rm dec} < 10^2$  the one-dimensional posterior is approximately flat. For this case, any value of  $z_{\rm dec}$  is allowed but is limited to  $N_{\rm eff,int} < 0.79$  at 68% C.L. ( $N_{\rm eff,int} < 2.34$  at 95% C.L.), but high- $z_{\rm dec}$  values are preferred at about 1- $\sigma$  (with a bound on  $z_{\rm dec}$  that is strongly prior dependent as discussed in the Table V caption). Low values of  $z_{\rm dec}$  require a low number of self-interacting extra relativistic species of about  $N_{\rm eff,int} < 0.5$  at  $1\sigma$  (with the fluidlike case allowing for a smaller value of  $N_{\rm eff,int} < 0.28$  at 68% C.L. or  $N_{\rm eff,int} < 0.50$  at 95% C.L.). Note that around  $z_{\rm dec} \sim 10,000$  there is a local maximum that allows up to about  $N_{\rm eff,int} < 1.2 \sigma$ .

TABLE V. Case 3: statistical information for our baseline configurations.  $\chi^2_{\rm eff} = -2 \ln \mathcal{L}$  is the effective chi square,  $\Delta\chi^2_{\rm eff}$  is with regard to the corresponding free-streaming case,  $\ln(E)$  is the Bayesian evidence, and  $E_{\rm int}/E_{\rm fs}$  is the Bayesian evidence ratio with regard to the corresponding free-streaming case.  $\chi^2_{\rm eff}$  is presented for the best-fit cosmology (giving the minimum effective chi square) and for the best fit of the high- $z_{\rm dec}$  mode. All credibility intervals are 68% C.L. centered around the mean unless otherwise noted. Note that at 95% C.L.  $N_{\rm eff,int} < 2.34$  ( $N_{\rm eff,int} < 0.50$  for fluidlike), and so, although one or more interacting species are disfavored, it is not ruled out by cosmological data (however, it is hard to accommodate a fluidlike neutrino species). The  $z_{\rm dec}$  bound is not reported in the table as it is strongly prior dependent. We find  $\log_{10}(z_{\rm dec}) > 4.0$  (68% C.L.) for the decoupling case for our standard prior range  $10^2 < z_{\rm dec} < 10^6$ , which was chosen because the posterior is flat below and above this range and the narrower prior range allows us to accurately probe the intermediate- $z_{\rm dec}$  range, while keeping the case computationally feasible. With a prior  $z_{\rm dec} < 10^9$ , we find  $\log_{10}(z_{\rm dec}) > 5.4$  (68% C.L.) and  $N_{\rm eff,int} < 1.10$  at 68% C.L. ( $N_{\rm eff,int} < 2.51$  at 95% C.L.). We instead refer to Fig. 11 for the  $z_{\rm dec}$  constraints.

	Free-streaming	Self-interacting (case 3)	Self-interacting (fluidlike)
	P18 + lens + BAO	P18 + lens + BAO	P18 + lens + BAO
$\overline{\omega_b}$	$0.02242 \pm 0.00014$	$0.02243 \pm 0.00014$	$0.02247 \pm 0.00015$
$\omega_{cdm}$	$0.1196 \pm 0.0010$	$0.1197 \pm 0.0010$	$0.1199 \pm 0.0010$
$100 \times \theta_s$	$1.04191 \pm 0.00032$	$1.04220^{+0.00033}_{-0.00066}$	$1.04261^{+0.00050}_{-0.0067}$
$\ln(10^{10}A_s)$	$3.043 \pm 0.015$	$3.042 \pm 0.016$	$3.036 \pm 0.017$
$n_s$	$0.9669 \pm 0.0038$	$0.9643^{+0.0055}_{-0.0041}$	$0.9621 \pm 0.0050$
$z_{\rm reio}$	$7.82 \pm 0.73$	$7.82 \pm 0.72$	$7.87 \pm 0.73$
$N_{ m eff,int}$	• • •	<0.79 (68% C.L.)	<0.28 (68% C.L.)
$\sum m$	<0.115 (95% C.L.)	<0.115 (95% C.L.)	<0.118 (95% C.L.)
$\overline{H}_0 \left[ \frac{(\text{km/s})}{\text{Mpc}} \right]$	$67.8 \pm 0.5$	$67.9_{-0.5}^{+0.6}$	$68.0 \pm 0.6$
$S_8$	$0.829 \pm 0.012$	$0.829 \pm 0.013$	$0.823 \pm 0.013$
ln(E)	$-0.5306 \times 10^3$	$-0.5309 \times 10^3$	$-0.5320 \times 10^3$
$E_{ m int}/E_{ m fs}$	•••	0.74	0.24
		Best fit	
$N_{ m eff,int}$	• • •	0.199	0.139
$\log_{10}(z_{\rm dec})$	• • •	3.084	• • •
$\chi^2_{ m eff}$	1017.32	1016.65	1017.05
$\Delta \chi^2_{ m eff}$	•••	-0.67	-0.28
	H	ligh-z <sub>dec</sub> mode best fit	
$N_{ m eff,int}$	• • •	0.020	• • •
$\log_{10}(z_{\rm dec})$	• • •	5.077	• • •
$\chi^2_{ m eff}$	• • •	1017.47	• • •
$\Delta \chi^2_{\rm eff}$	•••	+0.15	

- (iv) Figure 13. P18 + lens + BAO. Red (all free-streaming), blue (partially interacting), and purple (partially fluidlike).
- (v) Figure 13. P18 + lens + BAO + R19. Green (all free-streaming), yellow (partially interacting), and pink (partially fluidlike).

For this case, almost all  $z_{\text{dec}}$  values are allowed, and parameter space can roughly be split into three regions with slightly disfavored regions in between:

- (1) Nearly free-streaming at  $z_{\rm dec} \gtrsim 60,000$  extending up to standard neutrino decoupling (note that beyond  $z_{\rm dec} > 10^6$  the one-dimensional posterior is approximately flat up to standard neutrino decoupling).
- (2) A strongly interacting mode at around  $z_{\rm dec} \sim 10{,}000$ .
- (3) A fluidlike region from just before recombination until today, with a peak in the posterior shortly before recombination.

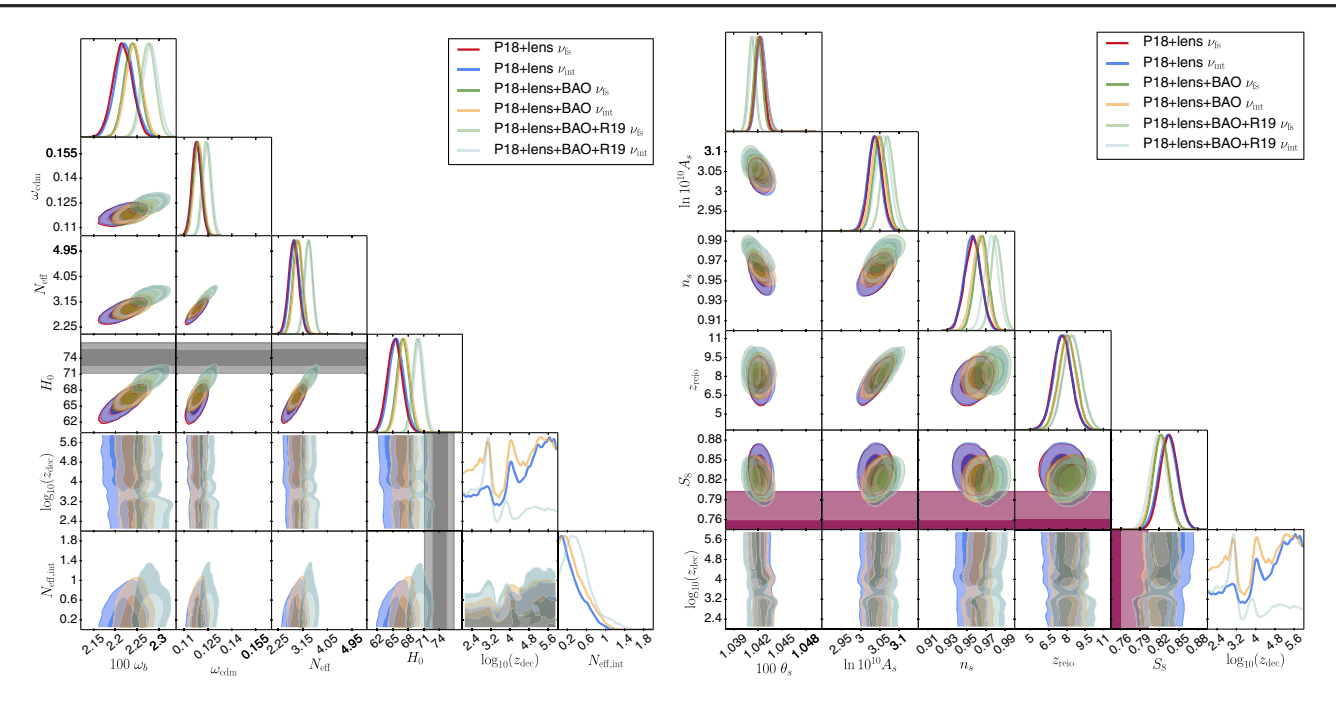


FIG. 12. Case 4: varying fraction of self-interacting relativistic species. All free-streaming (red, green, and light green) vs fraction of self-interacting (blue, yellow, and cyan) for Planck-only (red and blue), Planck + BAO (green and yellow), and Planck + BAO +  $H_0$  prior (light green and cyan). The gray bands correspond to the  $H_0$  measurement from Riess et al. [51], while the purple band is the  $S_8$  measurement from KiDS + VIKING-450 [134]. See Appendix C, Fig. 24 for the full parameter space plot. Left and right panels: both show the same cases, but different cosmological parameters. Left panel: energy density parameters. Right panel: power spectrum shape and amplitude parameters. Some contours are hard to see as the self-interacting cases are on top of the free-streaming comparison cases, e.g., red and blue, green and yellow, and light green and cyan. This is true for, e.g.,  $H_0$ , where there is negligible difference between the free-streaming and interacting cases except at low values of  $z_{\rm dec} \lesssim 2000$  in the fluidlike regime, making the combination of Planck and the  $H_0$  prior suspicious. The parameter space for the decoupling redshift,  $z_{\rm dec}$ , can be roughly separated into three regions, with slightly disfavored regions in between: 1) nearly free-streaming at  $z_{\rm dec} \lesssim 60,000$  (note the posterior is approximately flat up to standard neutrino decoupling), 2) a strongly interacting mode at around  $z_{\rm dec} \sim 10,000$ , and 3) a fluidlike region from just before recombination until today (the posterior is approximately flat below  $z_{\rm dec} < 10^2$ ), with a peak in the posterior shortly before recombination. At low  $z_{\rm dec} \lesssim 2000$ , in the fluidlike regime, we see  $H_0$  and  $S_8$  tensions are slightly alleviated compared to the free-streaming comparison cases (see  $z_{\rm dec}$ - $H_0$  and  $z_{\rm dec}$ - $S_8$  2-d plots for  $z_{\rm dec} \lesssim 2000$ ), while larger values for  $z_{\rm dec}$  show no improvement compared to the free-streaming cases.

The  $z_{\rm dec} \sim 10,000$  mode allows for up to  $N_{\rm eff,int} \lesssim 1$  at  $2\sigma$ , while the fluidlike regime is restricted to about  $N_{\rm eff,int} \lesssim 0.5$  unless the  $H_0$  prior is added, in which case a larger number of extra-relativistic species is allowed, up to around  $N_{\rm eff,int} \lesssim 1$  at  $1\sigma$ . We see there is a slight alleviation of the  $S_8$  (Fig. 12, right panel) and  $H_0$  (Fig. 12, left panel) tensions compared to the free-streaming case for low values of  $z_{\rm dec} \lesssim 2000$  (see  $z_{\rm dec}$ - $H_0$  and  $z_{\rm dec}$ - $S_8$  2-d plots for  $z_{\rm dec} \lesssim 2000$ ), with the change in  $S_8$  being the most significant. Given the relatively minor improvement in the

 $H_0$  tension compared to the free-streaming case, the combination with the  $H_0$  prior remains somewhat suspect.

However, if the results including  $H_0$  were to be trusted, we intriguingly find a preference for a fluidlike component, with a sharp peak in the posterior at around  $1000 < z_{\rm dec} < 2000$  (with a best fit of  $z_{\rm dec} = 1200$ ; see Table VI) and a flattening of the posterior at low- $z_{\rm dec}$  values (continuing until a decoupling today) at a higher level than the free-streaming part of parameter space, with a comparable parameter space volume. However, this would require a

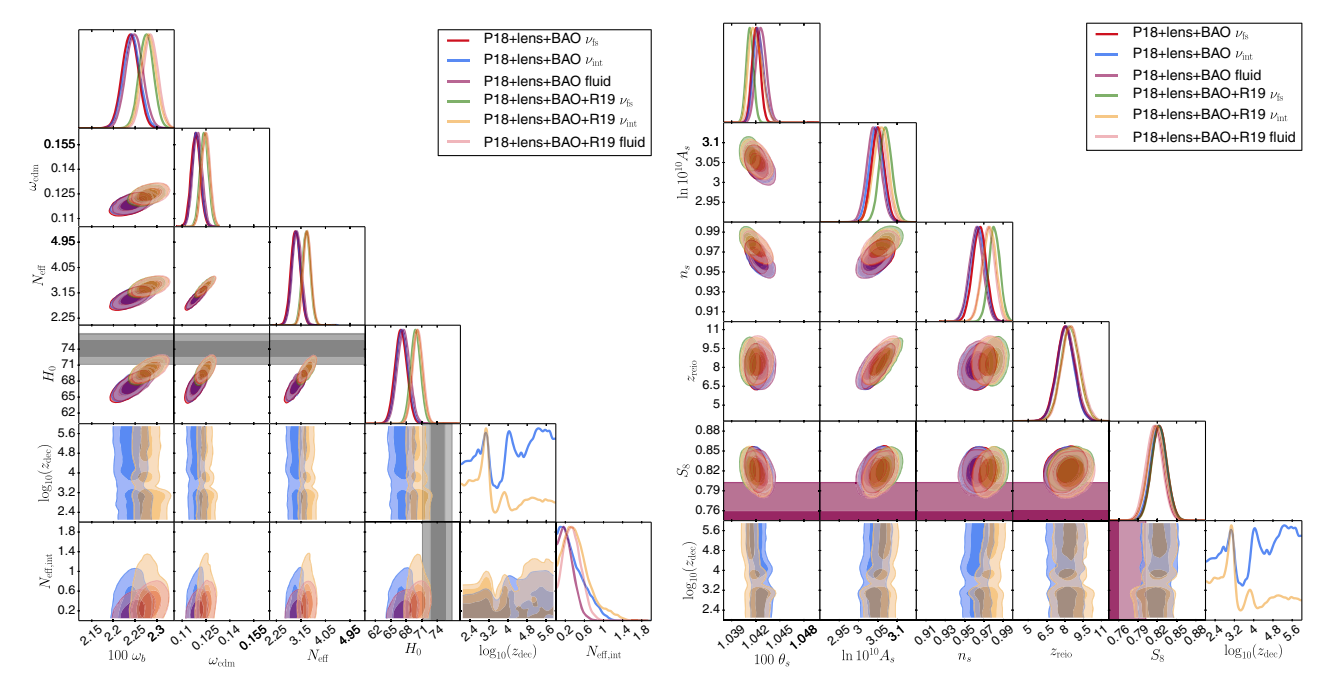


FIG. 13. Case 4: varying fraction of self-interacting relativistic species, including fluid. All free-streaming (red and green) vs fraction of self-interacting species interacting (blue and yellow) and fraction of fluidlike (purple and pink) for Planck + BAO (red, blue, and purple) and Planck + BAO +  $H_0$  prior (green, yellow, and pink). The gray bands correspond to the  $H_0$  measurement from Riess et al. [51], while the purple band is the  $S_8$  measurement from KiDS + VIKING-450 [134]. See Appendix C, Fig. 25 for the full parameter space plot. Left and right panels: both show the same cases, but different cosmological parameters. Left panel: energy density parameters. Right panel: power spectrum shape and amplitude parameters. Note that beyond  $z_{\rm dec} > 10^6$  up to standard neutrino decoupling and below  $z_{\rm dec} < 10^2$  the one-dimensional posterior is approximately flat. The fluidlike case only slightly alleviates the  $H_0$  and  $S_8$  tensions. Although the low- $z_{\rm dec}$  decoupling case at  $1000 < z_{\rm dec} < 2000$  (so, essentially fluidlike) does slightly better at the price of being somewhat fine-tuned, it still requires an external solution to the Hubble tension making the combination of Planck with the  $H_0$  prior somewhat suspect.

novel resolution to the  $H_0$  tension that fixes the value to a high number irrespective of the number of extra-relativistic species, without affecting these bounds.

To isolate the fluidlike region of parameter space, we include on Fig. 13 a fluidlike case with the decoupling redshift set to  $z_{\rm dec}=1$ . This makes it easier to derive numerical constraints; i.e., for the data combination P18 + lens + BAO + R19, the parameter constraints shift

from  $S_8 = 0.823 \pm 0.012$  (free-streaming) to  $S_8 = 0.815 \pm 0.013$  (fluid) and from  $H_0 = 69.8 \pm 1.0$  (free-streaming) to  $H_0 = 70.3 \pm 1.0$  (fluid). It is clear that this is only a marginal improvement in both cases. For a fluidlike species to help more with these tensions, we need a decoupling redshift in the relatively narrow interval of  $1000 < z_{\rm dec} < 2000$ , which is a somewhat fine-tuned solution (and still requires additional help in order to reach the  $H_0$  value from, e.g., Riess *et al.* [51]).

TABLE VI. Case 4: statistical information for our baseline configurations and the one including a prior on  $H_0$ .  $\chi^2_{\rm eff} = -2 \ln \mathcal{L}$  is the effective chi square,  $\Delta \chi^2_{\rm eff}$  is with regard to the corresponding free-streaming case,  $\ln(E)$  is the Bayesian evidence, and  $E_{\rm int}/E_{\rm fs}$  is the Bayesian evidence ratio with regard to the corresponding free-streaming case.  $\chi^2_{\rm eff}$  values are presented for the best-fit cosmology for each of the three modes, where the low- $z_{\rm dec}$  mode is the overall best fit of the run. All credibility intervals are 68% C.L. centered around the mean unless otherwise noted. For  $z_{\rm dec}$  bounds, we refer to Fig. 9, as this case is obviously multimodal and all of parameter space is allowed to some degree.

	Free-streaming			Self-interacting (case 4)			Self-interacting (fluidlike)	
	P18 + lens	+BAO	+R19	P18 + lens	+BAO	+R19	$\overline{P18 + lens + BAO}$	+R19
$\omega_b$	$0.02217 \pm 0.00022$	$0.02239 \pm 0.00019$	$0.02276 \pm 0.00017$	$0.02221 \pm 0.00022$	$0.02242^{+0.00018}_{-0.00020}$	$0.02281^{+0.00017}_{-0.00018}$	$0.02248 \pm 0.00020$	$0.02286 \pm 0.00017$
$\omega_{cdm}$	$0.1178 \pm 0.0028$	$0.1186 \pm 0.0029$	$0.1240 \pm 0.0026$	$0.1183^{+0.0027}_{-0.0030}$	$0.1191 \pm 0.0028$	$0.1247^{+0.0026}_{-0.0027}$	$0.1196 \pm 0.0029$	$0.1249 \pm 0.0027$
$100 \times \theta_s$	$1.04226 \pm 0.00054$	$1.04207 \pm 0.00052$	$1.04127 \pm 0.00046$	$1.04244^{+0.00054}_{-0.00066}$	$1.04238^{+0.00055}_{-0.00075}$	$1.04198^{+0.00068}_{-0.00094}$	$1.04269 \pm 0.00066$	$1.04226^{+0.00066}_{-0.00075}$
$\ln(10^{10}A_s)$	$3.038 \pm 0.017$	$3.050 \pm 0.017$	$3.071 \pm 0.017$	$3.036^{+0.017}_{-0.018}$	$3.044^{+0.018}_{-0.017}$	$3.058^{+0.020}_{-0.019}$	$3.040 \pm 0.018$	$3.054 \pm 0.019$
$n_s$	$0.9567 \pm 0.0085$	$0.9654 \pm 0.0070$	$0.9810 \pm 0.0059$	$0.9561^{+0.0086}_{-0.0082}$	$0.9633^{+0.0076}_{-0.0071}$	$0.9757^{+0.0073}_{-0.0070}$	$0.9622 \pm 0.0073$	$0.9745 \pm 0.0068$
$z_{\rm reio}$	$7.63 \pm 0.75$	$8.06 \pm 0.73$	$8.45 \pm 0.76$	$7.69_{-0.74}^{+0.72}$	$8.07^{+0.70}_{-0.72}$	$8.46 \pm 0.75$	$8.13 \pm 0.75$	$8.53 \pm 0.77$
$N_{ m eff}$	$2.81 \pm 0.18$	$2.95 \pm 0.17$	$3.35 \pm 0.15$	$2.85^{+0.18}_{-0.19}$	$2.98^{+0.16}_{-0.17}$	$3.37^{+0.14}_{-0.15}$	$3.00 \pm 0.17$	$3.37 \pm 0.15$
$N_{ m eff,int}$				<0.74 (95% C.L.)	<0.86 (95% C.L.)	$0.44^{+0.14}_{-0.37}$	<0.51 (95% C.L.)	$0.35^{+0.15}_{-0.22}$
$H_0 \left[ \frac{(\mathrm{km/s})}{\mathrm{Mpc}} \right]$	$65.4 \pm 1.4$	$67.0 \pm 1.2$	$69.8 \pm 1.0$	$65.7^{+1.4}_{-1.5}$	$67.2^{+1.1}_{-1.2}$	$70.1_{-1.0}^{+0.9}$	$67.5 \pm 1.2$	$70.3 \pm 1.0$
$S_8$	$\boldsymbol{0.835 \pm 0.014}$	$\boldsymbol{0.823 \pm 0.012}$	$\boldsymbol{0.823 \pm 0.012}$	$0.833 \pm 0.014$	$0.821\pm0.012$	$0.818 \pm 0.013$	$\boldsymbol{0.818 \pm 0.013}$	$0.815 \pm 0.013$
ln(E)	$-0.5275 \times 10^3$	$-0.5322 \times 10^3$	$-0.5399 \times 10^3$	$-0.5273 \times 10^3$	$-0.5317 \times 10^3$	$-0.5385 \times 10^3$	$-0.5325 \times 10^3$	$-0.5391 \times 10^3$
$E_{ m int}/E_{ m fs}$	• • •	• • •	• • •	1.18	1.57	3.94	0.71	2.19
			Best fit	(corresponding to lov	v-z <sub>dec</sub> mode)			
$N_{ m eff}$	2.798	2.937	3.321	2.807	2.924	3.376	2.982	3.365
$N_{ m eff,int}$				0.030	0.193	0.564	0.168	0.312
$\log_{10}(z_{\rm dec})$				3.038	3.077	3.078		
$\chi^2_{\rm eff}$	1012.85	1021.61	1036.65	1012.79	1021.01	1032.73	1021.22	1034.32
$\Delta\chi^2_{ m eff}$	• • •	• • •	• • •	-0.06	-0.60	-3.91	-0.39	-2.32
			Int	ermediate-z <sub>dec</sub> mode	best fit			
$N_{ m eff}$	• • •	• • •	• • •	2.768	2.930	3.463	• • •	• • •
$N_{ m eff,int}$	• • •	• • •	• • •	0.002	0.297	0.448	• • •	• • •
$\log_{10}(z_{\text{dec}})$	• • •	• • •	• • •	3.849	4.004	3.773	• • •	• • •
$\chi^2_{ m eff}$	• • •	• • •	• • •	1012.93	1021.46	1034.96	• • •	• • •
$\Delta\chi^2_{ m eff}$	• • •		• • •	+0.07	-0.15	-1.68	• • •	• • •
High-z <sub>dec</sub> mode best fit								
$N_{ m eff}$	• • •	• • •	• • •	2.954	2.924	3.321	• • •	• • •
$N_{\rm eff,int}$	• • •	• • •	• • •	0.012	0.028	0.305	• • •	• • •
$\log_{10}(z_{\text{dec}})$	• • •	• • •	• • •	5.542	5.860	5.180	• • •	• • •
$\chi^2_{\rm eff}$	• • •	• • •	• • •	1013.07	1021.74	1037.36	• • •	• • •
$\Delta \chi^2_{ m eff}$	•••	•••	•••	+0.22	+0.13	+0.71	•••	

#### VI. CONCLUSIONS

In this paper, we have produced comprehensive constraints on new neutrino self-interactions from CMB and BAO data. In comparing with data, we study a range of scenarios for neutrino self-interactions. While neutrino self-interactions are strongly constrained by terrestrial experiments, these constraints can be weakened by imposing the self-interactions on the neutrino mass eigenstates and limiting the number of states that participate (Fig. 2). We therefore consider cosmological constraints on self-interactions among all neutrino states as well as a variable fraction of the neutrino states. In the following, we summarize the main results of our analysis and discuss implications for particle physics.

We consider several different scenarios for neutrino interactions, dubbed *cases*, and summarized in Sec. III A, which are discussed case by case in the following (as a reference, our dataset choices are outlined in Sec. IV):

- (i) Case 1: all species interacting
  - P18 + lens and P18 + lens + BAO analyses: If we assume all neutrino species are interacting and allow for a free total amount of neutrinos ( $N_{\rm eff} = N_{\rm eff,int}$ ), we find two modes. The first mode (dubbed the "high-z<sub>dec</sub> mode") has similar cosmological parameters to the free-streaming case but allows values of  $z_{\rm dec}$  lower than the standard neutrino decoupling time; we find  $z_{\text{dec}} > 10^{5.1}$  at 95% confidence for P18 + lens + BAO. The second mode has a low value of  $z_{\text{dec}}$ ,  $z_{\text{dec}} = 10^{4.14 \pm 0.056}$  for P18 + lens+ BAO. The low- $z_{dec}$  mode also has a lower value of  $n_s$  (0.9226  $\pm$  0.0055 versus 0.9613  $\pm$  0.0071) and a lower value of  $N_{\rm eff}$  (2.57  $\pm$  0.14 versus 2.92  $\pm$ 0.17); here, both values are quoted for P18+ lens + BAO, but the trend is the same for P18 + lens alone. All other parameters remain similar between the two cases. The low- $z_{dec}$  mode is not an improved fit to the data, increasing the  $\chi^2_{\rm eff}$  by  $\approx 7$ . See Fig. 6 and Table I for complete parameter results.
  - P18 + lens + BAO + R19 analysis: Adding the local measurement of  $H_0$  from R19 increases the best-fit value of  $N_{\rm eff}$  to  $N_{\rm eff} = 3.30 \pm 0.15$  and eliminates the low- $z_{\rm dec}$  mode found above. The inferred cosmological parameters, including the value of  $N_{\rm eff}$ , are nearly identical for the interacting neutrino case and our free-streaming control. The neutrino decoupling epoch is bound at  $z_{\rm dec} > 10^{5.3}$  at 68% confidence. See Fig. 7 and Table II for complete results.
  - P18 + lens + BAO + R19, omitting high- $\ell$  polarization data: For comparison with Ref. [33], we also try eliminating high- $\ell$  CMB polarization data. In this case, the low- $z_{\rm dec}$  mode found with P18 + lens and P18 + lens + BAO mode reappears, but with shifted values of nearly all other cosmological parameters. Notably, the best-fit value of  $H_0$  is completely consistent with that from R19 alone,

- appearing to eliminate the Hubble tension. The value of  $S_8$  is also reduced slightly, somewhat alleviating the tension with low-redshift data. On the other hand, the low- $z_{\rm dec}$  mode is not actually an improved fit to the data ( $\chi^2_{\rm eff}$  increases by  $\approx$ 4). Separately, we have no *a priori* reason to eliminate the polarization data that forbids the existence of this mode. See Fig. 8 and Table III for complete results.
- (ii) Case 2: Two free-streaming species plus free amount of interacting species-If we force two neutrino states to be free-streaming to alleviate noncosmological constraints on neutrino interactions, P18 + lens + BAO analyses find bounds on  $N_{\rm eff} = 2.91^{+0.18}_{-0.17}$ , nearly unchanged from the control case in which all contributions to  $N_{\rm eff}$  are free-streaming,  $N_{\rm eff} = 2.92 \pm 0.17$ . A hint of a second low- $z_{\rm dec}$  mode appears at  $z_{\rm dec} \approx 10^{4.09}$ . This mode has a larger value of  $\theta_s$ , lower  $A_s$  and  $n_s$  but does not significantly shift other cosmological parameters (including  $H_0$  and  $S_8$ ). The hint of the low- $z_{dec}$  mode remains when adding R19, but the  $H_0$  tension is not relieved (the new value of  $H_0$  is the same as for free-streaming). The low- $z_{dec}$  mode is not isolated, so it is not straightforward to derive a bound on  $z_{\text{dec}}$  in this case. Complete results are presented in Fig. 9 and Table IV. For this scenario, we also provide constraints under the assumption that  $N_{\text{eff,int}}$  never decouples (that is, it is a fluid). For the fluid case, the values of  $n_s$  and  $N_{\text{eff}}$  are lowered by approximately 1-2 and  $0.5\sigma$ , respectively. The value of  $S_8$  is also lowered, somewhat reducing the tension with low-redshift data. The fluid model is, however, a worse fit to the data overall. Complete results are in Fig. 10 and Table IV. Figures 3 and 4 illustrate how changes to the CMB power spectra induced by the lower  $z_{dec}$  value are compensated by shifts in other cosmological parameters.
- (iii) Case 3:  $N_{\rm eff} = 3.046$ , varying fraction of interacting species—If we fix the total relativistic degrees of freedom to the Standard Model value of  $N_{\rm eff}$  = 3.046, but allow the interacting fraction to vary, we find upper bounds on the interacting component of  $N_{\rm eff,int}$  < 0.79 for P18 + lens + BAO at 68% confidence. The  $z_{dec}$  posterior shows a small local maximum at around  $z_{\rm dec} \sim 10,000$ . The region  $z_{\rm dec} \gtrsim 10^5$  is, however, preferred by the data (with  $N_{\rm eff,int} \lesssim 1$ , at about  $1\sigma$ ). The fluid case ( $z_{\rm dec} < 0$ ) further limits the interacting component to  $N_{\rm eff,int}$  < 0.28 at 95% confidence. The rest of the cosmological parameters are virtually unchanged between the free-streaming control case, the fit allowing some fraction of neutrinos to self-interact and decouple, and the fit allowing interacting neutrinos that never decouple. Complete results are given in Fig. 11 and Table V.

(iv) Case 4: Free total N<sub>eff</sub> and varying fraction of interacting species—Finally, if we allow  $N_{\text{eff.fs}}$  and  $N_{\rm eff,int}$  to vary independently, the values of  $A_s$  and  $n_s$ shift toward slightly lower values for all dataset combinations in comparison to the free-streaming control case. But other parameters, including  $N_{\rm eff}$ and  $H_0$ , are virtually unchanged. The upper bounds on  $N_{\rm eff.int}$  are 0.74 and 0.86 for P18 + lens and P18 + lens + BAO, respectively, both at 95% confidence. The interacting case is not in any less tension with R19 than the free-streaming control case. Intriguingly, there does appear to be hints of additional modes in  $z_{dec}$  at low, intermediate, and high values of  $z_{\rm dec}$  (appearing at  $z_{\rm dec} \approx 10^3$ ,  $10^4$ , and  $10^{5-6}$ ). The significance of the low- $z_{dec}$  mode increases dramatically with the inclusion of R19 data, and we find a substantial Bayesian evidence ratio of 3.94, yet the  $H_0$  tension is not resolved in this case, making the combination of discrepant datasets questionable. Complete results are given in Fig. 12 and Table VI. Additionally, in Fig. 13 and Table VI, we also present results for a fluid case that never decouples. In this case, we find a tighter bound on  $N_{\rm eff,int}$  of 0.51 for P18 + lens + BAO at 95% confidence, while  $S_8$  is slightly lowered compared to the free-streaming case, somewhat alleviating the tension with low-redshift data. When adding R19 a nonzero amount of interacting fluid is preferred at about 1.5 $\sigma$ , but since the  $H_0$  tension is not alleviated compared to the free-streaming case, the combination of discrepant datasets is questionable.

While we find some hints of additional strongly interacting neutrino modes, these are disfavored by the data overall. We conclude that self-interacting neutrinos are not cosmologically favored over free-streaming species but have not been ruled out for large enough  $z_{\rm dec}$  or small enough  $N_{\rm eff,int}$ . For large  $z_{\rm dec}$  or small  $N_{\rm eff,int}$ , self-interacting species are indistinguishable from free-streaming species as the earlier the decoupling or the lower the abundance, the less the self-interacting species has an effect on the CMB.

For the uniform and universal coupling,  $g_{ij} = g_\phi \delta_{ij}$  (case 1), we find the low- $z_{\rm dec}$  mode is not only disfavored by the cosmological data but is also ruled out experimentally (see Sec. II B). The high- $z_{\rm dec}$  mode places a bound on  $z_{\rm dec}$ , or equivalently on  $G_\nu$ , of  $\log_{10}(z_{\rm dec}) > 5.1$  (P18 + lens + BAO, 95% C.L.). This can be translated to  $G_\nu < 10^{-3.2}$  MeV<sup>-2</sup>. Note that this translation is computed under the assumption of the standard cosmology, but it is still valid as cosmological parameters for the high- $z_{\rm dec}$  mode agree with those for the standard cosmology with free-streaming neutrinos.

Partially interacting neutrinos are discussed in cases 2–4. For these cases, we focus only on the model where  $\nu_3$  is the only interacting neutrinos species,  $g_{ij} = g_{\phi} \delta_{3i} \delta_{3j}$ , as it has the weakest experimental bounds. The discussion of

extra dark radiation will be considered in follow-up work. For  $\nu_3$  to have self-interactions without beyond the Standard Model physics other than the Majoron, we need to have  $N_{\rm eff,int} \sim 1$ . From the results for case 2 in Table IV, we have a best-fit value of  $N_{\rm eff,int} = 0.787$  with  $\log_{10}(z_{\rm dec}) = 4.085 \ (G_{\nu} = 10^{-1.283} \ {\rm MeV^{-2}})$  for the lowerz decoupling mode or  $N_{\rm eff,int} = 0.822$  with  $\log_{10}(z_{\rm dec}) =$ 5.456 ( $G_{\nu} = 10^{-3.381} \text{ MeV}^{-2}$ ) for the higher-z decoupling mode. Both modes have  $\chi^2_{\rm eff}$  values comparable to the freestreaming neutrino case. The bounds on  $z_{dec}$  depend on the prior choice as stated in the caption of Table IV, but we can take the most conservative one,  $\log_{10}(z_{\text{dec}}) > 3.9$ (95% C.L.)  $(G_{\nu} < 10^{-0.99} \text{ MeV}^{-2})$ . We can consider this as the bound for interacting  $\nu_3$  because the mean value of  $N_{\rm eff}$  does not vary significantly with the value of  $z_{\rm dec}$ , as we can see in Fig. 10. Note that the bound on  $z_{dec}$  is relaxed by several orders of magnitude compared to the universal coupling case, as expected. From cases 3 and 4, we can deduce the bounds on  $N_{\rm eff,int}$ . Compared to the fluidlike case, allowing decoupling of self-interactions relaxes the bounds significantly. For case 3, where  $N_{\rm eff}$  is fixed to 3.046, we have  $N_{\rm eff,int}$  < 0.50 for the fluidlike case and  $N_{\rm eff,int}$  < 2.34 with decoupling (95% C.L.). For case 4, where  $\sum m$  is fixed, we have  $N_{\rm eff,int} < 0.51$  and  $N_{\rm eff,int} <$ 0.86 (95% C.L.) for the fluidlike and the decoupling cases,

Finally, we note that in cases 1 and 2 the modes with self-interacting neutrinos have mean values of the spectral index that are lower than the mean value for the free-streaming case. The allowed inflationary models could then be different in these cosmologies. For instance, if the constraints on the tensor-to-scalar ratio were unchanged in the interacting neutrino cosmology, then the lower value of  $n_s$  would favor natural inflation [136–138]. Neutrino free-streaming is, however, known to affect the tensor power spectrum (e.g., Ref. [139]), so constraints on the tensor-to-scalar ratio should differ somewhat in cosmologies where neutrinos self-interact until late times. We leave a study of this to a future work.

In summary, at present, CMB and BAO data exhibit no preference for nonstandard neutrino interactions. The cosmological constraints we have produced, though generally weaker, are complementary to laboratory constraints on neutrino interactions. On the other hand, the hints of additional modes with low values of neutrino decoupling demonstrate the potential for cosmological data to uncover new physics of neutrinos or other light relic particles. Considering an expanded suite of datasets, e.g., including galaxy survey data or other late-time probes, may shed further light on these scenarios and possibly rule out or strengthen the evidence for these hints. This goes beyond the scope of this paper and is something we leave to future work. Additionally, future CMB surveys are likely to improve constraints on these models, but we also leave a

study of the constraining power of future CMB datasets to a later work.

#### **ACKNOWLEDGMENTS**

We thank Peizhi Du and Christina Kreisch for useful discussions. We also thank Daniel Green and the referee for very useful feedback on the first version of the paper. We especially thank Kevin J. Kelly and Sam McDermott for providing the data in Ref. [47]. T.B. and M.L. are supported by U.S. DOE Grant No. DE-SC0017848. J. H. C. is supported by NSF Grant No. PHY-1914731, the Maryland Center for Fundamental Physics (MCFP), and the Johns Hopkins University Joint Postdoc Fund. J. H. C. was also supported in part by U.S. DOE Grant No. DE-SC0017938. Results in this paper were obtained using the

high-performance computing system at the Institute for Advanced Computational Science at Stony Brook University.

#### APPENDIX A: OPACITY FUNCTION

We compare the opacity functions with and without the Pauli-blocking factors in Sec. II. The approximation ignoring the Pauli-blocking factors gives  $\mathcal{O}(10\%)$  larger interaction rates  $\Gamma_{\nu}$ , which provides  $\mathcal{O}(1\%)$  smaller decoupling redshifts,  $z_{\rm dec}$ . In Fig. 14, we show the opacity functions for  $G_{\nu}=10^{-1}~{\rm MeV^{-2}}$  and  $G_{\nu}=10^{-3}~{\rm MeV^{-2}}$  as examples. For  $G_{\nu}=10^{-1}~{\rm MeV^{-2}}$ , we find  $z_{\rm dec}=5034$  for the full expression and  $z_{\rm dec}=4902$  for the approximation. For  $G_{\nu}=10^{-3}~{\rm MeV^{-2}}$ , we have  $z_{\rm dec}=96,367$  and  $z_{\rm dec}=93,859$ . The value of  $z_{\rm dec}$  is  $\mathcal{O}(1\%)$  smaller with

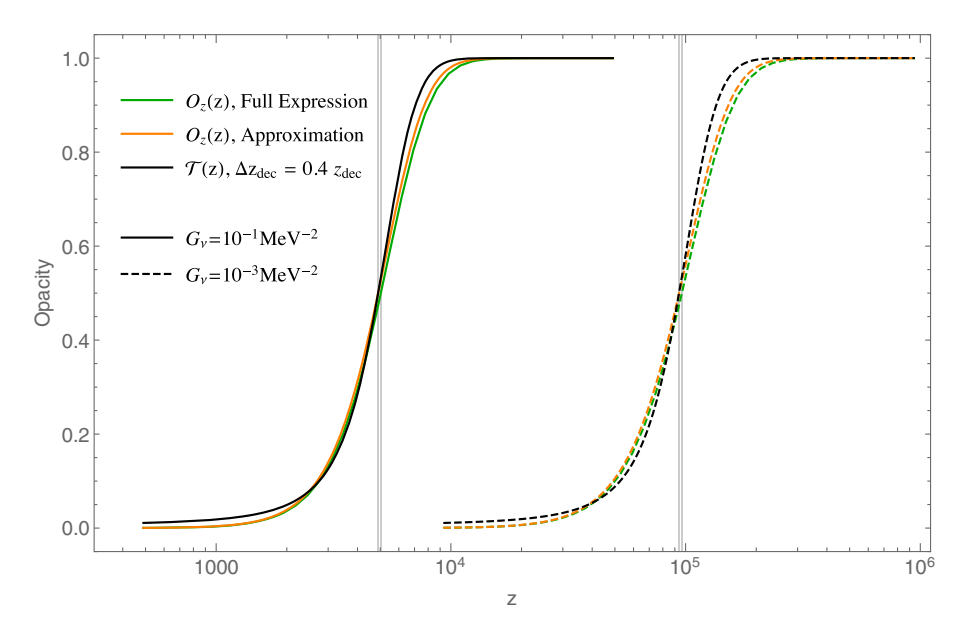


FIG. 14. Opacity in terms of z for  $G_{\nu}=10^{-1}~{\rm MeV^{-2}}$  (solid) and  $G_{\nu}=10^{-3}~{\rm MeV^{-2}}$  (dashed). Grid lines are z where opacity is 0.5. We also show the transition function  $\mathcal{T}(z)$  with corresponding  $z_{\rm dec}$  and  $\Delta z_{\rm dec}=0.4z_{\rm dec}$ .

the approximation. In addition, we show the corresponding transition functions [Eq. (13)] with  $\Delta z_{\rm dec} = 0.4 z_{\rm dec}$ , which we use in CLASS to implement the effects of neutrino self-interactions. We have checked that using the transition function to suppress higher  $(l \geq 2)$  moments of neutrino perturbations instead of using the opacity function yields only  $\mathcal{O}(0.1\%)$  difference in the power spectrum.

#### APPENDIX B: DECOUPLING WIDTH

In this Appendix, we test the impact of the choice in decoupling width on the spectra and the posterior distribution for one of our cases (the one referred to as case 2) for the dataset combination P18 +BAO. In Figs. 15 and 16, we show the difference ratio compared to a free-streaming cosmology when we vary the

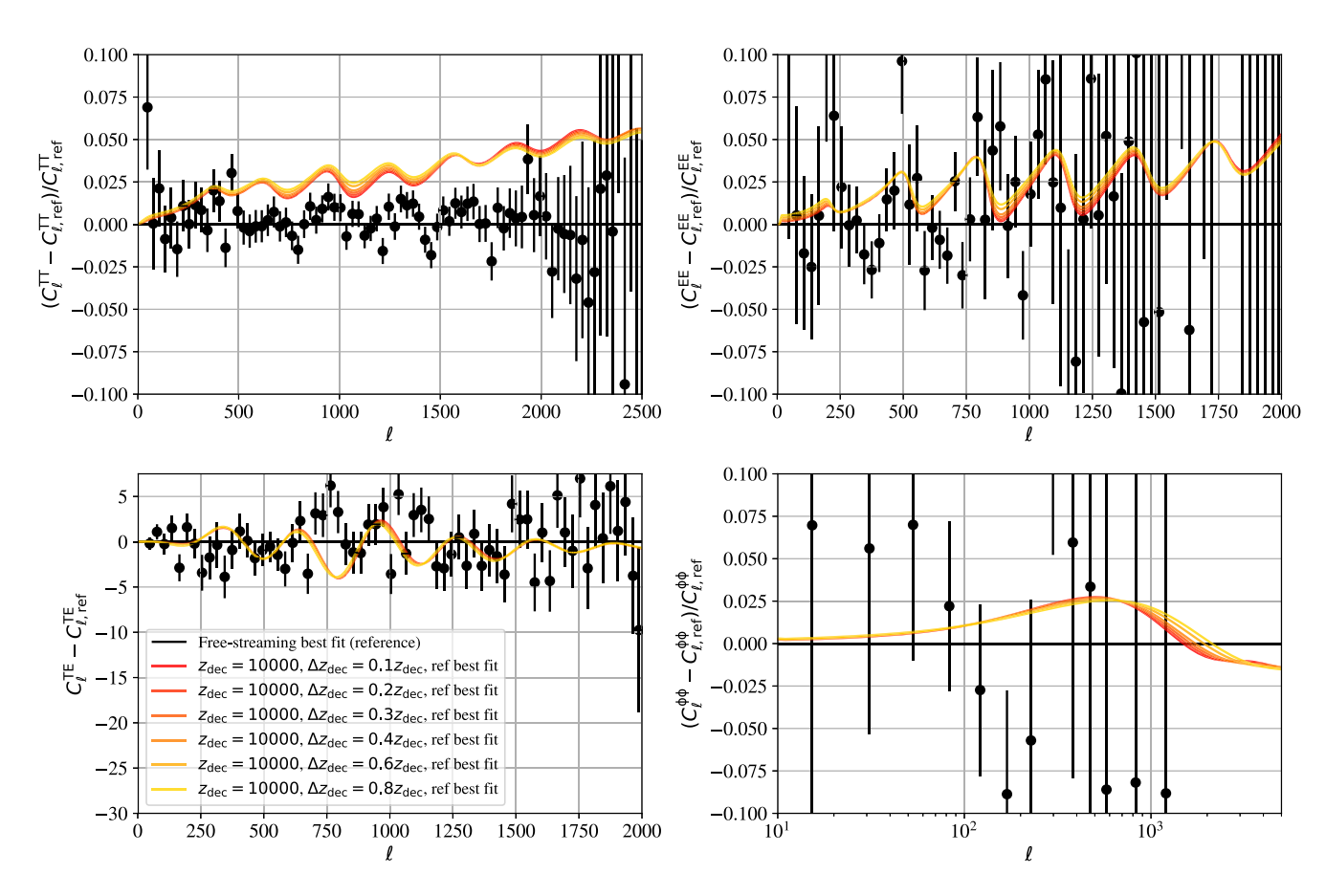


FIG. 15. Fractional differences of the CMB temperature (top left) and polarization (top right) autocorrelation and crosscorrelation (bottom left, showing difference rather than fractional difference) angular power spectra and the CMB lensing power spectrum (bottom right). All cases are compared to a free-streaming neutrinos comparison case with varying width of decoupling  $\Delta z_{\text{dec}}$  of 10% (more red) to 80% (more yellow) of the decoupling redshift of  $z_{\text{dec}} = 10,000$ .

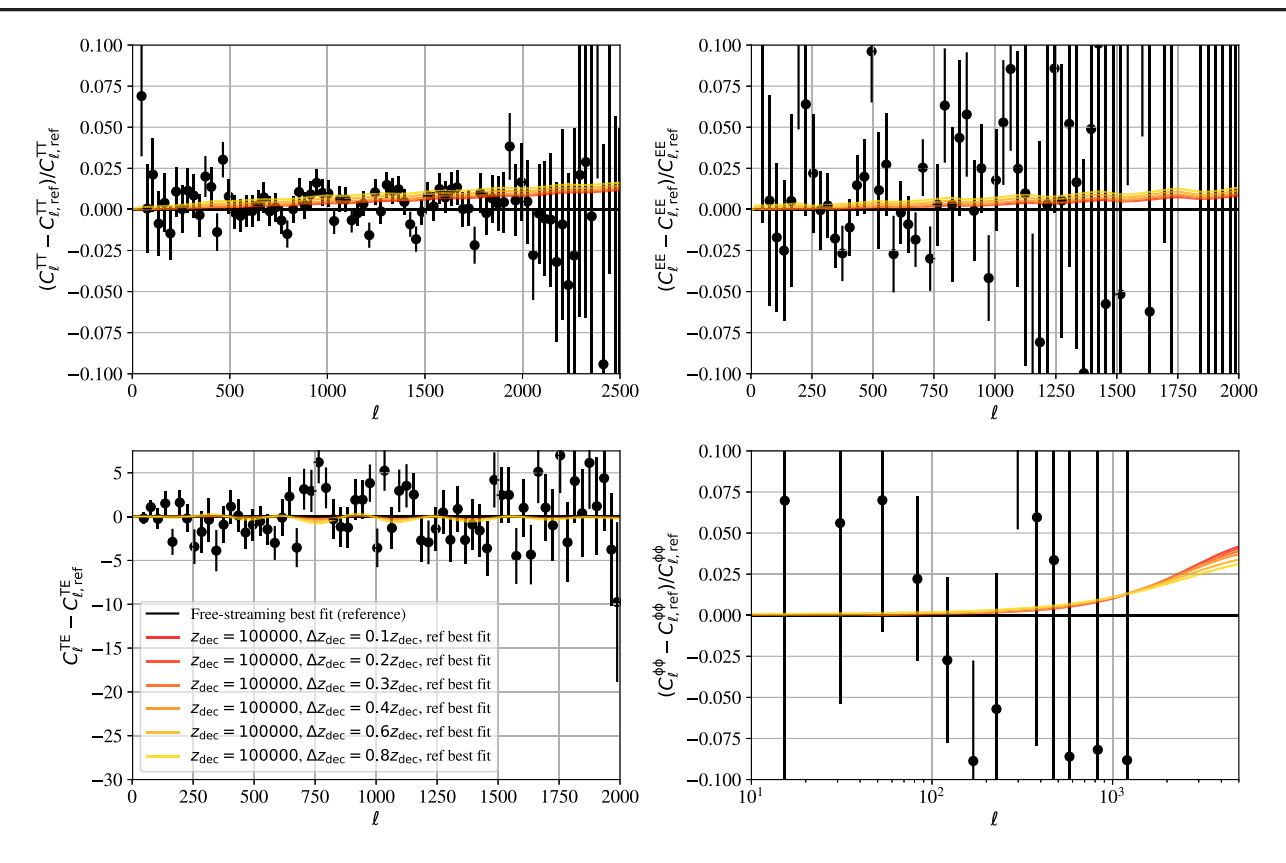


FIG. 16. Fractional differences of the CMB temperature (top left) and polarization (top right) autocorrelation and crosscorrelation (bottom left, showing difference rather than fractional difference) angular power spectra and the CMB lensing power spectrum (bottom right). All cases are compared to a free-streaming neutrinos comparison case with varying width of decoupling  $\Delta z_{\text{dec}}$  of 10% (more red) to 80% (more yellow) of the decoupling redshift of  $z_{\text{dec}} = 100,000$ .

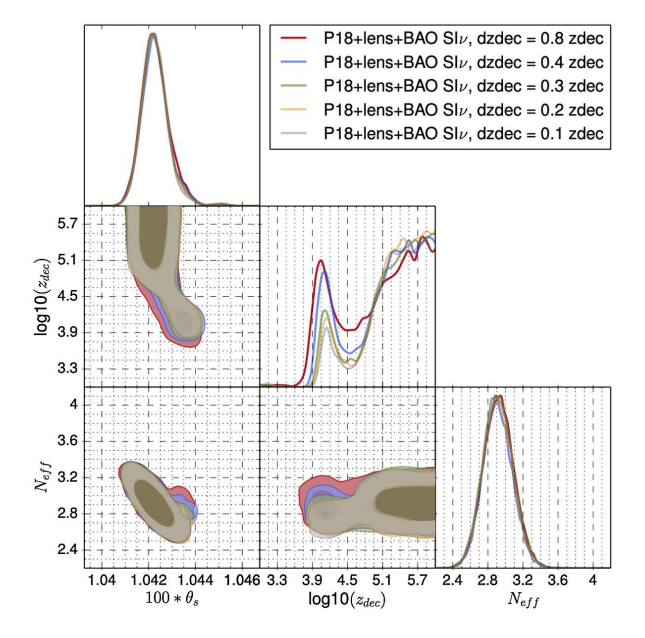


FIG. 17. *Case* 2: two free-streaming neutrinos plus self-interacting relativistic species. The figure shows select parameters for five runs with different decoupling widths of 10% (red), 20% (blue), 30% (green), 40% (yellow), and 80% (gray) of  $z_{\rm dec}$ . The MCMC runs otherwise have an identical setup and are for the data combination P18 + lens + BAO.

decoupling width from 10% to 80% for  $z_{\rm dec} = 10,000$  and  $z_{\rm dec} = 100,000$ , respectively. Qualitatively, they are similar and only differ at a subpercent level. We note that at the spectra level we found that with our baseline decoupling width of 40% of  $z_{\rm dec}$  we could reproduce the example spectra of Ref. [32] Figs 7–9 (but note that our value for  $z_{\rm dec}$  does not map perfectly onto theirs).

This does, however, translate to some difference in the posterior distribution, which is shown in Fig. 17. The low- $z_{\rm dec}$  mode persists for all decoupling widths, but a wider decoupling width shifts the mode to slightly lower values, and in general, lower  $z_{\rm dec}$  values are more disfavored for a narrower decoupling width. This extends to the intermediate- $z_{\rm dec}$  region, where a decoupling width of 10%–40% means the intermediate region is significantly more disfavored compared to the 80% decoupling width case. This might warrant further study in what kind of models could give rise to such a wide decoupling width, as it is easier to accommodate with cosmological data, but we leave this to future work.

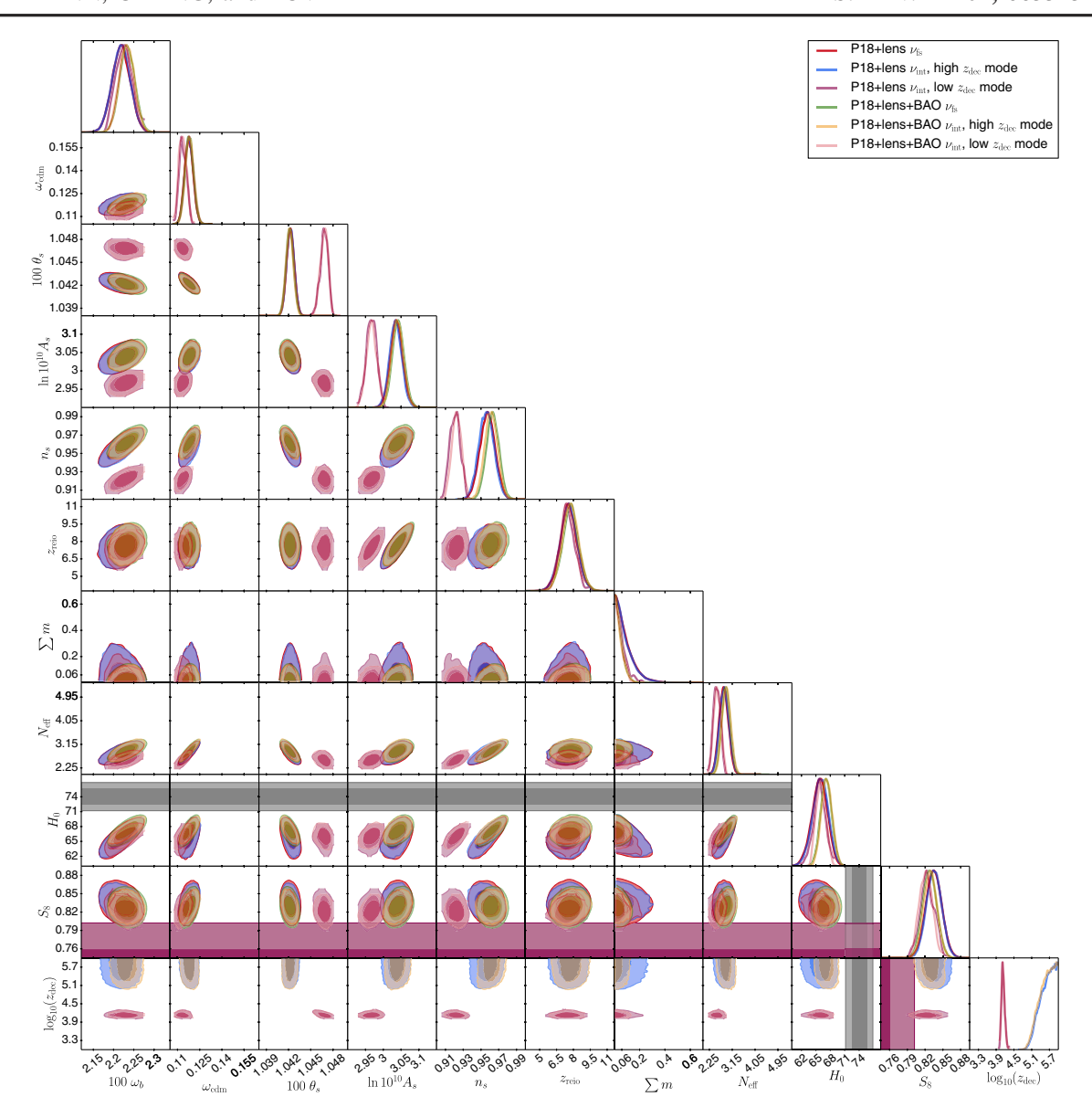


FIG. 18. Case 1: all species interacting. Full parameter space corresponding to Fig. 6.

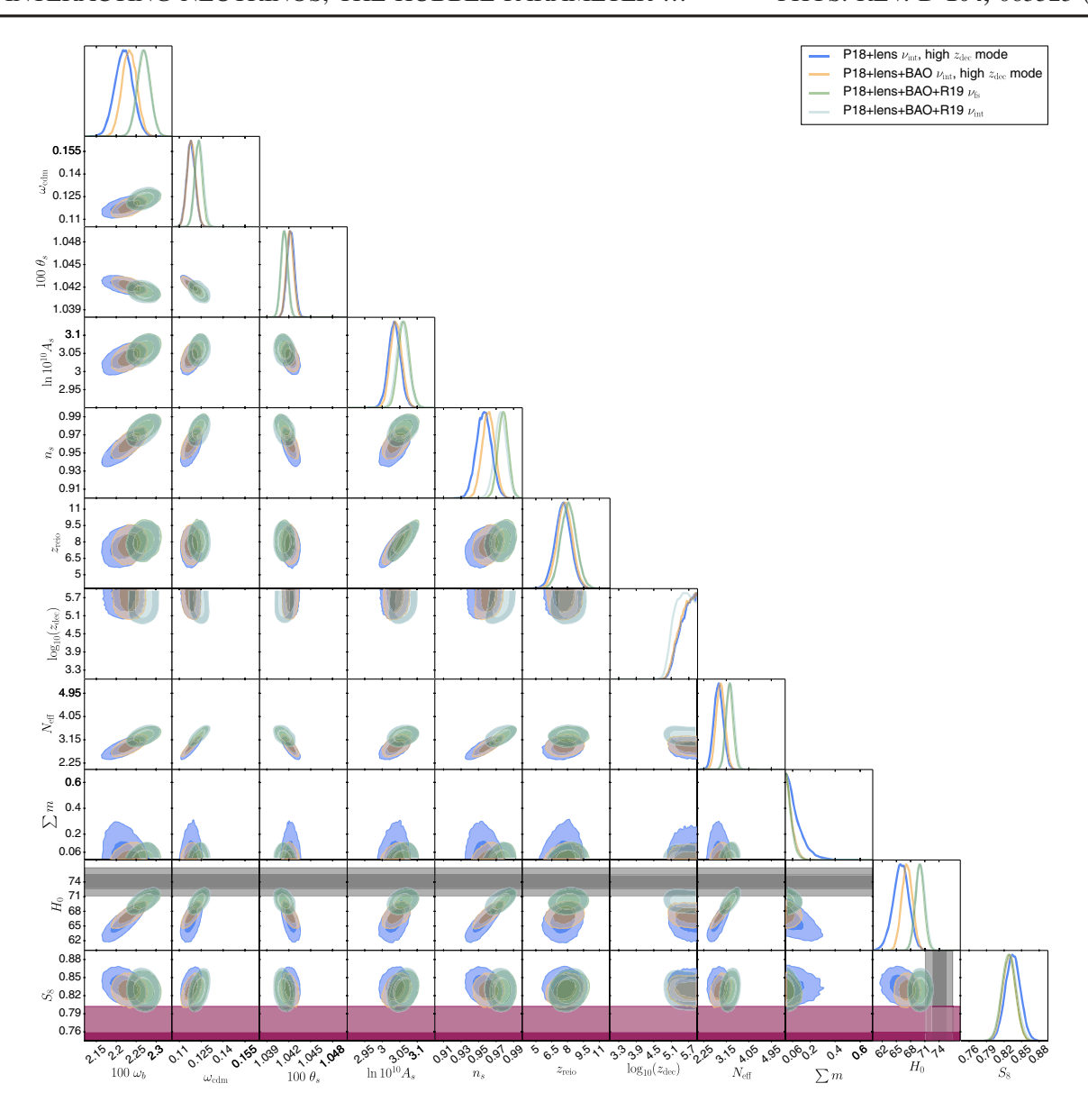


FIG. 19. Case 1: all species interacting, including  $H_0$  prior. Full parameter space corresponding to Fig. 7.

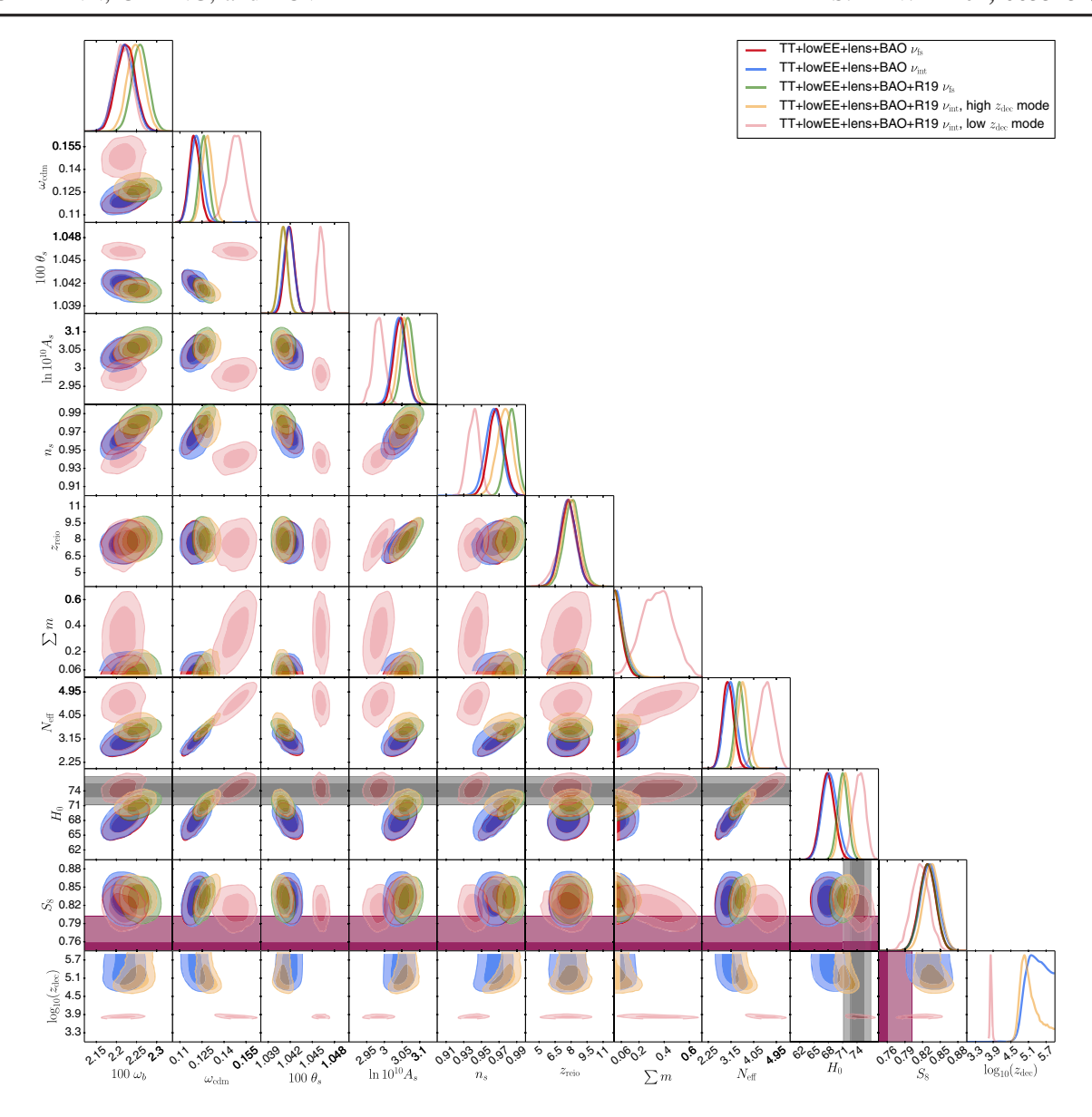


FIG. 20. Case 1: all species interacting, no high-\( \ell \) polarization. Full parameter space corresponding to Fig. 8.

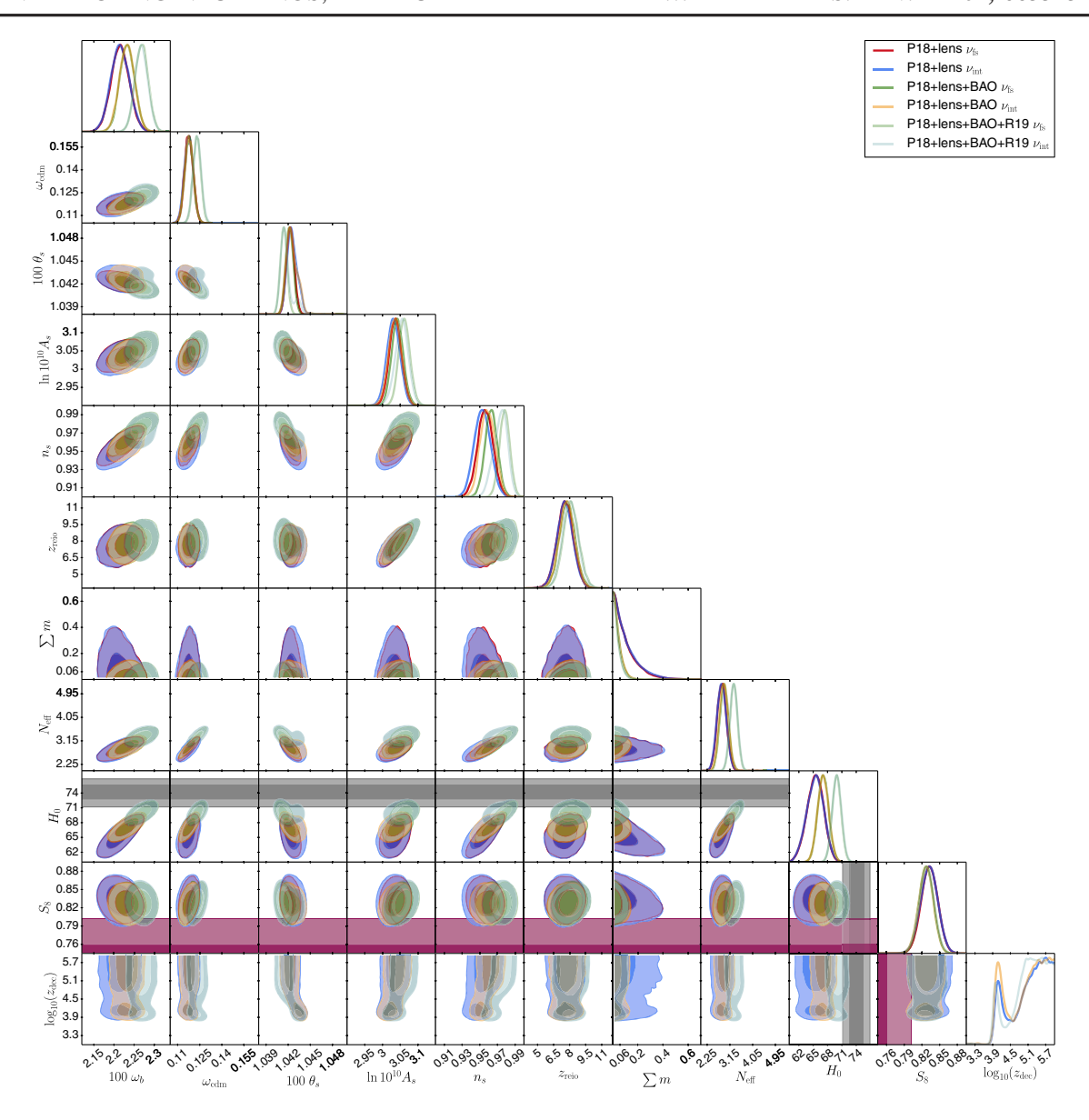


FIG. 21. Case 2: two free-streaming neutrinos plus self-interacting relativistic species. Full parameter space corresponding to Fig. 9.

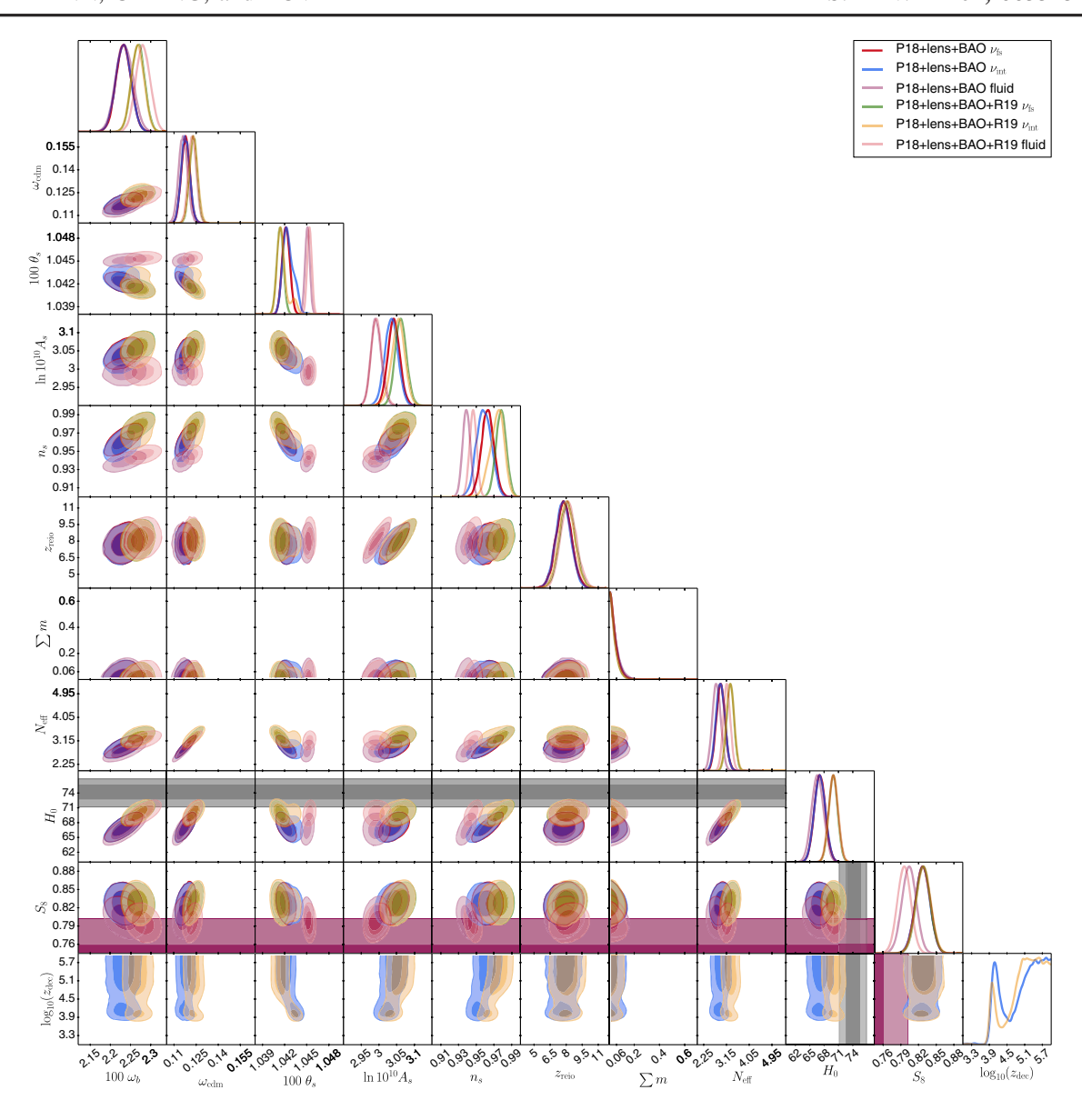


FIG. 22. Case 2: two free-streaming neutrinos plus self-interacting relativistic species, including fluidlike. Full parameter space corresponding to Fig. 10.

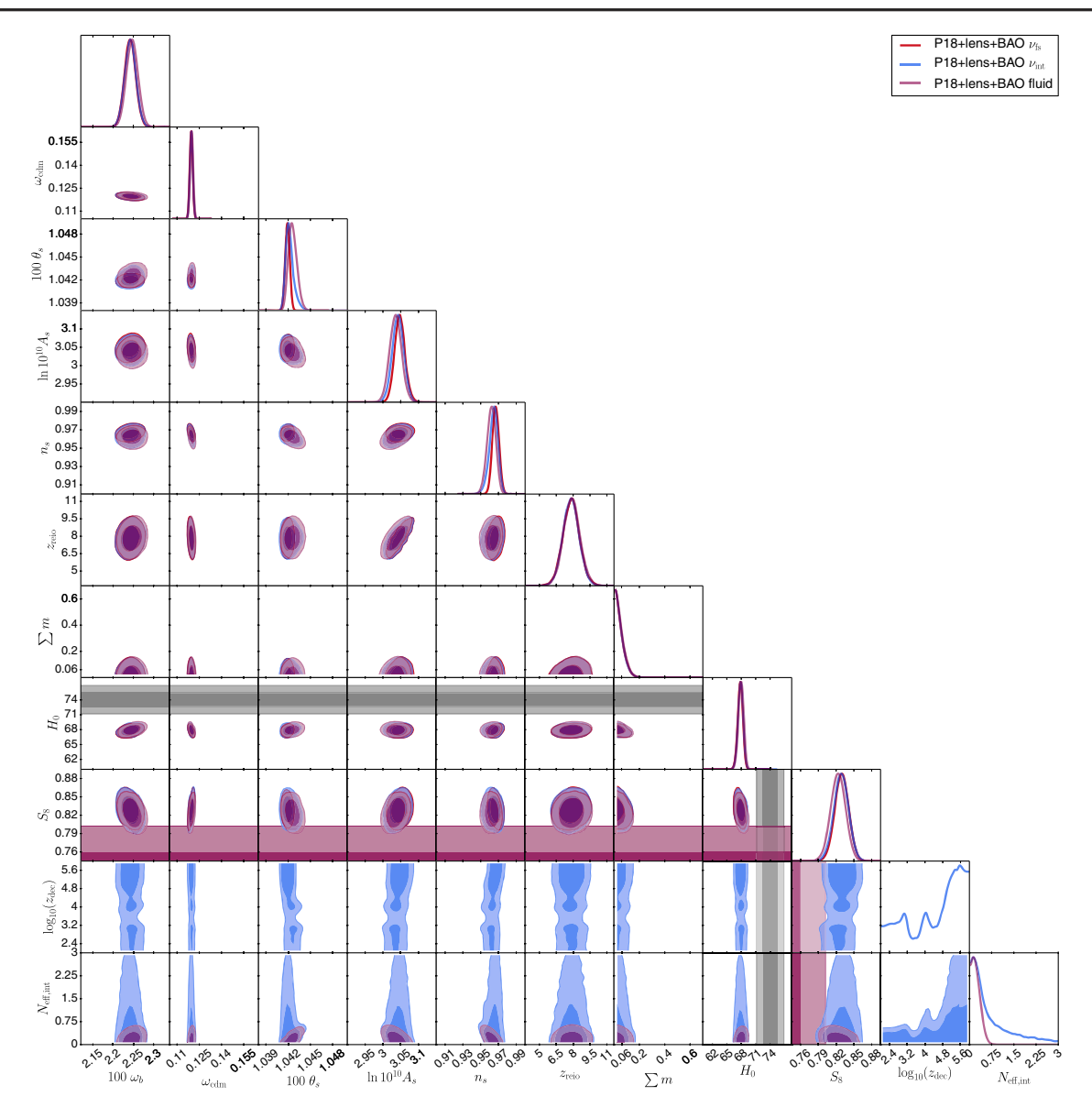


FIG. 23. Case 3: varying fraction of self-interacting relativistic species, including fluid-like, with fixed  $N_{\rm eff}=3.046$ . Full parameter space corresponding to Fig. 11.

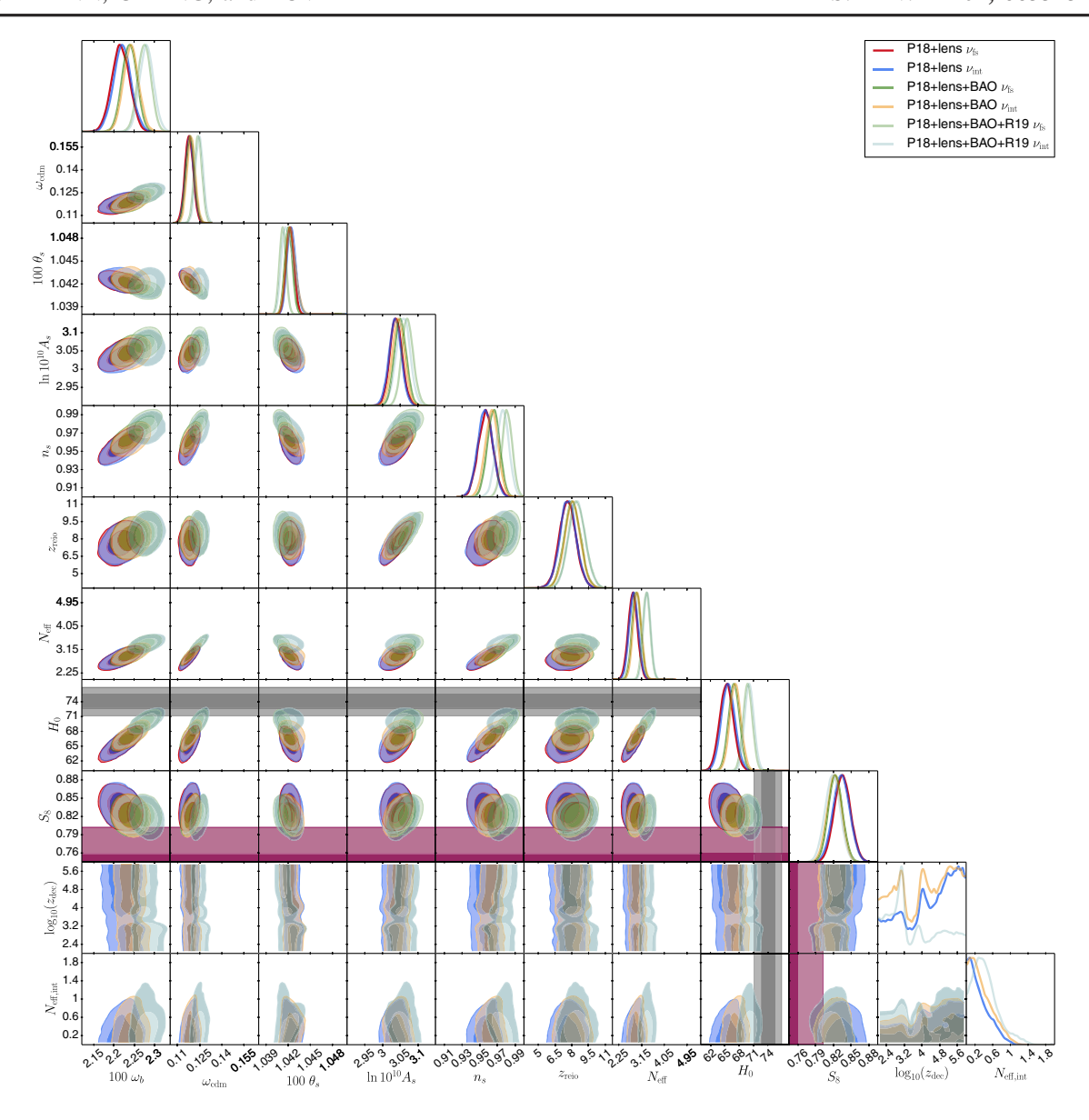


FIG. 24. Case 4: varying fraction of self-interacting relativistic species. Full parameter space corresponding to Fig. 12.

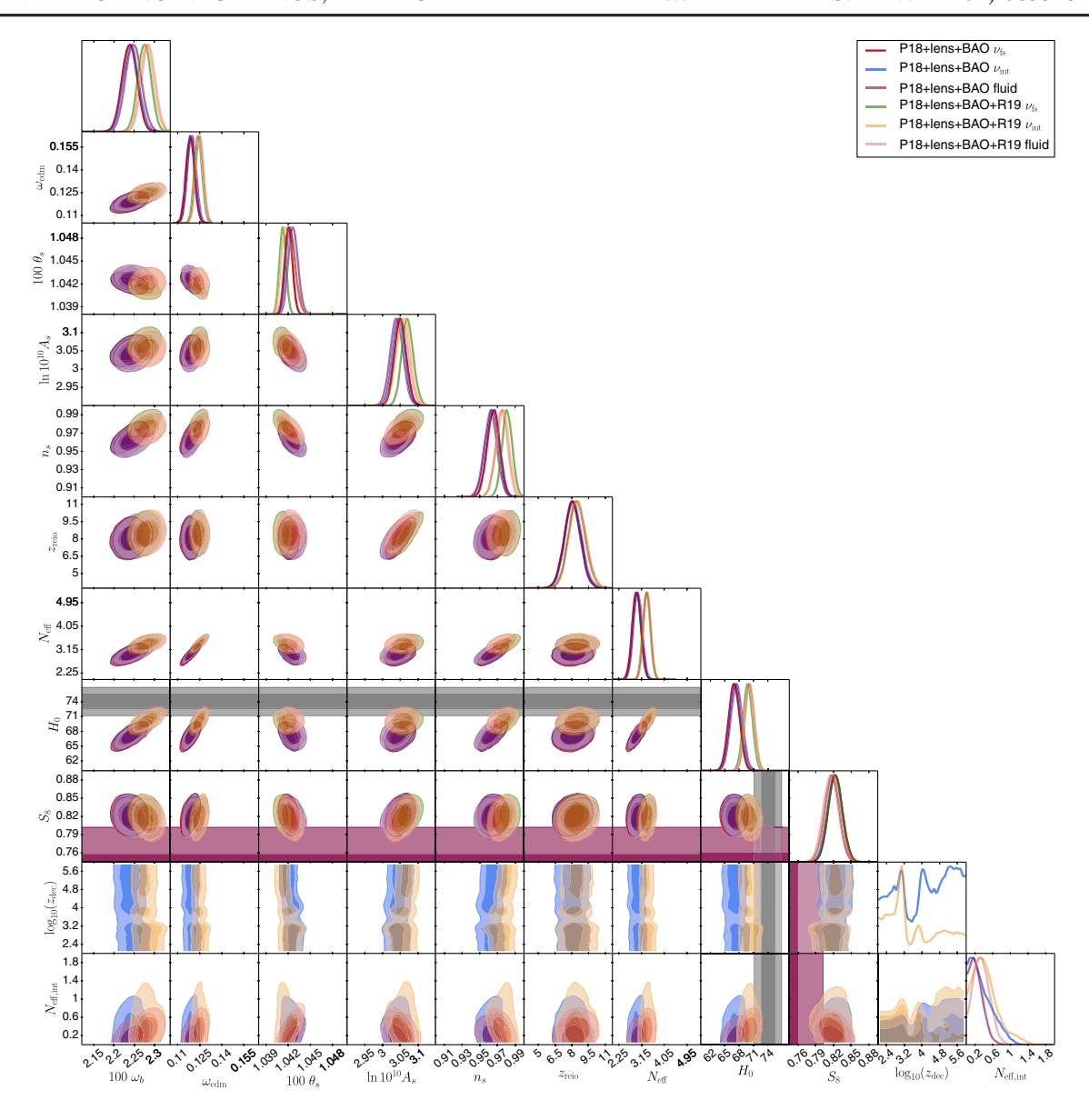


FIG. 25. Case 4: varying fraction of self-interacting relativistic species, including fluidlike. Full parameter space corresponding to Fig. 13.

## APPENDIX C: FULL PARAMETER SPACE PLOTS

In this Appendix, we show the full parameter space plots corresponding to the figures in Sec. V.

## APPENDIX D: CLASS PRECISION PARAMETERS AND MULTINEST SAMPLING SETTINGS

Although we added a new species with a different name, we will provide the settings used if someone were to add an interaction to the NCDM species as they are the same. To accurately compute the effect of self-interactions on a massive relativistic species using the NCDM framework

in CLASS, it is crucial to turn off the fluid approximation. This can be done by ensuring it never kicks in (alternately, one could use the ncdm\_fluid\_approximation flag) ncdm\_fluid\_trigger\_tau\_over\_tau\_k = 1e8
Aside from that, we set most of the other precision settings to an arbitrarily small value, although this could be tuned for greater efficiency:

```
tol_M_ncdm = 1e-10
tol_ncdm = 1e-10
tol_ncdm_synchronous = 1e-10
tol_ncdm_newtonian = 1e-10
tol_ncdm_bg = 1e-10
tol_ncdm_initial_w = 1e-10
```

Please see the file include/precisions.h (within newer CLASS versions) for details on what these parameters do and their default values.

To find all modes, we needed to increase the precision settings of the MultiNest sampler beyond commonly used values. We attribute this need to the many orders of magnitude covered by the parameters space in combination with the narrowness of some of the

modes compared to the wide allowed parameter space as the interactions asymptote to a free-streaming or fluidlike case. The settings we used were

- evidence tolerance = 0.005
- n live points = 4000

Please see the MultiNest documentation for details on what these parameters do.

- [1] K. Abazajian et al., arXiv:1204.5379.
- [2] P. Zyla *et al.* (Particle Data Group), Prog. Theor. Exp. Phys. (2020), 083C01.
- [3] K. N. Abazajian *et al.* (CMB-S4 Collaboration), arXiv:1610.02743.
- [4] S. Bashinsky and U. Seljak, Phys. Rev. D **69**, 083002 (2004).
- [5] Z. Bialynicka-Birula, Nuovo Cimento 33, 1484 (1964).
- [6] G. Raffelt and J. Silk, Phys. Lett. B 192, 65 (1987).
- [7] A. V. Berkov, Y. P. Nikitin, A. L. Sudarikov, and M. Y. Khlopov, Yad. Fiz. 46, 1729 (1987).
- [8] A. V. Berkov, Y. P. Nikitin, A. L. Sudarikov, and M. Y. Khlopov, Sov. J. Nucl. Phys. 48, 497 (1988).
- [9] K. M. Belotsky, A. L. Sudarikov, and M. Y. Khlopov, Phys. At. Nucl. 64, 1637 (2001).
- [10] Z. Chacko, L. J. Hall, T. Okui, and S. J. Oliver, Phys. Rev. D 70, 085008 (2004).
- [11] S. Hannestad, J. Cosmol. Astropart. Phys. 02 (2005) 011.
- [12] S. Hannestad and G. Raffelt, Phys. Rev. D **72**, 103514 (2005).
- [13] N. F. Bell, E. Pierpaoli, and K. Sigurdson, Phys. Rev. D **73**, 063523 (2006).
- [14] A. Friedland, K. M. Zurek, and S. Bashinsky, arXiv: 0704.3271.
- [15] A. Basboll, O. E. Bjaelde, S. Hannestad, and G. G. Raffelt, Phys. Rev. D 79, 043512 (2009).
- [16] M. Archidiacono and S. Hannestad, J. Cosmol. Astropart. Phys. 07 (2014) 046.
- [17] M. Archidiacono, S. Hannestad, R. S. Hansen, and T. Tram, Phys. Rev. D 91, 065021 (2015).
- [18] F. Forastieri, M. Lattanzi, G. Mangano, A. Mirizzi, P. Natoli, and N. Saviano, J. Cosmol. Astropart. Phys. 07 (2017) 038.
- [19] I.M. Oldengott, T. Tram, C. Rampf, and Y.Y. Wong, J. Cosmol. Astropart. Phys. 11 (2017) 027.
- [20] E. Di Valentino, C. Bøehm, E. Hivon, and F. R. Bouchet, Phys. Rev. D 97, 043513 (2018).
- [21] N. Song, M. Gonzalez-Garcia, and J. Salvado, J. Cosmol. Astropart. Phys. 10 (2018) 055.
- [22] G. Barenboim, P. B. Denton, and I. M. Oldengott, Phys. Rev. D 99, 083515 (2019).
- [23] I. Esteban and J. Salvado, J. Cosmol. Astropart. Phys. 05 (2021) 036.
- [24] Y. Du and J.-H. Yu, J. High Energy Phys. 05 (2021) 058.

- [25] R. Trotta and A. Melchiorri, Phys. Rev. Lett. 95, 011305 (2005).
- [26] R. F. Sawyer, Phys. Rev. D 74, 043527 (2006).
- [27] T. L. Smith, S. Das, and O. Zahn, Phys. Rev. D 85, 023001 (2012).
- [28] M. Gerbino, E. Di Valentino, and N. Said, Phys. Rev. D 88, 063538 (2013).
- [29] B. Audren *et al.*, J. Cosmol. Astropart. Phys. 03 (2015) 036.
- [30] P. Ade et al. (Planck Collaboration), Astron. Astrophys. 594, A13 (2016).
- [31] F.-Y. Cyr-Racine and K. Sigurdson, Phys. Rev. D 90, 123533 (2014).
- [32] L. Lancaster, F.-Y. Cyr-Racine, L. Knox, and Z. Pan, J. Cosmol. Astropart. Phys. 07 (2017) 033.
- [33] C. D. Kreisch, F.-Y. Cyr-Racine, and O. Doré, Phys. Rev. D **101**, 123505 (2020).
- [34] S. Ghosh, R. Khatri, and T. S. Roy, Phys. Rev. D **102**, 123544 (2020).
- [35] M. Escudero and S. J. Witte, Eur. Phys. J. C 80, 294 (2020).
- [36] H.-J. He, Y.-Z. Ma, and J. Zheng, J. Cosmol. Astropart. Phys. 11 (2020) 003.
- [37] M. Berbig, S. Jana, and A. Trautner, Phys. Rev. D 102, 115008 (2020).
- [38] A. Mazumdar, S. Mohanty, and P. Parashari, arXiv:2011 .13685.
- [39] A. Das and S. Ghosh, arXiv:2011.12315.
- [40] S. R. Choudhury, S. Hannestad, and T. Tram, J. Cosmol. Astropart. Phys. 03 (2021) 084.
- [41] K. S. Jeong and F. Takahashi, Phys. Lett. B 725, 134 (2013).
- [42] D. Baumann, D. Green, J. Meyers, and B. Wallisch, J. Cosmol. Astropart. Phys. 01 (2016) 007.
- [43] G. Choi, C.-T. Chiang, and M. LoVerde, J. Cosmol. Astropart. Phys. 06 (2018) 044.
- [44] N. Blinov and G. Marques-Tavares, J. Cosmol. Astropart. Phys. 09 (2020) 029.
- [45] G. Choi, T. T. Yanagida, and N. Yokozaki, J. High Energy Phys. 01 (2021) 127.
- [46] K. C. Y. Ng and J. F. Beacom, Phys. Rev. D **90**, 065035 (2014); **90**, 089904(E) (2014).
- [47] N. Blinov, K. J. Kelly, G. Z. Krnjaic, and S. D. McDermott, Phys. Rev. Lett. 123, 191102 (2019).
- [48] D. Green et al., arXiv:1903.04763.

- [49] A. G. Riess, L. Macri, S. Casertano, H. Lampeitl, H. C. Ferguson, A. V. Filippenko, S. W. Jha, W. Li, and R. Chornock, Astrophys. J. 730, 119 (2011); 732, 129(E) (2011).
- [50] A. G. Riess et al., Astrophys. J. 826, 56 (2016).
- [51] A. G. Riess, S. Casertano, W. Yuan, L. M. Macri, and D. Scolnic, Astrophys. J. 876, 85 (2019).
- [52] L. Verde, T. Treu, and A. Riess, Nat. Astron. 3, 891 (2019).
- [53] D. Scolnic et al., Astrophys. J. 859, 101 (2018).
- [54] E. Macaulay *et al.* (DES Collaboration), Mon. Not. R. Astron. Soc. **486**, 2184 (2019).
- [55] N. Aghanim *et al.* (Planck Collaboration), Astron. Astrophys. **641**, A6 (2020).
- [56] S. Aiola *et al.* (ACT Collaboration), J. Cosmol. Astropart. Phys. 12 (2020) 047.
- [57] M. Blomqvist et al., Astron. Astrophys. 629, A86 (2019).
- [58] A. Cuceu, J. Farr, P. Lemos, and A. Font-Ribera, J. Cosmol. Astropart. Phys. 10 (2019) 044.
- [59] N. Schöneberg, J. Lesgourgues, and D. C. Hooper, J. Cosmol. Astropart. Phys. 10 (2019) 029.
- [60] T. Abbott *et al.* (DES Collaboration), Mon. Not. R. Astron. Soc. **480**, 3879 (2018).
- [61] H. Hildebrandt et al., Astron. Astrophys. 633, A69 (2020).
- [62] S. Joudaki et al., Astron. Astrophys. 638, L1 (2020).
- [63] M. Asgari et al., Astron. Astrophys. 634, A127 (2020).
- [64] C. Heymans, T. Tröster, M. Asgari, C. Blake, H. Hildebrandt, B. Joachimi, K. Kuijken, C.-A. Lin, A. G. Sánchez, J. L. van den Busch *et al.*, Astron. Astrophys. 646, A140 (2021).
- [65] M. Asgari et al. (KiDS Collaboration), Astron. Astrophys. 645, A104 (2021).
- [66] E. van Uitert et al., Mon. Not. R. Astron. Soc. 476, 4662 (2018).
- [67] T. Hamana et al., Publ. Astron. Soc. Jpn. 72, 16 (2020).
- [68] T. M. C. Abbott *et al.* (DES Collaboration), arXiv:2105 .13549.
- [69] M. A. Buen-Abad, G. Marques-Tavares, and M. Schmaltz, Phys. Rev. D 92, 023531 (2015).
- [70] J. Lesgourgues, G. Marques-Tavares, and M. Schmaltz, J. Cosmol. Astropart. Phys. 02 (2016) 037.
- [71] M. A. Buen-Abad, M. Schmaltz, J. Lesgourgues, and T. Brinckmann, J. Cosmol. Astropart. Phys. 01 (2018) 008.
- [72] R. Krall, F.-Y. Cyr-Racine, and C. Dvorkin, J. Cosmol. Astropart. Phys. 09 (2017) 003.
- [73] M. Archidiacono, D. C. Hooper, R. Murgia, S. Bohr, J. Lesgourgues, and M. Viel, J. Cosmol. Astropart. Phys. 10 (2019) 055.
- [74] N. Becker, D. C. Hooper, F. Kahlhoefer, J. Lesgourgues, and N. Schöneberg, J. Cosmol. Astropart. Phys. 02 (2021) 019.
- [75] V. Poulin, T. L. Smith, T. Karwal, and M. Kamionkowski, Phys. Rev. Lett. 122, 221301 (2019).
- [76] J. C. Hill, E. McDonough, M. W. Toomey, and S. Alexander, Phys. Rev. D 102, 043507 (2020).
- [77] M. M. Ivanov, E. McDonough, J. C. Hill, M. Simonović, M. W. Toomey, S. Alexander, and M. Zaldarriaga, Phys. Rev. D 102, 103502 (2020).
- [78] G. D'Amico, L. Senatore, P. Zhang, and H. Zheng, J. Cosmol. Astropart. Phys. 05 (2021) 072.

- [79] F. Niedermann and M. S. Sloth, Phys. Rev. D 103, L041303 (2021).
- [80] F. Niedermann and M. S. Sloth, Phys. Rev. D 102, 063527 (2020).
- [81] F. Niedermann and M. S. Sloth, Phys. Rev. D 103, 103537 (2021).
- [82] M. Archidiacono, S. Hannestad, R. S. Hansen, and T. Tram, Phys. Rev. D 93, 045004 (2016).
- [83] M. Archidiacono, S. Gariazzo, C. Giunti, S. Hannestad, R. Hansen, M. Laveder, and T. Tram, J. Cosmol. Astropart. Phys. 08 (2016) 067.
- [84] M. Archidiacono, S. Gariazzo, C. Giunti, S. Hannestad, and T. Tram, J. Cosmol. Astropart. Phys. 12 (2020) 029.
- [85] J. Lesgourgues, arXiv:1104.2932.
- [86] Y. Chikashige, R. N. Mohapatra, and R. Peccei, Phys. Lett. 98B, 265 (1981).
- [87] Y. Chikashige, R. N. Mohapatra, and R. Peccei, Phys. Rev. Lett. 45, 1926 (1980).
- [88] K.-F. Lyu, E. Stamou, and L.-T. Wang, Phys. Rev. D **103**, 015004 (2021).
- [89] D. Bardin, S. M. Bilenky, and B. Pontecorvo, Phys. Lett. **32B**, 121 (1970).
- [90] M. S. Bilenky, S. M. Bilenky, and A. Santamaria, Phys. Lett. B 301, 287 (1993).
- [91] M. S. Bilenky and A. Santamaria, in *Neutrino Mixing: Meeting in Honor of Samoil Bilenky's 70th Birthday* (1999), pp. 50–61.
- [92] V. Brdar, M. Lindner, S. Vogl, and X.-J. Xu, Phys. Rev. D 101, 115001 (2020).
- [93] I. Esteban, M. Gonzalez-Garcia, A. Hernandez-Cabezudo, M. Maltoni, and T. Schwetz, J. High Energy Phys. 01 (2019) 106.
- [94] M. Park, C. D. Kreisch, J. Dunkley, B. Hadzhiyska, and F.-Y. Cyr-Racine, Phys. Rev. D 100, 063524 (2019).
- [95] G. Mangano, G. Miele, S. Pastor, and M. Peloso, Phys. Lett. B 534, 8 (2002).
- [96] G. Mangano, G. Miele, S. Pastor, T. Pinto, O. Pisanti, and P. D. Serpico, Nucl. Phys. **B729**, 221 (2005).
- [97] N. Y. Gnedin and O. Y. Gnedin, Astrophys. J. 509, 11 (1998).
- [98] S. Hannestad and J. Madsen, Phys. Rev. D 52, 1764 (1995).
- [99] A. F. Heckler, Phys. Rev. D 49, 611 (1994).
- [100] A. D. Dolgov and M. Fukugita, Phys. Rev. D **46**, 5378 (1992).
- [101] A. D. Dolgov, Phys. Rep. 370, 333 (2002).
- [102] A. D. Dolgov, S. H. Hansen, and D. V. Semikoz, Nucl. Phys. **B503**, 426 (1997).
- [103] S. Dodelson and M. S. Turner, Phys. Rev. D 46, 3372 (1992).
- [104] N. C. Rana and B. M. Seifert, Phys. Rev. D **44**, 393 (1991).
- [105] S. Esposito, G. Miele, S. Pastor, M. Peloso, and O. Pisanti, Nucl. Phys. **B590**, 539 (2000).
- [106] P. F. de Salas and S. Pastor, J. Cosmol. Astropart. Phys. 07 (2016) 051.
- [107] K. Akita and M. Yamaguchi, J. Cosmol. Astropart. Phys. 08 (2020) 012.

- [108] J. Lesgourgues and S. Pastor, Phys. Rep. 429, 307 (2006).
- [109] E. Di Valentino et al. (CORE Collaboration), J. Cosmol. Astropart. Phys. 04 (2018) 017.
- [110] S. Vagnozzi, E. Giusarma, O. Mena, K. Freese, M. Gerbino, S. Ho, and M. Lattanzi, Phys. Rev. D 96, 123503 (2017).
- [111] M. Archidiacono, S. Hannestad, and J. Lesgourgues, J. Cosmol. Astropart. Phys. 09 (2020) 021,
- [112] Z. Hou, R. Keisler, L. Knox, M. Millea, and C. Reichardt, Phys. Rev. D 87, 083008 (2013).
- [113] N. Aghanim *et al.* (Planck Collaboration), Astron. Astrophys. 641, A5 (2020).
- [114] N. Aghanim *et al.* (Planck Collaboration), Astron. Astrophys. 641, A8 (2020).
- [115] B. Audren, J. Lesgourgues, K. Benabed, and S. Prunet, J. Cosmol. Astropart. Phys. 02 (2013) 001.
- [116] T. Brinckmann and J. Lesgourgues, Phys. Dark Universe 24, 100260 (2019).
- [117] D. Blas, J. Lesgourgues, and T. Tram, J. Cosmol. Astropart. Phys. 07 (2011) 034.
- [118] J. Lesgourgues and T. Tram, J. Cosmol. Astropart. Phys. 09 (2011) 032.
- [119] F. Feroz and M. P. Hobson, Mon. Not. R. Astron. Soc. 384, 449 (2008).
- [120] F. Feroz, M. P. Hobson, and M. Bridges, Mon. Not. R. Astron. Soc. 398, 1601 (2009).
- [121] F. Feroz, M. P. Hobson, E. Cameron, and A. N. Pettitt, Open J. Astrophys. 2, 10 (2019).
- [122] J. Buchner, A. Georgakakis, K. Nandra, L. Hsu, C. Rangel, M. Brightman, A. Merloni, M. Salvato, J. Donley, and D. Kocevski, Astron. Astrophys. 564, A125 (2014).
- [123] F. Beutler, C. Blake, M. Colless, D. Jones, L. Staveley-Smith, L. Campbell, Q. Parker, W. Saunders, and F. Watson, Mon. Not. R. Astron. Soc. 416, 3017 (2011).

- [124] A. J. Ross, L. Samushia, C. Howlett, W. J. Percival, A. Burden, and M. Manera, Mon. Not. R. Astron. Soc. 449, 835 (2015).
- [125] S. Alam *et al.* (BOSS Collaboration), Mon. Not. R. Astron. Soc. **470**, 2617 (2017).
- [126] L. Anderson *et al.* (BOSS Collaboration), Mon. Not. R. Astron. Soc. **441**, 24 (2014).
- [127] J. L. Bernal, T. L. Smith, K. K. Boddy, and M. Kamionkowski, Phys. Rev. D 102, 123515 (2020).
- [128] P. Lemos, F. Khlinger, W. Handley, B. Joachimi, L. Whiteway, and O. Lahav, Mon. Not. R. Astron. Soc. 496, 4647 (2020).
- [129] W. Handley and P. Lemos, Phys. Rev. D **103**, 063529 (2021).
- [130] G. Benevento, W. Hu, and M. Raveri, Phys. Rev. D 101, 103517 (2020).
- [131] D. Camarena and V. Marra, Mon. Not. R. Astron. Soc. 504, 5164 (2021).
- [132] G. Efstathiou, Mon. Not. R. Astron. Soc. 505, 3866 (2021).
- [133] L. Knox and M. Millea, Phys. Rev. D 101, 043533 (2020).
- [134] A. H. Wright, H. Hildebrandt, J. L. van den Busch, C. Heymans, B. Joachimi, A. Kannawadi, and K. Kuijken, Astron. Astrophys. 640, L14 (2020).
- [135] N. Aghanim *et al.* (Planck Collaboration), Astron. Astrophys. **594**, A11 (2016).
- [136] P. A. R. Ade *et al.* (BICEP2, Keck Array Collaborations), Phys. Rev. Lett. **121**, 221301 (2018).
- [137] Y. Akrami et al. (Planck Collaboration), Astron. Astrophys. 641, A10 (2020).
- [138] K. Freese, J. A. Frieman, and A. V. Olinto, Phys. Rev. Lett. 65, 3233 (1990).
- [139] S. Weinberg, Phys. Rev. D 69, 023503 (2004).